# POLITECNICO DI TORINO

Collegio di Ingegneria Chimica e dei Materiali

**Corso di Laurea Magistrale**

**in Ingegneria Chimica e dei Processi Sostenibili**

Tesi di Laurea Magistrale

# Thermal treatments on Cassava products

## Experimental and modelling study

**Relatori**

Prof. Davide Fissore

**Candidato**

Simone Cavalera

Ottobre 2022

## SOMMARIO

# 1 Introduzione

La manioca (*Manihot esculenta Crantz*) è una coltura tipica delle zone sub tropicali di Africa, Asia e Sud-America. Le foglie e la radice sono utilizzate come nutrimento per l'uomo e per gli animali. La forma e le proprietà delle foglie dipendono dalla varietà e dalle condizioni ambientali, mentre la parte legnosa dello stelo è utile per la propagazione vegetativa asessuata. Nella radice si sviluppa invece la conversione dei metaboliti (oligosaccaridi) provenienti dalle foglie, l'unica parte della pianta in cui avviene la fotosintesi, per la biosintesi enzimatica dell'amido. La qualità e quantità di quest'ultimo dipendono dalla varietà e dalle condizioni ambientali. L'importante quantità di amido presente nelle radici della manioca, la rende una fonte energetica utile a fronteggiare la sempre crescente domanda di alimenti nei paesi in via di sviluppo. Questa coltura ha la capacità di crescere in terreni poco fertili e con gradi di acidità considerevoli, richiedendo basse quantità di acqua, ed è per questo motivo che la sua importanza ampiamente riconosciuta soprattutto per gli ecosistemi fragili, o in cui non si riesce a fronteggiare il sempre crescente costo dei fertilizzanti. In più, le operazioni di raccolta e trattamenti post-raccolta danno lavoro a 500 milioni di persone nel mondo. Secondo i dati della FAO, nel 2020 sono state prodotte circa trecentomila tonnellate di manioca, il 64% delle quali in Africa, con la Nigeria come maggior produttore, seguita dalla Repubblica democratica del Congo e il Ghana. Un altro 27% arriva invece dall' Asia, soprattutto dalla Thailandia, mentre il restante 9% è quasi tutto allocato nell'America del Sud. Nonostante il ruolo da protagonista la che manioca gioca nell'approvvigionamento alimentare mondiale, la sua produzione, soprattutto in Africa, è ancora affidata a piccoli produttori che utilizzano metodi artigianali e tradizionali per il suo trattamento post-raccolta.

La manioca presenta tre limiti principali: il basso contenuto proteico, il rapido deterioramento post-raccolta e la tossicità di alcune varietà dovuta al contenuto di composti cianogeni. La shelf-life della radice dopo la raccolta va dalle 48 alle 72 ore, dopo le quali va incontro a due tipi di deterioramento: gli acidi cumarici si attivano a causa del danneggiamento del tessuto esterno della manioca dovuto alla raccolta, e ossidano la radice donandole un colore scuro e poco appetibile dal consumatore; in seguito, la degradazione microbica interviene a rendere il prodotto non più consumabile. Questo limite pregiudica fortemente le possibilità commerciali di questo prodotto, ed è dunque necessario cercare di arginarlo: coltivazione preferenziale di varietà a più lenta degradazione, refrigerazione e rivestimento con cere sono metodi che trovano largo impiego. Tuttavia, la disidratazione rimane il metodo più efficiente per diminuire il contenuto umido delle radici, inibendo così la crescita microbica, diminuire la quantità di composti cianogeni fino ad annullarne la tossicità per l'organismo umano, e ridurre il peso del prodotto facilitando così il suo trasporto.

I prodotti derivati ma manioca maggiormente creati in Africa sono farine, semole o paste fermentate. Il processo inizia con la raccolta delle radici e il trasporto nell'unità di trasformazione dove, se necessario, inizia la fermentazione (radici intere in acqua, o dopo sminuzzamento all'interno di involucri specifici). Se non viene condotta la fermentazione le radici vengono pelate (manualmente o meccanicamente), lavate e poi macinate, ottenendo così una polpa. I passaggi successivi sono quelli di disidratazione meccanica e termica, a seguito delle quali una seconda macinazione del prodotto porta alla farina. Come visibile in Figure 1, alcuni di questi step possono essere bypassati se le radici hanno un basso quantitativo di composti al cianuro.

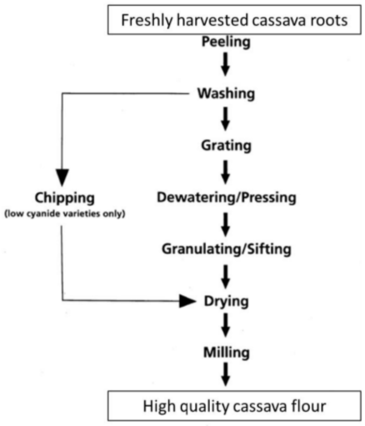

*Figure 1 Schema degli step principali per la produzione di farine da manioca non fermentata*

Fra le varie fasi di lavorazione, quella che richiede un maggior dispendio energetico è quella di disidratazione termica. Per questo motivo, in un'ottica di industrializzazione del processo produttivo che porta alle farine di manioca, è importante studiare i processi meccanici di dewatering antecedenti l'essiccazione, in quanto giocano un ruolo chiave nel consumo energetico di quest'ultimo. Le principali operazioni che possono essere eseguite in questo senso sono: centrifugazione, filtrazione sottovuoto e compressione. L'analisi e la modellazione di questi trattamenti sono importanti al fine del loro efficientamento e sono stati trattati da Chiadò Rana[1] nel suo lavoro di tesi.

L'essiccazione della manioca, al giorno d'oggi in Africa è condotta principalmente al sole, con tempi dipendenti dalle condizioni atmosferiche esterne, e che possono andare dai 7 ai 14 giorni. Questo procedimento può portare allo sviluppo di micotossine sui prodotti, che non saranno più consumabili e rappresenteranno uno scarto. Si rende necessario quindi velocizzare l'essiccazione ed incrementare la qualità del prodotto finito, rendendo quest'ultima indipendente dalle condizioni atmosferiche. A questo proposito possono essere utilizzati diversi essiccatori comunemente impiegati nell'essiccazione di alimenti: forni, cabinet dryers, essiccatori a tamburo o flash. Molti di questi processi di essiccazione artificiale prevedono la convezione di una corrente di aria calda sul prodotto, il modo tale da provocare l'evaporazione dell'acqua dalla superficie, creando allo stesso tempo un gradiente di concentrazione fra quest'ultima e il bulk del prodotto, inducendo quindi la diffusione del contenuto umido interno. Di conseguenza, la progettazione di un essiccatore efficiente passa dalla caratterizzazione e dalla modellazione del comportamento della manioca durante questo tipo di disidratazione.

Il focus del presente lavoro è quello di analizzare il comportamento a drying di diversi prodotti derivanti da manioca, rappresentativi di diversi gradi di lavorazione effettuati sul prodotto: manioca grezza, polpa di manioca ottenuta macinando le radici, e polvere di manioca ottenuta pressando meccanicamente la polpa. L'essiccazione è stata condotta in apparecchiature pilota dove le caratteristiche dell'aria per quanto riguarda temperatura, umidità relativa, velocità e direzione del flusso potevano essere impostate dall'utente. Il comportamento a disidratazione dei vari prodotti è stato analizzato a temperature dai 40°C agli 80°C, con umidità relative dagli 8% al 21% e velocità da 0.7 a 1.8 m/s. L'analisi è stata estesa a due tipi di essiccazione*: parallel flow drying*, in cui l'aria incontra il prodotto lateralmente, e *cross flow drying* dove invece l'aria attraversa il prodotto perpendicolarmente.

Successivamente si è passati alla parte di modellazione, per la quale è stato utilizzato il modello di Lambert et al. [2]. Gli scambi di materia ed energia considerati sono sia superficiali (convezione) che interni (diffusione), e le equazioni alla base del modello sono concepite per tenere conto di diverse geometrie: cilindro, sfera e lastra. Il prodotto è trattato come un "thin layer" dal momento che le caratteristiche dell'aria nell' attraversare il prodotto rimangono pressocché invariate. Al fine di applicare il modello al caso della manioca è stato necessario reperire le proprietà strutturali e termo-idriche del nostro prodotto. Al fine di fare ciò, una combinazione di ricerca bibliografica, misure dirette e utilizzo di algoritmi di minimizzazione dello scarto si sono resi necessari. Quest'ultima tecnica è stata utilizzata per l'identificazione del coefficiente di diffusione sulla base dei risultati sperimentali, dal momento che i dati di letteratura fornivano un intervallo troppo ampio di valori per trattarsi dello stesso medium, e una scelta di un valore rispetto ad un altro si sarebbe rivelata priva di fondamento.

# 2 Materiali e metodi

Il lavoro presentato è diviso in due parti: una riguardante l'analisi sperimentale del comportamento a drying di prodotti derivanti da manioca, e una riguardante la modellazione di questo processo.

## 2.1 Analisi sperimentale del comportamento a drying di prodotti derivanti da manioca

L'analisi ha previsto, a valle della produzione dei vari campioni, una loro caratterizzazione a livello geometrico e strutturale, prima e dopo averli sottoposti al processo di disidratazione in essiccatori convettivi in scala pilota. Nelle sottosezioni seguenti, una descrizione dei metodi di ottenimento dei prodotti, delle apparecchiature impiegate per il loro essiccamento e della procedura utilizzata.

### 2.1.1 Ottenimento dei prodotti

Per la parte sperimentale è stata acquistata, in una sola volta, una quantità di manioca sufficiente a condurre tutti gli esperimenti, in modo da non avere discrepanze per quanto riguarda le varietà e i vari livelli di maturazione. Questo ha portato alla necessità di uno stoccaggio che non pregiudichi la qualità dei campioni e non modifichi il loro comportamento a drying. Il metodo migliore si è rivelato essere un rapido congelamento a -25°C che favorisca la nucleazione dei cristalli rispetto al loro accrescimento, e una conservazione a -15°C fino al momento dell'utilizzo, in cui i campioni sono poi scongelati in un bagno termico a 30°C. Una verifica sperimentale ha poi confermato la trascurabilità degli effetti di questo tipo di stoccaggio sul comportamento a drying dei prodotti.

Dei cilindri di manioca (Figure 2) sono stati ottenuti direttamente dalla radice per mezzo di un coltello circolare. Le dimensioni dei cilindri sono di 17 mm e 50 mm rispettivamente per il diametro e l'altezza, misurati con rilevamento diretto per mezzo di un calibro. Una verifica sperimentale dell'influenza della lunghezza dei cilindri sul comportamento a drying è stata effettuata ai fini della modellazione, ed ha rivelato che le dimensioni sono tali da essere approssimate con sufficiente precisione a quelle di cilindro di lunghezza infinita, nonché la maggior tendenza dei meccanismi diffusivi a svilupparsi radialmente piuttosto che longitudinalmente.

*Figure 2 Cilindri di manioca grezza*

*Figure 3 a) Polpa di manioca b) Polvere di manioca*

Macinando dei pezzi di radice di manioca, privata della corteccia, all'interno di un "Magimix" si ottiene una polpa (Figure 3a), che quando viene pressata meccanicamente all'interno di una pressa a pistone perde parte del suo contenuto umido, trasformandosi nella polvere visibile in Figure 3b, un prodotto simile a quello che viene effettivamente essiccato in Africa per la produzione di farina. Inoltre, a fini di un analisi comparativa dell'effetto dei diversi gradi di processamento della manioca sull'essiccazione, si è proceduto ad uniformare le geometria, formando dei cilindri, delle stesse dimensioni di quelli ottenuti con cassava grezza, anche con la polpa (Figure 4a) e con la polvere. Questi ultimi sono stati prodotti a due diverse porosità (Figure 4b minore porosità, Figure 4c maggiore porosità).

*Figure 4 a) cilindri di polpa di manioca b) cilindri di polvere di manioca a minore porosità c) cilindri di polvere di manioca a più elevata porosità*

### 2.1.2 Procedura

Prima di sottoporre i vari prodotti a disidratazione, viene misurato il loro contenuto umido prelevandone un campione e mantenendolo ad una temperatura di 100°C per 24 ore. Lo stesso viene fatto a valle dell'operazione di essiccamento. In Table 1 dei valori medi di contenuto umido per i diversi prodotti, e la deviazione standard rilevata fra i diversi esperimenti.

*Table 1 Contenuto umido iniziale e finale dei diversi prodotti derivati da manioca*

| **Prodotto** | **$X_0$ (d.b.)** | **Dev_std su $X_0$** | **$X_f$ (d.b.)** | **Dev_std su $X_f$** |
|---|---|---|---|---|
| Cilindri grezzi | 1.465 | 0.0199 | 0.0672 | 0.025 |
| Polpa | 1.5 | / | 0.0395 | / |
| Polvere | 0.760 | 0.0085 | 0.046 | 0.0166 |

L'operazione di drying è quindi condotta su apparecchiature pilota per convezione di una corrente di aria calda. Durante l'operazione, si esegue la pesatura dei prodotti ad intervalli irregolari, determinati dall'utente a seconda dalla velocità di essicamento dell'alimento, non costante nel tempo. Ipotizzando che la perdita di peso sia interamente dovuta alla perdita d'acqua da parte dell'alimento (ipotesi verificata a valle con un bilancio di materia), i valori di peso e di contenuto umido iniziale permettono quindi di ottenere delle curve di drying ($X$ vs $t$) e di drying rate ($dX/dt$ vs $X$).

Gli esperimenti sono condotti in cross flow o in parallel flow, con temperature per l'aria di 40°C, 60°C o 80°C alle quali corrisponde un'umidità relativa del 21% nel primo caso e dell'8% negli altri due. Per la maggior parte degli esperimenti, la velocità dell'aria è impostata su un valore di circa 1.8 m/s. Tuttavia, valori di velocità più bassi sono stati altresì esplorati impiegando un secondo essiccatore pilota sul quale la velocità dell'aria era più facilmente modulabile. Quando possibile, si è cercato di assicurare un certo numero di ripetizioni dello stesso esperimento, al fine di assicurarne una buona ripetibilità e di validare dunque la procedura seguita.

### 2.1.3 Essiccatori pilota

L'apparecchiatura maggiormente utilizzata durante la fase sperimentale è stata il loop dryer (Figure 5) dei laboratori di CIRAD.

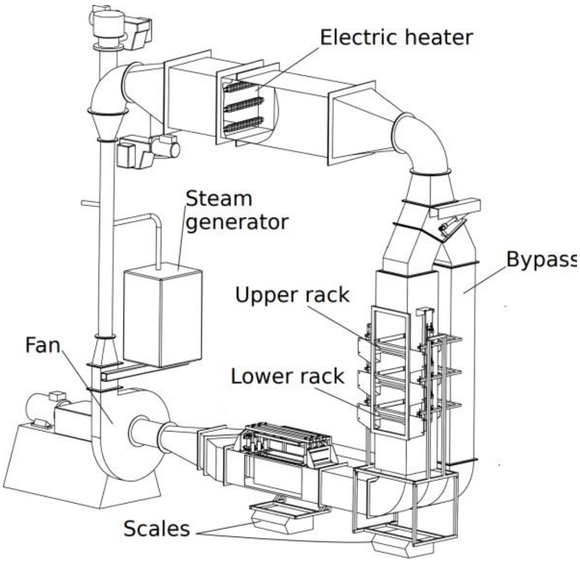

*Figure 5 Schema compositivo del loop dryer di CIRAD*

L’essiccatore si compone di due camere: una nella quale il flusso d’aria incontra perpendicolarmente il prodotto (con tre vassoi per i prodotti da essiccare) e una in cui l’aria arriva lateralmente. Il fluido è movimentato grazie ad una ventola la cui frequenza di rotazione è controllabile dall’utente. Altri parametri controllabili sono la temperatura dell’aria (per mezzo dell’heater elettrico) e la sua umidità relativa (per mezzo dell’evaporatore). L’operazione di record del peso durante l’operazione avviene automaticamente ad intervalli impostati dall’utente, e prevede che l’aria venga fatta passare nel circuito di bypass durante la pesata. I risultati sono poi registrati all’interno di un semplice file di testo e sono messi a disposizione dell’utente per l’elaborazione.

Il limite principale di questa apparecchiatura si è dimostrato essere il valore minimo di velocità raggiungibile per l’aria: non era possibile, infatti, impostare valori inferiori a 1.8 m/s. Inoltre, data l’assenza di un condensatore, non tutti i valori di umidità relativa sono ottenibili, relativamente alla temperatura utilizzata. Infine, non è possibile operare il macchinario a temperature inferiori a 40°C. Al fine di investigare valori più bassi di velocità del fluido, degli esperimenti sono stati condotti su un secondo essiccatore presente dei laboratori A.T.A: questa apparecchiatura, seppur necessitava di pesare manualmente i prodotti durante il procedimento, consentiva di modulare la velocità del fluido fino ad un valore minimo di 0.7 m/s. Entrambe le apparecchiature consentivano una verifica delle caratteristiche dell’aria mediante sensori esterni, disponendo di accessi in punti strategici. I dettagli di tale verifica sono oggetto dell’Annex 1.

### 2.1.4 Caratterizzazione geometrica e strutturale del prodotto

Come anticipato, una caratterizzazione geometrica e strutturale dei prodotti è stata condotta, in particolare per quanto riguarda la misura di densità e porosità al picnometro, la granulometria effettuata sulla polvere di manioca, e la valutazione dello stringimento a cui sono soggetti i prodotti durante asciugatura. Quest’ultimo sarà poi utile in fase di modellazione per scegliere il modello più adeguato a descrivere il comportamento della manioca a drying.

#### *2.1.4.1 Misura di densità e porosità dei prodotti*

Allo scopo di misurare densità e porosità dei prodotti, è stato impiegato un picnometro a elio, la cui procedura di impiego ha previsto le seguenti fasi:

1. Una certa quantità di prodotto è inserita, dopo pesatura, in un recipiente di volume noto
2. Il recipiente è chiuso ermeticamente e riempito con una quantità nota di elio
3. Viene misurata la pressione del gas nella camera

4. Dalla legge dei gas perfetti si ricava il volume occupato dal gas, corrispondente al volume che non è occupato dal prodotto e dai pori dello stesso con un diametro inferiore a quello delle molecole di elio ($d_{He}$ = 256 · $10^{-12}$ m)
5. Per sottrazione si ottiene quindi il volume del campione, che risulta essere una somma di diversi contributi: $V_{sample} = V_{dry\ matter} + V_{water} + V_{pore<dHe}$.
   Per dedurre un valore della porosità che includa i pori più piccoli, è necessario calcolare il volume occupato dalla materia secca: si macina quindi finemente il prodotto al fine di ottenere uno strato in cui la porosità possa ritenersi nulla, e si ripete la procedura. Il volume occupato dall'acqua è facilmente dedotto dalla conoscenza del contenuto umido iniziale e del valore di densità dell'acqua.

I valori di densità e porosità così ottenuti sono riassunti in Table 2

*Table 2 Valori di densità e porosità prodotti misurati al picnometro*

| Prodotto | Densità | Porosità |
|---|---|---|
| Polvere rimacinata | 1479 +/- 8 [kg/m$^3$] | 0% |
| Cilindri di manioca grezza | 1090 +/- 17 [kg/m$^3$] | 43% |
| Polvere di manioca | 1300 +/- 12 [kg/m$^3$] | 72% |

Tali risultati, seppur leggermente inferiori sono in accordo con quanto rilevato da Escobar et al. (1565 kg/m$^3$ per la polvere rimacinata).

### *2.1.4.2 Particle size distribution*

Al fine di effettuare una caratterizzazione geometrica della polvere, sono stati combinati due tipi di granulometria, una condotta attraverso vassoi agitati in serie, disposti di griglie con luci di passaggio via via decrescenti, e l'altra condotta sulle particelle più grandi (quelle che rimangono sulla griglia a maglie più larghe) mediante analisi d'immagine. L'operazione è stata condotta sulla polvere secca così da effettuare una granulometria che non sciogliesse gli agglomerati, come invece succede se viene effettuata in aspersione d'acqua sulla polvere umida, e che risultasse quindi essere più rappresentativa delle condizioni reali.

Nel primo tipo di granulometria, la dimensione caratteristica delle particelle si è assunto essere intermedia fra la luce di passaggio della griglia antecedente e quella sulla quale la particella si è effettivamente fermata. È chiaro come, per le particelle nel primo vassoio, questo non sia possibile, ed è necessario l'intervento dell'analisi d'immagine per tenere conto dell'eterogeneità delle loro dimensioni. Quest'ultima tecnica sfrutta la capacità del software ImageJ di calcolare la superficie e il perimetro delle particelle a partire da una foto: la dimensione caratteristica corrisponderà quindi al diametro di una sfera avente area superficiale uguale a quella rilevata per le particelle. La combinazione di queste due tecniche porta all'ottenimento delle seguenti curve di distribuzione granulometrica e di frequenza cumulata rispetto al diametro delle particelle, rispettivamente in Figure 6 e Figure 7. Il diametro medio il $d_{50}$ risultano essere rispettivamente 1.639 mm e 0.589 mm.

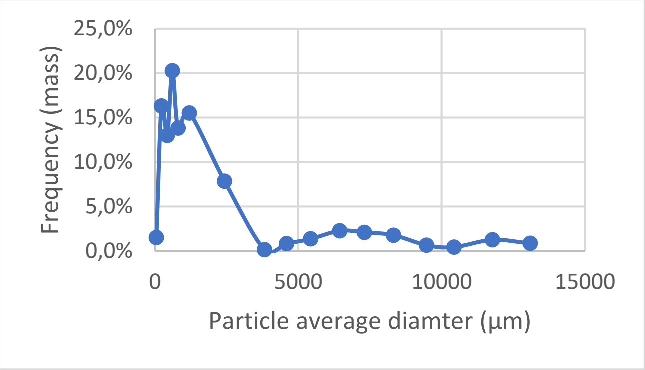

*Figure 6 Distribuzione granulometrica sulla polvere secca*

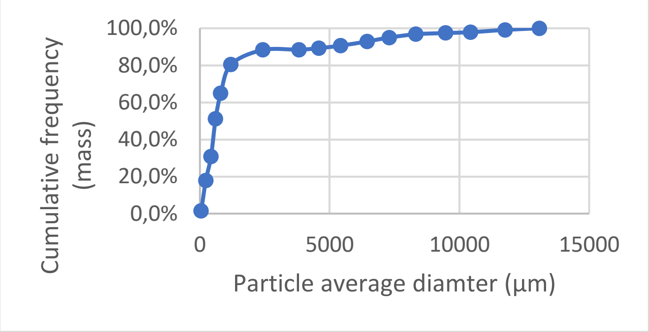

*Figure 7 Frequenza cumulata rispetto al diametro medio delle particelle per la polvere secca*

#### 2.1.4.3 Valutazione dello stringimento

Una misura delle dimensioni a monte e a valle dell'essiccazione è stata effettuata sui diversi prodotti. Una misura diretta di lunghezza e diametro è stata possibile solo per i cilindri, per mezzo di un calibro. La leggera deformazione della forma cilindrica a valle dell'essiccamento ha renso necessaria la misura del diametro attraverso la variazione di volume di una quantità nota di olio in un cilindro graduato; la lunghezza era ancora misurabile con buona approssimazione per mezzo del calibro. In Table 3 i risultati delle misure di stringimento su cilindri.

*Table 3 Dimensioni e stringimento dei cilindri di manioca grezza*

| Dimensione | Before drying | After drying | Stringimento |
|---|---|---|---|
| Diametro | 16,96 [mm] | 13,288 [mm] | 21,65 % |
| Lunghezza | 49,94 [mm] | 38,38 [mm] | 23,14 % |
| Volume | 45111,4 [mm$^3$] | 21279,8 [mm$^3$] | 52,82 % |

Una misura indiretta dello spessore dello strato di polvere è stata ottenuta invece riproducendo in piccola scala, in un recipiente di volume noto, la disposizione della polvere nel vassoio dell'essiccatore, e attraverso una proporzione si è ottenuta una stima dello spessore medio in condizioni reali. Uno stringimento medio dello strato di prodotto del 14.55% è stato rilevato in questo modo.

Si potrebbe teoricamente valutare lo stringimento delle singole particelle attraverso la granulometria. Tuttavia, l'elevato contenuto umido iniziale della polvere, rende necessario effettuare la granulometria in aspersione d'acqua, che non offre risultati comparabili con la granulometria condotta sul prodotto secco.

## 2.2 Modello di disidratazione della manioca

### 2.2.1 Numeri di Biot e meccanismi controllanti

I meccanismi di scambio di materia ed energia che concorrono alla disidratazione degli alimenti sottoposti ad una corrente di aria calda sono principalmente di due tipi: superficiali, ossia l'evaporazione dell'acqua sulla superficie del prodotto, o interni, ossia la diffusione dell'acqua dal bulk del prodotto verso la superficie. La valutazione dei numeri di Biot termico e di materia è utile a capire se ci sono meccanismi controllanti:

$$Bi_{th} = \frac{h \cdot L_c}{\lambda_a}$$

Dove $h$ $(\frac{W}{m^2 \cdot K})$ è il coefficiente di convezione, $Lc$ (m) la lunghezza caratteristica e $\lambda_a$ $\left(\frac{W}{m \cdot K}\right)$ la conduttività termica.

$$Bi_{mat} = \frac{D_{eff} \cdot L_c}{k_{mat}}$$

Dove $D_{eff}$ è il coefficient di diffusione effettivo $\left(\frac{m^2}{s}\right)$ $k_{mat}$ $\left(\frac{m}{s}\right)$ è il coefficiente di trasferimento di materia.

È importante notare che il coefficiente $h$ è calcolato, nella maggior parte dei casi, mediante l'analogia di Chilton-Colbun:

$$h = \frac{Nu \cdot \lambda_a}{L_{eq}}$$

dove Nu è il numero di Nusselt e $L_{eq}$ è una lunghezza equivalente. Questo ha portato a calcolare un valore di $h$ per il caso dei cilindri di circa 93 $[\frac{W}{m^2 \cdot K}]$, e di circa 196 $[\frac{W}{m^2 \cdot K}]$ nel caso della polvere in cross flow drying. Nel caso della polvere in parallel flow è stato calcolato un valore di circa 17.72 $[\frac{W}{m^2 * K}]$.

*Table 4 Numeri di Biot termico e di materia per i diversi prodotti*

| | Polvere in cross flow | Cilindri | Polvere in parallel flow |
|---|---|---|---|
| **BI_th** | 0.236 | 1.378 | 0.164 |
| **Bi_mat** | 5.27E+03 | 6.29E+04 | 3.86E+04 |

Dai risultati possiamo notare come per il prodotto in polvere i fenomeni convettivi siano controllanti rispetto a quelli conduttivi, dal momento che $Bi_{th} < 1$. Questo non è completamente applicabile al caso dei cilindri. $Bi_{mat} >> 100$ per tutti i prodotti significa che nel modello vanno considerati sia i meccanismi diffusivi che quelli convettivi

### 2.2.2. Il modello di drying

Il modello che utilizziamo è stato sviluppato da Lambert et al[2] e fa parte dei "*simplified white box models*" i quali prevedono la risoluzione di equazioni differenziali alle derivate parziali provenienti dallo sviluppo di bilanci che partono dalle leggi di Fick e di Fourier. Il termine "simplified" si riferisce al fatto che in questo caso le geometrie considerate sono ideali e gli scambi sono monodimensionali.

Il modello si basa sulle seguenti ipotesi:

1. Il prodotto ha proprietà uniformi e isotrope con trasferimento di calore e massa solo in direzione radiale.

2. Si assume una geometria ideale di cilindro infinito, lastra infinita o sfera: lo stringimento e il rigonfiamento sono considerati trascurabili.
3. Si trascura il trasferimento di calore per conduzione tra le particelle.
4. Si trascura il coefficiente di espansione termica
5. L'evaporazione avviene solo sulla superficie delle particelle, così come la convezione di massa e di calore.
6. La conduzione del calore e la diffusione dell'acqua liquida avvengono invece all'interno della particella.

Il modello è stato sviluppato sia per l'essiccazione “Thin layer” che per quella “Deep bed”, dove quest'ultima è vista come una successione di “Thin layers” in cui si verificano fenomeni di trasferimento tra aria e prodotto dopo ogni strato. In questo caso, sono necessari bilanci di calore e di massa per l'aria dopo ogni strato attraversato. Nel nostro caso, consideriamo solo il comportamento “Thin layer”, poiché le proprietà dell'aria che attraversa il prodotto nell'essiccatore non sembrano essere modificate.

Dalle leggi di Fick e di Fourier, i bilanci di materia ed energia portano alle seguenti equazioni:

$$\left(\frac{\partial X_t^{r,z}}{\partial t}\right) = \frac{1}{r^n}\frac{\partial}{\partial r}\left(r^n D_{eff}\frac{\partial X_t^{r,z}}{\partial r}\right)$$

$$\left(\frac{\partial Tp_t^{r,z}}{\partial t}\right) = \frac{1}{\rho_{dm}\left(Cp_{dm} + X_t^{r,z}Cp_w\right)r^n}\ \frac{\partial}{\partial r}\left(r^n\lambda_{eff}\frac{\partial Tp_t^{r,z}}{\partial r}\right)$$

Per risolvere tali equazioni abbiamo bisogno di condizioni al contorno:

1. Contenuto umido della particella ritenuto costante: $\left(\frac{\partial X_t^{0,z}}{\partial r}\right) = 0$
2. Temperatura uniforme nella particella: $\left(\frac{\partial Tp_t^{0,z}}{\partial r}\right) = 0$
3. $\rho_{dm}\left(\frac{\partial X_t^{R,z}}{\partial r}\right) = \dot{m} = k\frac{M_w}{R}\left(\frac{a_w P_v^{sat}\left(Tp_t^{R,Z}\right)}{Tp_t^{R,z}} - \frac{RHPv^{sat}(Ta_t^z)}{Ta_t^z}\right)$
4. $\lambda_{eff}\left(\frac{\partial Tp_t^{R,z}}{\partial r}\right) = h\left(Tp_t^{R,z} - Ta_t^z\right) - \dot{m}\,\Delta H_v\left(Tp_t^{R,z}\right)$

Nelle equazioni, *Tp* è la temperatura del prodotto, *X* il suo contenuto d’acqua, $M_w$ è la massa molare dell’acqua, *Ta* è la temperatura dell’aria, $\Delta H_v$ è il calore latente di evaporazione dell’acqua $\left({}^{J}/_{Kg}\right)$, $a_w$ è l’attività dell’acqua e RH l’umidità relativa dell’aria.

Tali equazioni sono risolte numericamente mediante il metodo dei volumi finti.

### 2.2.3 Stima delle proprietà termo-idriche della manioca

Alcune proprietà termo-idriche della manioca sono essenziali all’applicazione del modello, e molte di queste sono dipendenti da variabili di stato come temperatura e composizione. Per la quasi totalità di queste proprietà, una revisione della letteratura è stata sufficiente per ricavare dei valori affidabili dei vari coefficienti. Questo non si è dimostrato vero per il coefficiente di diffusione, per il quale si è resa necessaria una procedura di identificazione parametrica.

#### *2.2.3.1 Capacità termica*

La maggior parte della letteratura trascura la dipendenza della capacità termica dalla temperatura, ma mantiene quella dalla composizione. Choi et al. hanno sviluppato la seguente equazione:

$$c_p = 4.180 \cdot X + 1.711 \cdot x_{protein} + 1.929 \cdot x_{fat} + 1.547 \cdot x_{carbohydrate} + 0.908 \cdot x_{ash}$$

Altri modelli generici e sono disponibili, così come misure di questa proprietà sulla manioca anidra condotte da Gevaudan et al., che hanno portato a scegliere un valore di 1.50 [kJ·kg$^{-1}$·K$^{-1}$] per il nostro prodotto. Questo valore può essere utilizzato con buona approssimazione per gran parte delle varietà di manioca.

### 2.2.3.2 Conducibilità termica

Anche nel caso nella conducibilità termica abbiamo delle equazioni generiche dipendenti dalla composizione, come quelle proposte da Okos e Sweat:

$$k = 0.628 \cdot X + 0.21 \cdot x_{protein} + 0.10 \cdot x_{fat} + 0.24 \cdot x_{carbohydrate} + 0.37 \cdot x_{ash}$$

$$k = 0.58 \cdot X + 0.155 \cdot x_{protein} + 0.16 \cdot x_{fat} + 0.25 \cdot x_{carbohydrate} + 0.135 \cdot x_{ash}$$

La conducibilità di calore non è facilmente misurabile su un mezzo poroso. Nonostante ciò, Gevaudan et al. ha utilizzato fonti di calore impulsive e continue per misurarla rispettivamente su polpa di manioca al 50% e al 52% di umidità w.b., a diverse porosità. La misura può essere approssimata in modo soddisfacente con il valore ricavato dalle equazioni generiche solo per i valori di porosità più bassi, altrimenti la differenza relativa è molto elevata. Njie[40] ha misurato la conduttività con la tecnica DSC, concludendo che il modello Sweat è in grado di prevedere bene il valore della conduttività termica solo al di sotto di un contenuto di umidità del 60% w.b. L'effetto delle differenze di composizione varietale è risultato trascurabile dall'applicazione delle due equazioni. La conduttività della manioca può essere confrontata con quella calcolata per i granuli di amido con una buona corrispondenza, secondo il lavoro di Drouzas et al [46], quando il contenuto di umidità è compreso tra 0 e 40%. A un contenuto di umidità molto basso si verificano modifiche nella densità e nella porosità, che portano a una forte diminuzione della conduttività.

Per ottenere un valore per k, di solito si distinguono due situazioni: se la conducibilità termica non ha una forte influenza, è accettabile un valore di k = 0,22 [W· m$^{-1}$· K$^{-1}$], se invece la conducibilità è rilevante, si può utilizzare il valore trovato per i granuli di amido da Drouzas et al. Nel nostro caso in base alla composizione si è scelto un valore di 0.4 [W· m$^{-1}$· K$^{-1}$].

### 2.2.3.3 Adsorbimento/Desorbimento

La stabilità del prodotto nelle procedure di essiccazione è fortemente legata all'attività dell'acqua e al comportamento del prodotto in adsorbimento/desorbimento. Per questo motivo, per la modellizzazione del processo di essiccazione della manioca è necessario definire anche l'isoterma di adsorbimento dell'acqua, in modo da avere una relazione tra il contenuto di umidità e l'attività dell'acqua nel prodotto all'equilibrio. Il lavoro di revisione della letteratura eseguito da parte di Van Der Werf et al. ha portato alle seguenti equazioni per la curva di adsorbimento/desorbimento e il relativo calore liberato durante il processo:

$$X = \left(\frac{\exp(-0.0142998 \cdot T_K)}{-\log(a_w)}\right)^{1/1.83388}$$

$$L_p = 7.0903 \cdot X^{-1.792} + L_v$$

Dove $L_v$ è il calore latente di evaporazione dell'acqua$\left(\frac{J}{kg}\right)$. In Figure 8 e Figure 9 le rappresentazioni delle suddette curve

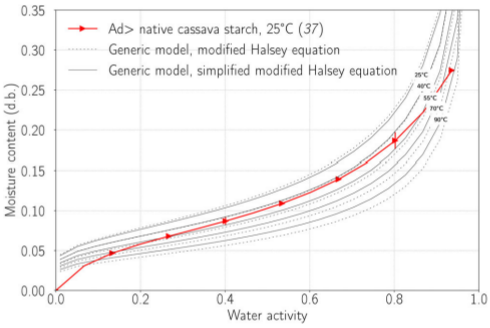

*Figure 8 Isoterma di adsorbimento/desorbimento per la manioca, dal lavoro di fitting eseguito da Van Der Werf et al.*

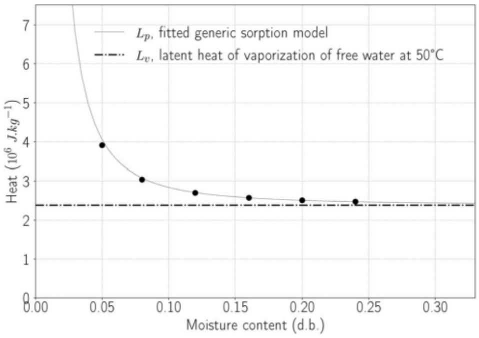

*Figure 9 Calore di adsorbimento della manioca comparata a quello di evaporazione dell'acqua libera*

### 2.2.3.4 Il coefficiente di diffusione

Il coefficiente di diffusione è una proprietà intrinseca del materiale, principalmente dipendente dalla sua struttura interna, dal contenuto umido e dalla temperatura. La pratica più comune per dedurre il coefficiente di diffusione non è la sua misura diretta, complicata a causa del gran numero di parametri da controllare, ma si basa su curve di drying sperimentali e la diffusività e dedotta attraverso la legge di Fick. In Table 5, i valori del coefficiente di diffusione trovati dai vari autori per diversi prodotti derivati da manioca.

*Table 5 Diffusività effettiva dell'acqua in diversi prodotti derivanti da manioca*

| **Prodotto** | **$D_{eff}$ ($m^2 \cdot s^{-1}$)** | **Initial moisture (% w.b.)** | **Air T (°C)** | **Drying equipment** | **Reference** |
|---|---|---|---|---|---|
| Farina di manioca | $1.74 \cdot 10^{-10}$ | 45 | 140 | Conductive rotatory dryer | Sanni et al. [22] |
| Gari | $4.51 \cdot 10^{-10}$ | 45 | 200 | Conductive rotatory dryer | Sanni et al. [22] |
| Manioca macinata e fermentata | $1.32–3.52 \cdot 10^{-9}$ | * | 115-230 | Bench rotatory dryer | Ademiluyi et al[41] |
| Chips di manioca | $2.43–4.52 \cdot 10^{-11}$ | 82 | 60-80 | Tunnel dryer | Stephen Ajala et al. [53] |
| Chips di manioca | $7.31-8.06 \cdot 10^{-7}$ | 13 | 60 | Hot air tray dryer | T.Tunde-Akintunde et al[54] |
| Chips di manioca | $3-30 \cdot 10^{-11}$ | ** | 55 | Convective tunnel dryer | Lopez-Ortiz et al. [55] |
| Pellets di manioca | $1.4-2.3 \cdot 10^{-9}$ | 76-78 | 66-81 | Convective tray dryer | Onyemazuwa et al.[56] |
| Chips di manioca | $1.57-2.15 \cdot 10^{-9}$ | ** | 40-70 | Cabinet dryer | Chavez-Méndez et al.[57] |

* Polpa di manioca pressata ad un contenuto umido w.b. del 45%

** Contenuto umido delle radici di cassava di circa 60-65% w.b.

Nonostante una certa discrepanza fra i vari valori sia attesa (ci aspettiamo che le scaglie o i pellet di manioca abbiano una diffusività diversa rispetto alla polpa di manioca gelatinizzata), il range di valori esplorato è troppo ampio per appartenere allo stesso medium, e osservando i risultati non si nota una precisa correlazione fra la struttura del materiale e il coefficiente di diffusione trovato. Una possibile ragione può essere attribuita alle diverse condizioni sperimentali delle apparecchiature di essiccazione, della temperatura dell'aria e del contenuto iniziale di umidità o, più probabilmente, ai diversi metodi di analisi.

Per questo motivo si è reso necessario utilizzare un algoritmo di identificazione parametrica basata sulle curve di drying ottenute nei vari esperimenti. I parametri identificati sono quelli dell'equazione dipendente dalla temperatura che definisce il coefficiente di diffusione:

$$D_{eff}(T) = a \cdot \exp\left(-\frac{b}{T_p}\right)$$

I parametri di tale equazione sono inizializzati ai seguenti valori validi per l'amido, il componente prevalente nella manioca:

$a = \ 5.321 \cdot 10^{-6}\ [m^2/s], b = 1.511\ [K]$

Quando implementato su Python, il metodo di Nelder-Mead minimizza lo scarto fra la curva sperimentale e quella simulata mediante il seguente parametro:

$$j = \frac{(X_{simu} - \ X_{exp})}{X_{exp} \cdot N_p}$$

dove $X_{simu}$ è il contenuto di umidità dei punti della curva simulate, $X_{exp}$ sono quelli della curva di essiccazione sperimentale, e $N_p$ è il numero di punti della curva sperimentale. La procedura si arresta quando una certa tolleranza sul valore di *j* è raggiunta oppure il numero massimo di iterazioni è stato ecceduto.

L'identificazione dei parametri dell'equazione è eseguita in prima battuta sulla base degli esperimenti condotti sui cilindri di manioca grezza, dal momento che la loro caratterizzazione geometrica è più facile e precisa, e sono poi applicati agli altri prodotti al fine di verificare il fitting della curva di essiccazione sperimentale con quella simulata che ne deriva. I valori ottenuti sono poi stati validati attraverso identificazione dei parametri condotta prima sulla base degli esperimenti sulla polvere, e poi su tutte le geometrie allo stesso tempo.

## 2.2.4 Data processing

### *2.2.4.1 Modellazione di una popolazione di particelle con un ampio range di dimensioni*

La polvere di manioca essiccata in parallelo è approssimabile come una placca di materiale poroso sottoposta ad una corrente di aria calda, mentre in cross flow come una popolazione di sfere indipendenti. In quest'ultimo caso, sono necessarie delle precisazioni riguardo al modo in cui sono state condotte le simulazioni.

Dalla granulometria abbiamo ottenuto diverse classi di particelle, ciascuna in un intervallo di dimensioni e caratterizzata da una frazione massica rispetto al totale. Quindi, le simulazioni venivano effettuate con ogni valore di dimensione delle particelle, ottenendo un insieme di curve di essiccazione simulate, ciascuna corrispondente a un raggio diverso per le particelle. La curva simulata finale sarà il risultato di una ponderazione delle varie curve, effettuata sulla base della loro frequenza, ossia la loro frazione in massa rispetto al totale. In questo modo la curva ottenuta si dimostra essere una migliore approssimazione delle condizioni reali rispetto all'uso del solo diametro medio o mediano. Nella Figure 10 un esempio di curva simulata (*D<sub>eff</sub>* ottimizzato) e sperimentale. Le varie curve grigie (sempre più scure al diminuire del raggio) visibili nell'immagine sono le cinetiche ottenute con ogni valore del diametro ottenuto dalla granulometria. La curva blu è quella finale, ottenuta con la tecnica appena descritta.

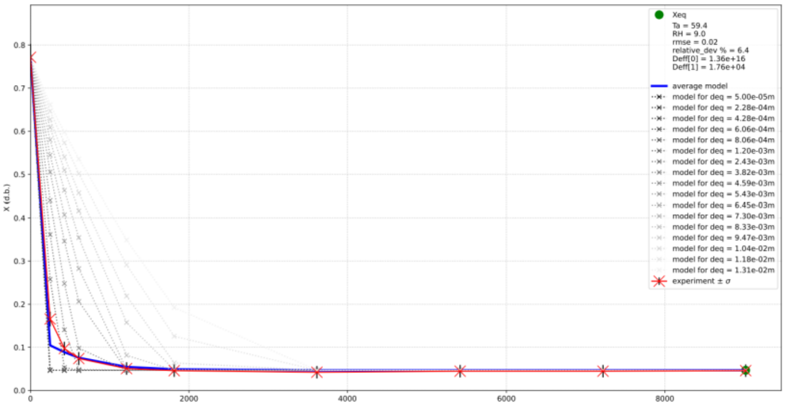

*Figure 10 Curva di essiccazione simulata ottenuta per ponderazione e somma delle cinetiche simulate con ogni raggio dalla granulometria*

# 3 Risultati e discussione

Nella presente sezione sono descritti i risultati ottenuti sia nella parte sperimentale (curve di drying e di drying rate), sia nella parte di modellazione (in particolare l'identificazione del coefficiente di diffusione). Sui vari esperimenti sono stati condotti test di ripetibilità che in tutti i casi hanno fornito esito positivo, validando la procedura impiegata e descritta nella sezione 2.1.2. Al fine di una migliore comprensione e di una lettura più scorrevole dei risultati che seguono, si specificano qui alcune peculiarità comuni:

- Ad una temperatura dell'aria di 40°C corrisponde sempre un'umidità relativa del 21%, mentre a 60°C e 80°C dell'8%. La velocità dell'aria, a meno che non sia diversamente specificato, si attesta su un valore di circa 1.8 m/s.
- I confronti riguardanti gli esperimenti con la polvere sono fatti sulla base di un egual spessore iniziale dello strato di prodotto, e non sulla base della quantità in grammi. Se non diversamente specificato, lo spessore medio iniziale dello strato è di 4 mm
- I risultati della parte sperimentale sono rappresentati da due curve: una curva di essiccazione ($X$ vs $t$) e una di velocità di essiccazione ($dX/dt$ vs $X$). Per quanto riguarda la prima, questa è ottenuta a partire dal valore di contenuto in acqua iniziale del prodotto, mentre quello finale misurato è mostrato in figura come verifica di quello calcolato. È altresì presente il valore di equilibrio ottenuto mediante le curve di adsorbimento.

## 3.1 Analisi del comportamento ad essiccazione dei prodotti derivanti da manioca

### 3.1.1 Polvere in cross flow

In Figure 11 una comparazione fra esperimenti di essiccazione della polvere di manioca in cross flow, condotti a diverse temperature (40°C curva rossa, 60°C curva blu e 80°C curva verde). L' aspetto delle curve mostra che la prima fase di essiccazione è assente, quindi in queste prove non è visibile alcuna fase di "warm up". Al contrario, si riscontra una rapida diminuzione iniziale del contenuto di umidità in tutte le condizioni, sebbene sia più rilevante con l'aumento della temperatura dell'aria. La velocità, nel grefico di destra, ha un andamento decrescente con diverse pendenze: l'essiccazione del prodotto è inizialmente molto veloce quando il meccanismo convettivo è più rilevante, per poi diminuire a valori più bassi di umidità dove la diffusione è invece il fenomeno limitante. La ragione di questa evidenza è la limitazione imposta alla diffusione dalla struttura dell'alimento e la diminuzione del gradiente di concentrazione interno durante l'asciugatura.

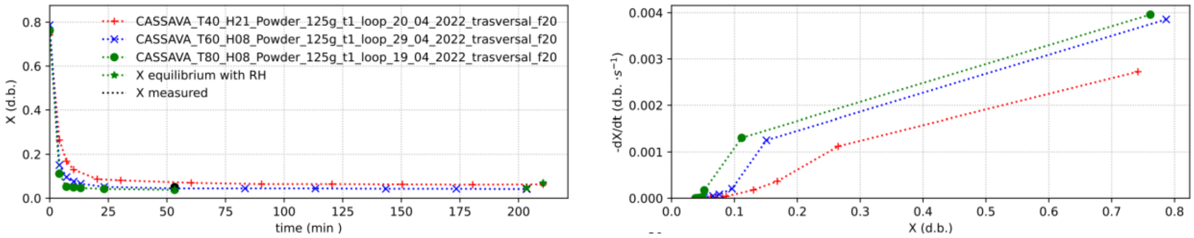

*Figure 11 Confronto tra le cinetiche sulla polvere nell'essiccazione a flusso trasversale in diverse condizioni d'aria: T=40 HR=21% (curva rossa),T=60 HR=8% (curva blu),T=80 HR=8% (curva verde)*

### 3.1.2 Cilindri in cross flow

In Figure 12 una comparazione fra esperimenti di essiccazione dei cilindri di manioca grezza in cross flow, condotti a diverse temperature (40°C curva verde, 60°C curva blu e 80°C curva rossa). La cinetica di essiccazione è molto più lenta rispetto al caso della polvere e la fase di " warm-up" è qui visibile, soprattutto nel grafico della velocità di essiccazione, in cui l'andamento decrescente con diverse pendenze già visto per la polvere, è ora preceduto da un trend crescente e poi circa costante.

I cilindri espongono al flusso di aria calda una superficie minore rispetto alla polvere e la distanza che l'umidità deve percorrere diffondendo dal bulk verso la superficie, dove viene rimossa per convezione, è maggiore. Questo spiega la differenza nel tempo necessario al contenuto umido per raggiungere un valore di equilibrio e dà ragione del fatto che la velocità di essiccazione è di un ordine di grandezza inferiore a quella che caratterizza il prodotto macinato e pressato.

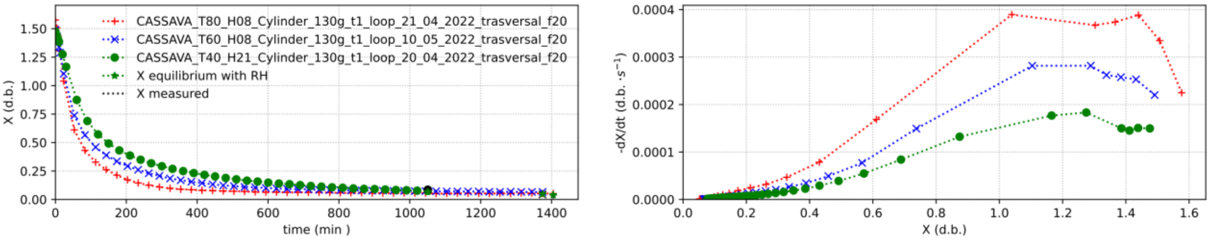

*Figure 12 Confronto tra le cinetiche sui cilindri di manioca cruda nell'essiccazione a flusso trasversale in diverse condizioni d'aria: T=40 HR=21% (curva verde), T=60 HR=8% (curva blu), T=80 HR=8% (curva rossa)*

### 3.1.3 Cilindri di polpa e polvere di cassava in cross flow

In Figure 13 si può vedere un confronto fra le curve ottenute su cilindri di manioca grezza (curva rossa), di polpa (curva blu), e di polvere (curva verde per i cilindri a più elevata porosità e grigia per quelli meno porosi). Il risultato interessante del confronto mostrato nel grafico di sinistra della Figure 13 consiste nel fatto che quasi nessuna differenza è rilevabile tra le curve di essiccazione. Quindi, i vari livelli di lavorazione sembrano avere un'influenza trascurabile sulla forma della curva. Inoltre, anche l'effetto della porosità sembra essere trascurabile, in quanto le curve di drying rate si sovrappongono per la maggior parte del processo di essiccazione. Non ci sono ragioni chiare alla base di questa evidenza, che sembra suggerire che la struttura cellulare dei prodotti abbia una scarsa influenza sul comportamento dei prodotti di manioca in disidratazione e, di conseguenza, sulla diffusività dell'acqua. Tuttavia, è possibile formulare alcune ipotesi. Il diverso livello di lavorazione, passando dalla radice alla polpa e poi alla polvere, modifica la struttura interna delle fibre e delle cellule del prodotto. Anche il contenuto di umidità iniziale varia tra i vari prodotti, con un effetto, anche se minore, sui meccanismi di trasferimento dell'umidità interna. L'evaporazione dell'acqua in superficie dipende invece dalle condizioni dell'aria che si avvicina alla superficie e dalla superficie stessa. Il contenitore esterno utilizzato sui cilindri di povere altamente porosi e su quelli realizzati con la polpa influenza il flusso dell'aria, che deve passare attraverso la griglia dell'oggetto prima di raggiungere il prodotto: la sezione di passaggio cambia e la velocità varia insieme a una variazione dell'aerodinamica nei pressi dei cilindri. Una combinazione di questi e altri fattori può essere ipotizzata come possibile causa dei risultati ottenuti.

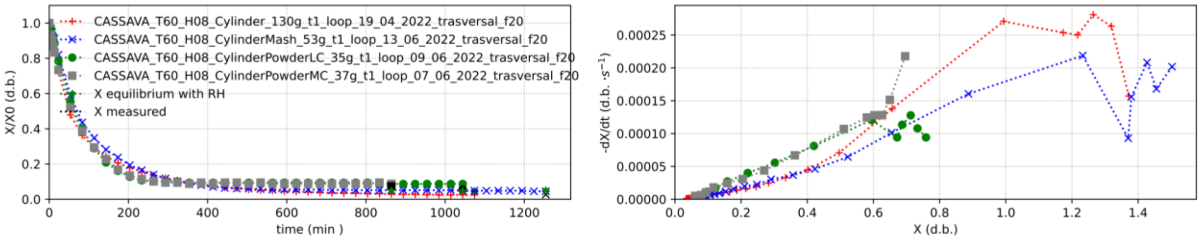

*Figure 13 Confronto tra tutti i prodotti cilindrici: curva rossa per i cilindri grezzi, curva blu per quelli realizzati con la polpa, curva verde per i cilindri realizzati con polveri ad alta porosità, curva grigia per quelli realizzati con polveri a bassa porosità*

### 3.1.4 Polvere in parallel flow

In Figure 14 una comparazione fra esperimenti di essiccazione della polvere di manioca in parallel flow, condotti a diverse temperature (40°C curva blu, 60°C curva verde e 80°C curva rossa). In Figure 15 vediamo invece un confronto fra le curve di essiccamento e di velocità di essiccamento fra la polvere in cross flow (curva rossa) e in parallel flow (curva blu) drying a 60°C. Ciò che salta all'occhio è la grande differenza tra i due metodi in termini di velocità di asciugatura. Nei grafici di destra, dove *dX⁄dt* è tracciato rispetto al contenuto di umidità su base secca, si calcola una differenza di circa un ordine di grandezza tra i tassi di essiccazione in modalità laterale e trasversale. Ciò si riflette anche nel grafico di sinistra, dove si può notare che il tempo necessario al contenuto di umidità per raggiungere il valore di equilibrio nelle prove in flusso trasversale, anche se è leggermente diverso a seconda della temperatura della prova, rimane di gran lunga inferiore rispetto a quello necessario nell'essiccazione laterale. La superficie esposta direttamente al flusso d'aria è maggiore nel caso del flusso trasversale e ciò consente un'evaporazione più rapida sulla superficie: ciò è visibile nella parte iniziale delle curve di essiccazione, fase guidata dai meccanismi convettivi, con una pendenza molto ripida. In questo caso, infatti, l'aria è costretta ad attraversare lo strato di polvere, le cui particelle sono quindi circondate dal gas caldo. Nel caso dell'essiccazione laterale, invece, l'aria lambisce le facce esterne dello strato, creando una sorta di percorso preferenziale che evita la caduta di pressione dovuta all'attraversamento, e quindi "girando" sostanzialmente intorno allo strato anziché attraversarlo. Pertanto, nel caso del flusso parallelo, la geometria del prodotto è meglio approssimata da una lastra porosa, rispetto alle sfere come nel caso del cross flow.

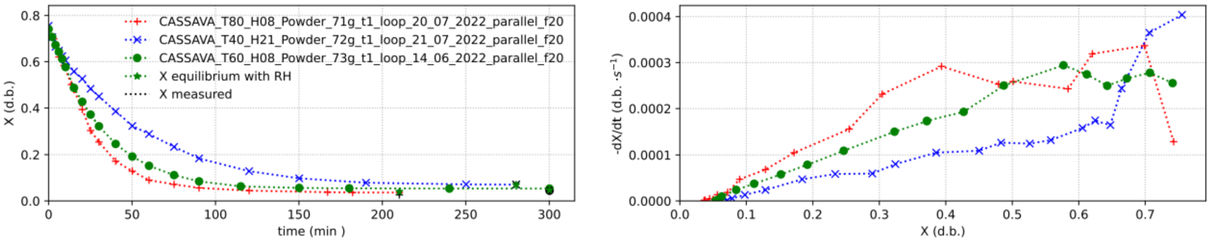

*Figure 14 Confronto tra le cinetiche sulla polvere di manioca nell'essiccazione a flusso parallelo in diverse condizioni d'aria: T=40 HR=21% (curva blu), T=60 HR=8% (curva verde), T=80 HR=8% (curva rossa)*

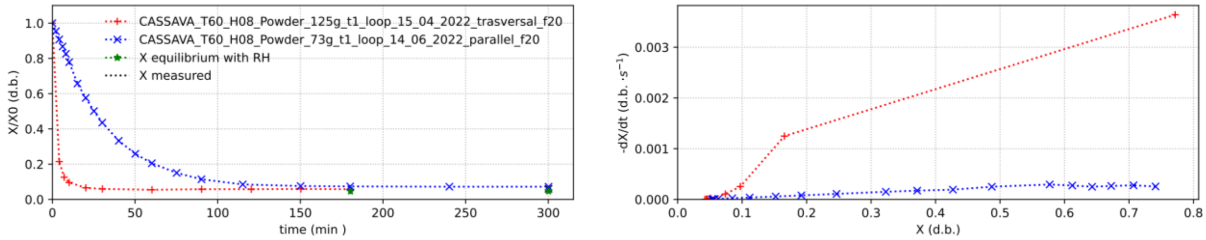

*Figure 15 Confronto della cinetica e del tasso di essiccazione tra parallel drying (curve rosse) e cross drying (curve blu) sulla polvere di manioca. T = 60°C HR = 8%*

### 3.1.5 Cilindri in parallel flow

In Figure 16 una comparazione fra esperimenti di essiccazione sui cilindri di manioca in parallel flow, condotti a diverse temperature (40°C curva verde, 60°C curva blu e 80°C curva rossa). La curva della velocità di essiccazione mostra in questo caso, soprattutto per le prove a 40 °C e 80 °C, un primo andamento crescente, seguito da uno quasi costante e da un'ultima parte decrescente. Ciò rispecchia la curva teorica completa di drying rate che comprende anche la fase di "warm-up". La parte costante della curva è rappresentativa della fase in cui l'evaporazione superficiale avviene con la stessa velocità necessaria all'umidità per raggiungere la superficie e "rabboccarla". La fase decrescente è solitamente legata al fatto che la diffusione è sempre più limitata dalle barriere fisiche e dalla diminuzione del gradiente di concentrazione. La curva di essiccazione ottenuta dall'esperimento a 60°C è più vicina a quella a 80°C rispetto a quella a 40°C nella prima parte, dove la convezione è il fenomeno limitante. In Figure 17 abbiamo invece un confronto fra i cilindri sottoposti ad essiccazione trasversale (curva rossa) e in parallelo (curva blu). Le differenze tra i due metodi di essiccazione sono meno pronunciate in questo caso. Infatti, non abbiamo rilevanti differenze per quanto riguarda la superficie esposta, e le discrepanze che si osservano tra i due metodi possono essere imputabili maggiormente all'aerodinamica all'interno delle due diverse camere di essiccazione trasversale e laterale.

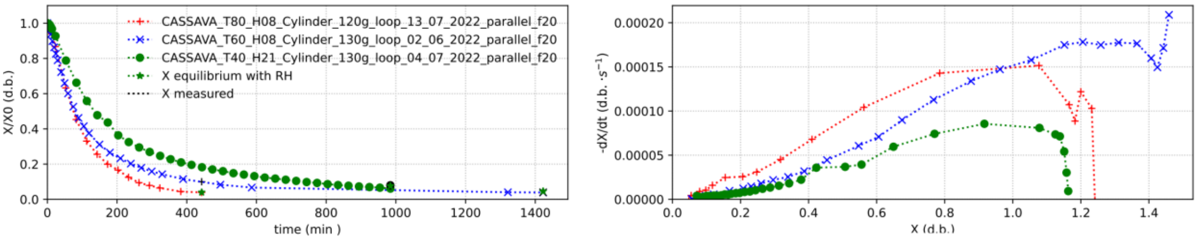

*Figure 16 Confronto delle cinetiche e delle velocità di essiccazione ottenuti da prove su cilindri di manioca cruda in essiccazione laterale. T = 40°C HR = 21% (curva verde), T = 60°C HR = 8% (curva blu), T = 80°C HR = 8% (curva rossa)*

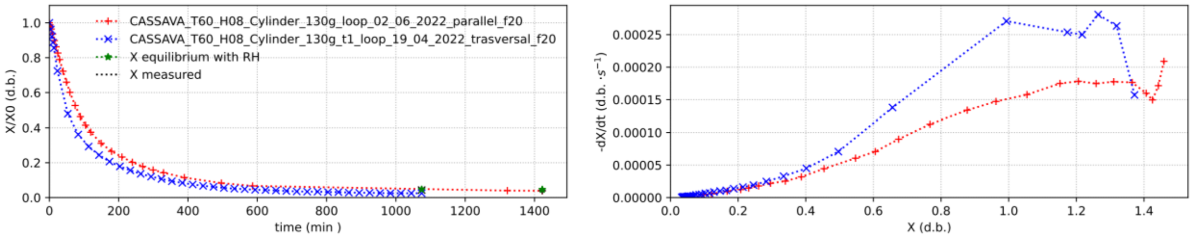

*Figure 17 Confronto di cinetica e di velocità tra l'essiccazione parallela (curve blu) e incrociata (curve rosse) su cilindri grezzi di manioca. T = 60°C HR = 8%*

## 3.2 Modellazione del drying di manioca

Come accennato nella sezione "Materiali e metodi", per applicare il modello è necessario definire meglio la diffusività, in quanto l'ampia gamma di valori per il coefficiente di diffusione trovati in letteratura non consente di fare affidamento su uno preciso per i nostri prodotti. Nelle sottosezioni successive saranno mostrati dei grafici dove le curve di essiccamento ottenute mediante gli esperimenti sono messe a confronto con le curve simulate. Le curve sperimentali sono rappresentate in rosso, e i loro punti mostrano una error bar la cui ampiezza rappresenta la deviazione standard fra i vari esperimenti condotti nelle stesse condizioni. Le curve simulate sono invece rappresentate in blu.

### 3.2.1 Identificazione parametrica – Cilindri

L'identificazione è stata condotta utilizzando tre curve sperimentali di essiccazione di cilindri di manioca grezza a tre diverse temperature in flusso incrociato.

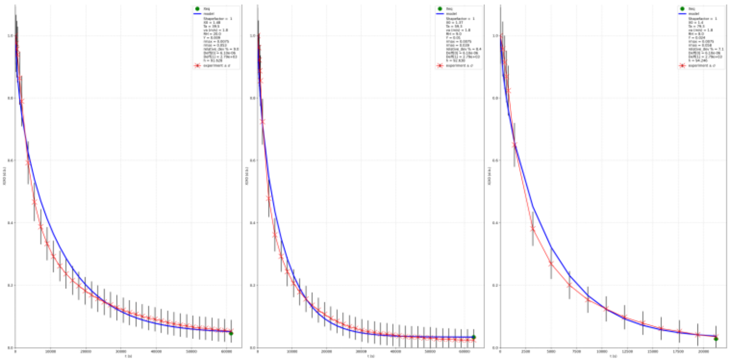

*Figure 18 Curva simulata e sperimentale per la cinetica dei cilindri di manioca grezza in flusso trasversale a (da sinistra a destra) 40°C, 60°C e 80°C*

I parametri identificati per l'equazione del coefficiente di diffusione sono:

$$a = 0.00610\ [m^2/s]\ ;\ b = 2790\ [K]$$

I valori esplorati per il coefficiente di diffusione vanno da $0.6 \cdot 10^{-9}$ a $2.2 \cdot 10^{-9}$ $\left[\frac{m^2}{s}\right]$.

I parametri identificati con i cilindri sono stati poi applicati alle curve di essiccazione della polvere in cross flow, per verificare se la corrispondente curva simulata è in grado di riprodurre in modo soddisfacente la curva sperimentale di essiccazione del prodotto sferico in cross flow. Nella Figure 19 abbiamo nove curve di essiccazione, disposte su tre livelli: sul primo livello abbiamo le tre curve di essiccazione disponibili a 40°C, sul secondo quelle a 60°C e sull'ultimo quelle a 80°C. Si nota subito che la curva simulata blu è una buona approssimazione di quella sperimentale in tutti i casi, con un range di deviazione relativa che va dal 12,6% al 14,7% per gli esperimenti a 40°C, dall'8,2% al 10,7% per quelli a 60°C e dal 6% al 15,3% per quelli a 80°C. In Figure 20 vediamo invece l'applicazione dei parametri ai casi dei cilindri di polpa e polvere, con un fitting che presenta un range di deviazione standard dagli 8.4% ai 12.8%. Infine, in Figure 21 abbiamo l'applicazione dei parametri ai trial condotti sulla polvere in parallel flow drying, simulata come una lastra di materiale poroso. Da sinistra a destra abbiamo esperimenti di drying condotti a 40°C, 60°C e 80°C, e in tutti e tre i casi la curva simulata approssima con una sufficiente accuratezza quella sperimentale, mostrando una deviazione standard che va dai 2.5 ai 7.2 punti percentuali.

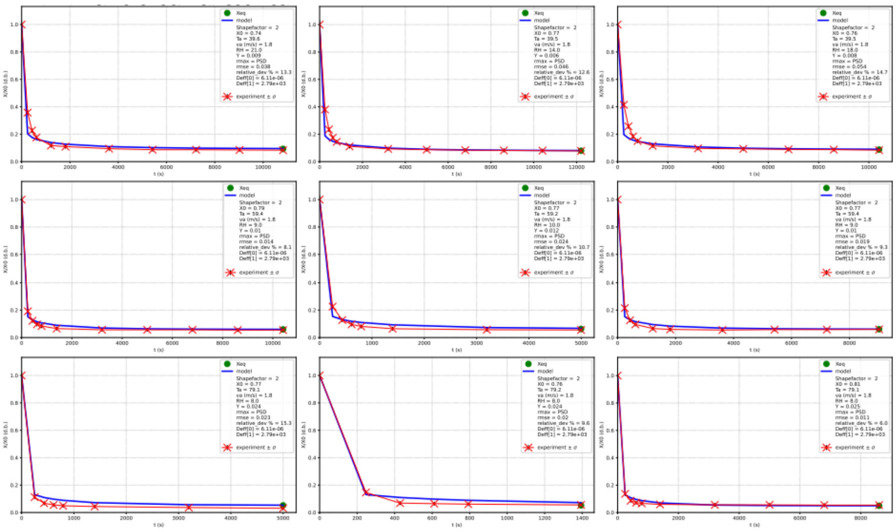

*Figure 19 $D_{eff}$ da identificazione su cilindri applicati su tutte le cinetiche della polvere di manioca in flusso trasversale a 3 diverse temperature*

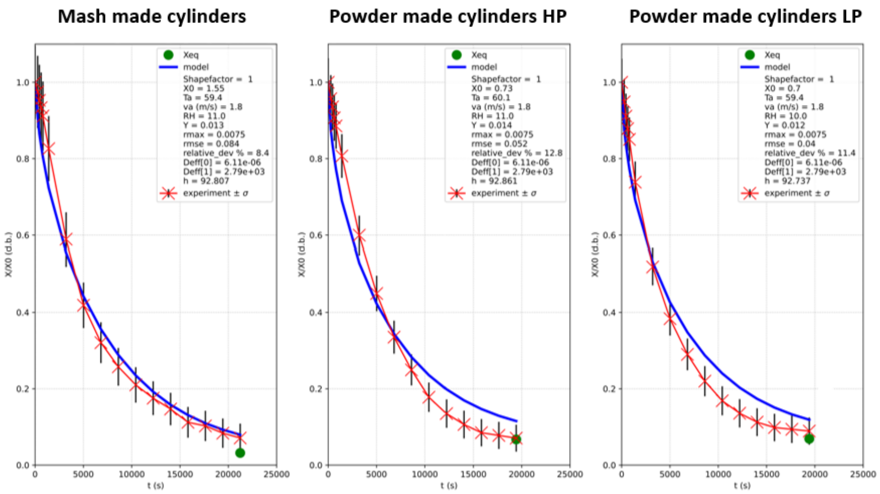

*Figure 20 $D_{eff}$ dall'identificazione su cilindri applicati alla cinetica dei cilindri di polpa e polvere ad alta porosità e a bassa porosità. Cross flow a 60°C*

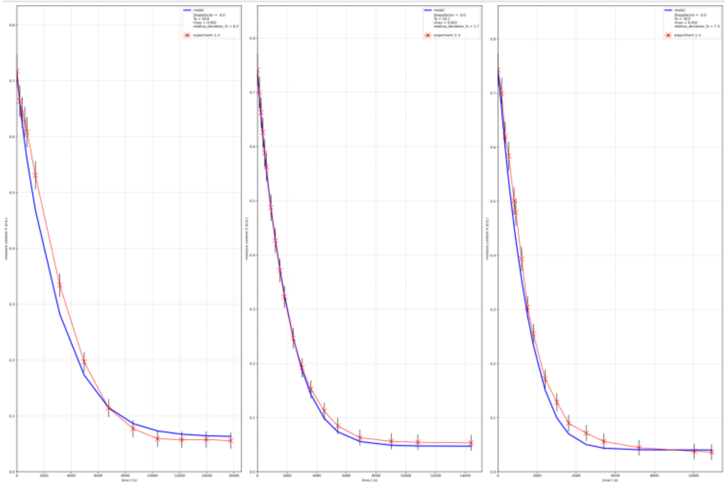

*Figure 21 $D_{eff}$ dall'identificazione su cilindri applicato alle cinetiche della polvere in parallel flow rispettivamente, da sinitra a destra, a 40°C, 60°C e 80°C*

### 3.2.2 Validazione dei valori ottenuti

Al fine di validare i valori identificati per i parametri dell'equazione del coefficiente di diffusione, sulla base delle curve dei prodotti cilindrici, altre identificazioni sono state condotte sugli altri prodotti. L'obiettivo era verificare se, identificando i parametri su curve sperimentali diverse, il loro valore non si allontanasse molto da quelli ottenuti in precedenza. La prima identificazione è stata condotta sulla base delle curve sperimentali relative ai prodotti in polvere sottoposti a essiccazione laterale. I parametri emersi dell'equazione per $D_{eff}$ emersi sono i seguenti:

$$a = 0.0000188\ [m^2/s]\ ;\ b = 3190\ [K]$$

con un range di valori esplorati per il coefficiente di diffusione che va dai $0.5 \cdot 10^{-9}$ to $2.2 \cdot 10^{-9}$ $[m^2/s]$.

Infine, con l'aiuto di un computer con una potenza di calcolo maggiore, i parametri sono stati identificati su tutte le cinetiche disponibili, allo stesso tempo.

I parametri in questo caso sono: $a = 0.00000633\ [m^2/s]\ ;\ b = 2813.07\ [K]$

con un range di valori esplorati per il coefficiente di diffusione che va dai 0,42$\cdot 10^{-9}$ to 2,2$\cdot 10^{-9}$ $[m^2/s]$. In Figure 22 gli andamenti del coefficiente di diffusione con la temperatura per le 3 diverse coppie di parametri identificate.

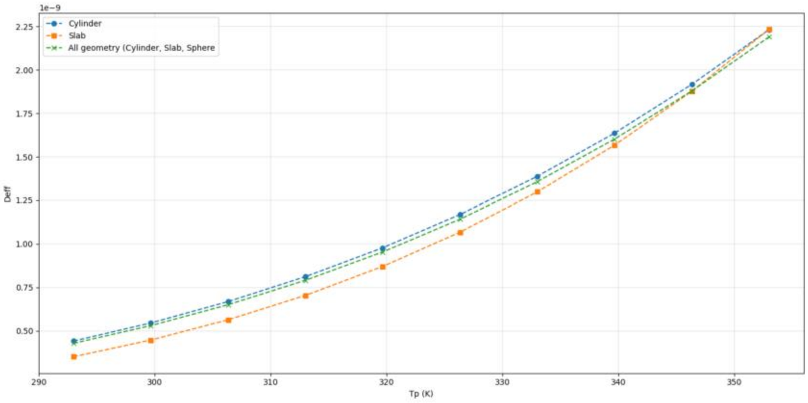

*Figure 22 Grafico $D_{eff}$ vs T. Comparazione fra curve*

# 4 Conclusioni

In questa tesi, il comportamento dei prodotti derivati dalla manioca sottoposti a essiccazione è stato studiato sperimentalmente. Poi, un modello convettivo e diffusivo esistente è stato applicato al caso della manioca.

## 4.1 Studio sperimentale dell’essicazione della manioca

Come risultato delle sperimentazioni, dalle varie prove sono state ricavate le curve di essiccazione e di velocità di essiccazione. Come conclusioni principali è doveroso sottolineare le seguenti:

1. L'essiccazione a flusso trasversale è molto più veloce di quella in flusso parallelo, soprattutto se applicata alla polvere.
2. Il diverso livello di lavorazione sembra avere un impatto trascurabile sul comportamento a essiccazione di prodotti a geometria unificata.

In riferimento alla prima conclusione, un ulteriore studio del consumo energetico fornirà maggiori informazioni e prospettive di scalabilità di questo tipo di procedura, che si è dimostrata un modo più semplice e veloce di essiccare la polvere di manioca rispetto al flusso parallelo. In questo contesto, un primo passo può essere lo studio della velocità dell'aria, poiché ha una forte influenza sia sulla procedura di essiccazione sia sul consumo energetico. Per quanto riguarda la temperatura, si può fare un bilancio del dispendio energetico per aumentare la temperatura dell'aria e del guadagno in termini di aumento della velocità di essiccazione. Per quanto riguarda la seconda conclusione, sarà utile approfondire lo studio per comprendere i fattori esterni che hanno influenzato i risultati. Una conoscenza più approfondita può anche essere un punto di partenza per indagare l'utilità e il livello delle procedure di disidratazione meccanica, solitamente applicate nei trattamenti della manioca prima dell'essiccazione termica. Anche in questo caso, il confronto tra i vari consumi energetici gioca un ruolo fondamentale nella definizione del percorso più efficiente da seguire. In generale, alcuni esperimenti su un essiccatore di scala maggiore, abbinati a una stima del fabbisogno energetico, possono essere un primo passo utile per verificare ulteriormente il comportamento dei prodotti durante il drying, limitando i problemi legati all'utilizzo di apparecchiature pilota per quanto riguarda l'aerodinamica, e per stimare la fattibilità di un ulteriore scale-up fino al livello industriale.

## 4.2 Modelling dell’essiccazione della manioca

Poiché in letteratura è stato trovato un ampio intervallo di valori per quanto riguarda il coefficiente di diffusione, è stato necessario identificarlo basandosi sulle curve di essiccazione sperimentali precedentemente ottenute, poiché lo studio bibliografico non ha fornito alcun valore affidabile ma solo un intervallo di maggiore probabilità. Su questa base, il modello è stato implementato su Python ed è stata effettuata l’identificazione dei parametri di un’equazione dipendente dalla temperatura per il coefficiente di diffusione, utilizzando il metodo Nelder-Mead. Dapprima l’identificazione è stata effettuata sulla base delle curve sperimentali riguardanti i cilindri di manioca grezza, trovando dei valori che permettevano di ottenere una soddisfacente approssimazione delle curve sperimentali anche degli altri prodotti. Successivamente l’identificazione è stata estesa, e nuovi parametri sono stati trovati basandosi sulle curve sperimentali di tutti gli altri prodotti. I valori risultati non si discostano di molto da quelli ottenuti sui cilindri, e sono in accordo con la letteratura e con i valori trovati nell’Abaco di Fourier, e confermano quindi l’affidabilità del risultato ottenuto. L'identificazione del coefficiente di diffusione conclude la parte relativa alla caratterizzazione del prodotto e apre la strada alla successiva fase di dimensionamento di un impianto di essiccazione ottimizzato per una determinata capacità, in un'ottica di valutazione dei costi e quindi di applicabilità dell'impianto stesso in condizioni reali (Africa e Sud America).

## Sommario

# 1 Introduction

## 1.1 The research centre

The present Thesis is based on a research work conducted in the research centre of CIRAD (“Centre de Cooperation Internationale en Recherche Agronomique pour le Développement”) in Montpellier, an organism working on the sustainable development of tropical and Mediterranean countries. The internship was part of the RTB (Root Tubers and Bananas) project launched by CGIAR (“Consultative Group on International Agricultural Research”), and to which CIRAD is among the partners.

*Figure 1 Cirad logo*

*Figure 2 RTB project logo*

## 1.2 Cassava - characteristics, production, and limits

Cassava (*Manihot esculenta Crantz*) is a crop typical of tropical countries, and it is part of the *Euphorbiaceus* family of the Amazon region[1]. Domesticated in Brazil more than 4000 years ago, cassava cultivations spread in South America and Caribbean Islands in the post-Columbian time, before being exported is Africa after the Spanish and Portuguese conquer of the seventieth century. In Asia was instead probably introduced from Latin America around eighteenth century [2].

Three main parts composes the physiology of this plant, root, stem, and leaf, and apart from the stem, all are used as nourishing for people and animals. Cassava contains a large quantity of starch that is an important source of energy, ad its roots can go from 0.5 to 2 kg for a length going from 15 to 100 cm. The shape and the property of the leaf depend on the variety and environmental conditions, while the woody part of the stem is used as cuttings for commercial productions. The latter is also useful for vegetative and asexual propagation of the species[3]. Looking at Figure 3 we can see the typical structure of the root. Periderm and cortex are the components of the peel, and they are in turn composed by the cortical parenchyma, phloem vessels and sclerenchyma (a system of xylem vessels and starch). Here we have the conversion of metabolites (oligosaccharides) coming from the leaf (the only place where photosynthesis occurs)[4], by means of the phloem vessels, are enzymatically converted for the starch biosynthesis and storing in the root. The quantity and quality of the starch vary according to the variety and the environmental conditions[5].

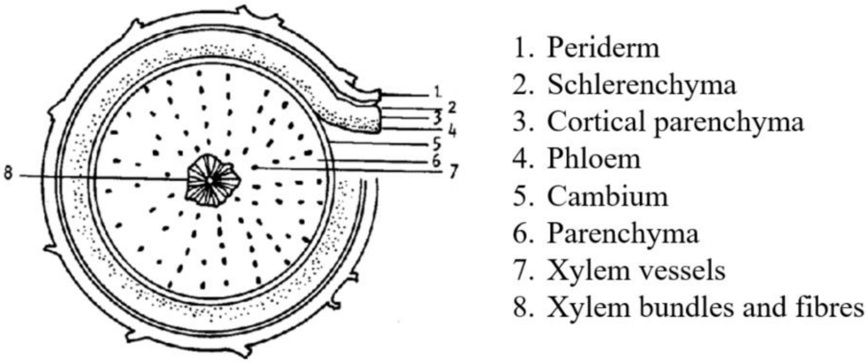

*Figure 3 Transversal view of a cassava root.*[4] *with modifications*

For developing countries of Africa, South America and Asia, cassava represents one of the widely consumed crops, with an always increasing production. Thanks to its nutritional properties, is in the fourth position as main energy supplier, after rise, sugar, and maize. Employment for 500 million workers is given by cassava cultivation and post-harvesting operations. A production of more than 300 MTons was detected by FAO for the age 2020, that gives to cassava a place between the most important crops for human diet on a world basis. Africa is the main producer, detaining the 64% of the worldwide production, especially in Nigeria (60 MTons in 2020, almost 20% of the overall world production), Democratic Republic of Congo, and Ghana. Asia is the second producer, contributing for the 27% of the total, with Thailand in the front raw with an annual production of 29 MTons. The remaining 9% is approximately entirely allocated in South America. [6]

Despite the leading role played by cassava in the world food supply, its production nowadays still relies mostly on small producers. Thanks to the ability to withstand in poorly fertile or acid soils and the low amount of water needed, cassava has a primary importance in fragile ecosystems [7]. Consequently, accounting also the increased cost of soil fertilizers, in some countries cassava is replacing maize, as evidenced by the fact that average soil yields in Africa increased by only 33% in the 1990s, while cassava production increased by 70%[8]

Nevertheless, casava presents three main limits: post harvesting fast perishing, low protein content and toxicity of some varieties. Fresh roots have a shelf life of 48-72 hours after which two types of deterioration start: internal change of colour due to oxidation caused by coumaric acids (activated when the tissue is damaged, as after harvesting)[7] followed by microbial deterioration. This drawback strongly affects the cassava chance to play a leading role in the world crop market, because oxidation leads to aesthetic results that are not compatible with consumer purchase, while microbial degradation activity changes its texture and flavour, making it no longer consumable. In order to limit this problem, cassava varieties with longer shelf-life could be preferentially cultivated or genetic modifications can be applied. Improvement of storage techniques can also be a valid way: refrigerating the roots for 4 weeks at 3°C will give to the root a more spongier consistence but will preserve the flavours; paraffin wax coating of the roots is widely used for prolonging the shelf life up to 4 months[9]. Anyway, the widely used method to elongate the shelf life of cassava is by dehydrating it, creating an uncomfortable environment for the microorganisms to grow. For what regards the toxicity of some variety of cassava, it is due to the presence of cyanogenic glucosides as linamarin and lotaustralin. The cyanogen presence can be reduced with many processes: desiccation, grinding, fermentation or roasting[9].

## 1.3 Cassava derived products and main transformation process

Depending on the final product, different transformations are possible according to the country considered. Nine different groups of cassava products can be distinguished in Africa according to Ugwu et al.[10]: cooked fresh roots, flours, *gari* (granulated roasted cassava), granulated cooked cassava, fermented pastes, sedimented starches, drinks, leaves and medicines.

For what regards flours, we must differentiate between fermented and unfermented ones. The fermentation process can occur in water before grating or in polypropylene after grating. Fermentation changes the taste of cassava, approaching it to the local taste of the country, while removing undesired cyanide particles. Fermentation can be conducted in different ways according to the final product desired and the considered geographic area. The main fermented cassava derived products are the following:

- *Gari:* typical of Nigeria and West Africa, involves the processing steps of peeling, washing, grating, fermenting for 3 up to 5 days, pressing in polypropylene sacks and finally roasting. It's usually consumed with hot water [11].
- *Lafun:* the product is put into water for 2 up to 5 days after peeling, dewatering in propylene sacks, drilling, and milling[12].
- *Attiéke:* is a granulated product obtained by peeling, cutting into pieces, washing, mashing, fermenting (fermented mash is added to the fresh one in order to initialize fermentation) and then dewatered and sun-dried. In some countries, like the Ivory Coast, steaming is previewed before consuming.

For the "sweet" variety of cassava, fermentation is not mandatory because usually the percentage of cyanogenic compounds is very low. In Figure 4 the production process for unfermented products: peeling, grating, and dewatering with piston presses or centrifuges, granulation, sun-drying and milling are the main steps. Grating, dewatering and granulation can be skipped in some cases, like happens in less developed areas[13].

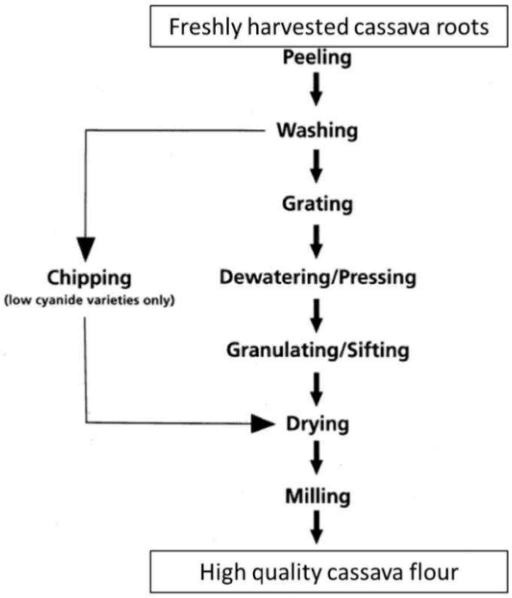

*Figure 4 Scheme of the main step for the production of high-quality cassava unfermented floor. Figure from* [13] *with modifications*

To produce the flours, the traditional method foreseen, both for fermented and unfermented ones, the following steps: harvesting and transportation, roots preparation (pealing mechanical of by hand), grating and drying. The grating stage is important for starch extraction, and it consists of mechanical grinding of the roots until a mash is obtained. Drying is the final stage and, especially in Africa, is often sun-driven, with 7 to 14 days duration and with the risk of fungus and mycotoxin development. As an alternative, pneumatic dryers are used[14].

## 1.4 Cassava mechanical dewatering

The use of dryers is required to reduce the time needed for drying both to reduce the risk of toxic elements origination and in a perspective of industrialization of the process to face the always increasing demand. Thermal treatments are the most energy intensive processes in cassava flours production[15], so a prior mechanical dewatering can be done in order to diminish the moisture content before dying: this represents an important step because on its yield depends also the energy consumption of the thermal drying. The three main mechanical treatments that can be applied are centrifugation, vacuum filtration, and compression dewatering.

Centrifugation and automatic filter press are normally employed in starch industries, but they are very expensive, and they require specialized staff for use and maintenance. For this reason, these equipment are not usually found in small-medium realities, where artisanal mechanical presses are usually employed like the ones of Figure 5 (small unit) and Figure 6 (medium unit).

*Figure 5 Artisanal mechanic press. Small unit in Benin*

*Figure 6 Artisanal mechanic press. Medium unit in Benin*

As mentioned, centrifugation can be another option for mechanical dewatering of cassava, even if is demonstrated that is efficiency is too low and can be overcame by easier presses like the one in Figure 6. Moreover, the subsequent use of a flash dryer requires an initial moisture content of the product of around 35% [w.b.] in order to avoid undesired gelatinization of the starch during the procedure, that can lead to higher energy consumption. A study of compression- filtration for the optimization of a press, and subsequently of an entire processing line, was carried out by Chiadò Rana[16] as part of the project that also comprehends the work conducted on thermal treatments and detailed in this Thesis (see section 1.1). The objective was to be able to predict the final moisture content of the goods accounting for: initial mash moisture content and mass, filtration area, pressure applied and elapsed time.

## 1.5 Thermal drying of cassava

Thermal treatments are conducted on cassava both to lower the amount of water, disempowering the microbial activity, and to diminish the amount of cyanide.

*Figure 7 Dried cassava chips. Source: FAO (2006)*

### 1.5.1 Sun-drying

As mentioned, at present sun-drying is the most used technique for cassava treatment, principally for its simplicity. It consists of spreading the pieces of Cassava on the ground or in raised outdoor platforms, and to turn them over at intervals using a shovel or a rake[17]. The main drawback is known to be the time required and the connected risk of mycotoxins onset. The drying time needed, according to the work conducted by Wareing et al. [18] on *kokonte* is of 7 to 14 days in dry season and from 8 to 14 on the rainy one. In order to shorten these times, many techniques can be used, as an example by acting on the shape and size of the pieces, use of inclined trays or concrete drying floors. In the case of cassava chips dried in Ghana, thanks to a machine developed by the International Institute Of Tropical Agriculture and drying in raised trays and polythene sheets, led to obtainment of ah high quality product with a drying time of two days[19].

### 1.5.2 Oven drying

Cassava can be also artificially dried in ovens where the atmosphere is under control. The advantages in the use of ovens, lies in the reduced space needed for drying, reduce labour, reduced time, and independence on the weather conditions. In addition, a better quality control can be achieved together with a strong reduction in mould and bacteria contamination of the good. The operation is conducted at temperatures going from 45°C to 165°C, with better results under 100°C, and is followed by cooling, packing in sacks or polyethylene bags and storing on raised platforms in dry and airy place (damp warm environment are preferably avoided) [17].

### 1.5.3 Cabinet drying

Other existing artificial drying techniques for cassava are the following: drum drying, freeze drying, kiln drying, tunnel drying, flash drying and cabinet drying. In the latter, chips of cassava thinly cut are loaded on a tray, and fresh air enters the cabinet drawn by the fan through the heater coils. The air crossing the food trays, dries it with a rate depending on the chip size, loading density and initial moisture content[17].

### 1.5.4 Flash drying for starch production

In Thailand, where cassava is processed on a large scale to produce starch, a production of 200 tons per day on 24 hours working plant is assured by a well-organized distribution network and transport infrastructures. Flash drying is conducted after mechanical dewatering, with two classes of operations that can be carried out depending on the thermal source: simple hot air or thermal oil. Temperature fluctuation is found out when air is used as heat exchanger medium, so a gradual transition to the thermo-oil is in progress for most of the installations. The entrained fluidized bed theory is at the basis of the functioning of a pneumatic dryer. Wet starch is introduced thanks to a feeding device like an hummer mill, useful to break up the product in small particles that can enter the air flow, are dried and then separated from the gas with cyclones[20]. In a common Thailand plant, 100 t/h of hot air at around 200°C are sent into the tubes of the flash dryer. The starch cake goes from 38% to 12% moisture content in 6 s, and 9 to 10 tons of dry starch is obtained each hour[21]. Temperature fluctuation in a problem that is strongly related to the initial moisture content of the feed and, as mentioned, its effect and was studied by Chiadò Rana[16] an part of the RTB project. Moreover, the pneomatic drying was analized and modelled by Chapuis et al.[20] with the aim of designing an small-scale flash dryier that, despite the scale, is efficient and suitable for cassava processing in Africa. The study led to the development of a one dimensional model for the description of drying particles using water diffusion driven mechanisms. This gave the possibility to calculate velocity, moisture content and temperature profile of the drying particles, crucial to obtain the design guidelines for the dryer.

### 1.5.5 Rotatory drying

On a theoretical basis, a rotatory convective dryer was conceived by Sanni et al.[22], as it's effectively used for various agricultural and non-agricultural materials. No actual application of this kind of apparatus on cassava is found in literature even if its use is feasible[23] and can bring to an increased production capacity and quality. In this work, the effect of drying parameters on the product moisture content is studied, for fermented ground cassava. Conductive contact drying is in this case the main mechanism of heat transfer, and temperatures of 70°C and 90°C were used for the experiments. During drying, the effect on the various thermo-hydro property of the product as effective moisture diffusivity, thermal conductivity and heat capacity were investigated, as well as some structural ones as the bulk porosity. Finally, a study of the specific energy consumption and rotatory dryer efficiency was derived. The latter value was found to be around 31%, increased with respect to the previous works and suitable for cassava processing application.

## 1.6 Drying behaviour analysis and modelling for cassava products in convective drying

Artificial drying is needed to shorten the times required to diminish the moisture content and the amount of cyanide in the products. This need is also mandatory to avoid the onset of mycotoxins and consequently to reduce the waste. Moreover, dried products are easier to store and transport and have a longer shelf life. The development of efficient drying systems can therefore help small producers, especially from Africa, to earn a place in the international market for this product.

In this perspective, since most of the drying techniques seen include convection of hot air on the product, the design of an efficient dryer starts from the characterization of the product during convective drying

### 1.6.1 Analysis of the behaviour in drying

In the following sections of this Thesis, an analysis of the behaviour in drying of different products is conduced, accounting for different processing stages of cassava: raw roots, mash resulted by milling, and powder obtained by pressing mechanically the mash to diminish its water content. No fermentation occurs in this case. Downstream of the production of the samples, before subjecting the various products to drying, a study of their geometric and structural characteristics such as density and porosity was conducted. For a meaningful comparative study of the various levels of processing, the geometry of the samples was uniformized: cylinders made of raw root, mash and powder with different porosity were produced. Nonetheless, the cassava powder was also subjected to drying arranged in a layer, since the production of cassava flour in sub-tropical countries provides for starting from this type of configuration.

Two pilot convective dryers were employed for the experimentation, where air velocity, temperature, relative humidity, and direction with respect to the product could be set by the user. By virtue of this, lateral and cross flow drying was studied, with an air temperature of 40°C to 80°C, a relative humidity between 8% and 21%, and an air velocity between 0.7 and 1.8 m/s.

The outcomes are presented in the form of curves of drying and drying rate, comprehensive of comparisons between the various products and air conditions.

### 1.6.1 Modelling cassava drying

The model used accounted for both surface (convective) and internal (diffusive) heat and mass transfers as the evaluation of the heat and matter Biot number didn’t allow to neglect one of these mechanisms. It was an existing model developed by C. Lambert et al[24] conceived for different geometries: ideal cylinders, spheres and infinite slab. The product is treated as a “thin layer” since negligible variations in the air characteristics were found across the product. The powder in cross flow is simulated as independent spheres, while in parallel flow their behaviour in drying is better simulated by a slab as it will be shown in the section “Results and Discussion”.

In order to apply the model to the case of cassava, some hydro-thermal properties of the latter were investigated both by literature review, direct measurement and parameter identification algorithm. Thermal conductivity, sorption isotherms and heat capacity were derived from literature; the convective coefficient was obtained by adimensional correlations (Nusselt) or by measuring the temperatures of products and air during drying, and deriving it from an energy balance. The diffusion coefficient was instead identified with the Nelder Mead root minimization technique implemented on phyton and based on the experimental drying curves previously obtained.

# 2 Materials and methods

This section is divided into two main parts. The first one regards the experimentation aimed to obtain a complete and reliable study of the behaviour of cassava derived products during drying, and it comprises a characterization of the products used, the pilot drying equipment and the air parameter, with a detailed explanation of the procedure employed to derive the drying kinetics. The second part focuses on the modelling part of this Thesis, with a description of the main equations and assumption made in the model, of the methods used to solve the differential equations resulting from the balances, and of the attainment of the product parameters needed for the application of the model to the case of cassava.

## 2.1 Experimental analysis of cassava drying

The experimental study for the analysis of the behaviour of cassava products in drying comprises the following steps:

- Manufacturing of the samples from Cassava roots
- Drying of products in pilot dryers, using cross or parallel air flow
- Characterization of the air flow: temperature, velocity, and relative humidity
- Characterization of the products before and after drying.

All these steps have the aim to obtain repeatable drying kinetics, useful to derive a study of the cassava products drying and to represent the basis for the modelling part.

### 2.1.1 Samples production

After a first phase of determining the best way to conduct the experiments, a big batch of cassava was employed to produce all the goods needed in the experimental work. The objective was to minimize discrepancies that there could be among the different roots, according to the quality and the different level of ripening.

#### *2.1.1.1 Storage of products: vacuum and deep freezing*

To find the best way to store our products, a comparative study between fresh and thawed cassava was conducted to investigate the presence of significative differences among the two on the drying kinetics. The outcomes revealed that no consistent variations can be appreciated between the fresh samples and the ones that were first frozen and then thawed. This allowed us to operate a deep freezing on the products at -25°C, then to store them at -15°C and to defrost each sample just before the trial using a thermal bath at 30°C (Figure 8). The freezing procedure is made on products in vacuum bags, and nucleation of crystals is favoured with respect to growing, in order to modify the cell structure of the goods the least we can. The Figure 9 shows a comparison of four drying curves, two of which are referred to fresh cassava powder (grey and green curves) and two to the thawed one (red and blue curves). Negligible differences can be observed and no significant effect of deep-freezing on drying kinetics can be noticed.

Moreover, in an earlier part of the project in which filtration-compression dewatering of cassava was investigated, an evaluation of the cells breakage was conducted according to the Escobar Salamanca work[25] The evaluation was made on the basis of the fact that cassava roots store the glucose produced by photosynthesis both in intracellular and extracellular compartments, in the form of starch. The latter, according to Defloor et al.[26], can be detected in granulometry with a particle diameters lower than 10-15 µm, and can be easily removed from the thawed cassava by rinsing. As a consequence, a comparison of the starch measured by granulometry on fresh cassava and the one retained on a mesh sieve after rinsing the thawed one, gave as a result a negligible difference[16]

*Figure 8 Thermal bath at 30°C used for the de-freezing of Cassava*

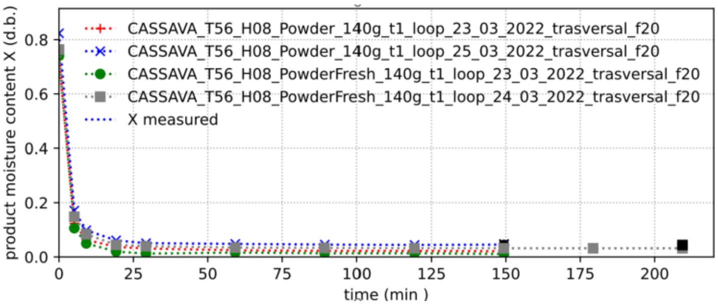

*Figure 9 Comparison between drying curves obtained with fresh and thawed cassava powder*

### *2.1.1.2 Manufacturing of powder*

The powder product comes from roots that are first manually pealed and then ground into a "Magimix" instrument, finally resulting into a mash (Figure 10). A part of the mash is stored, under vacuum and frozen, and will be also used for experimentations.

*Figure 10 Cassava mash after roots grinding*

Another part, before being stored, underwent mechanical pressing into a piston press: the pressure mechanically lowers the water content of the cassava, as well as the quantity of starch. The result is the cassava powder (Figure 11).

*Figure 11 Cassava powder obtained by mechanically pressing the mash*

### 2.1.1.3 Manufacturing of raw cassava cylinders

The cylinder-shaped products were instead produced with a circular piece cutter (Figure 12) able to penetrate the root and to derive cylinders from it. These latter can have different length and diameter according to the dimension of the instrument used. As a first attempt, we tried to obtain very thin and long specimens that can better approximate cylinders of infinite length for modelling. Unfortunately, the mechanical resistance of the cassava didn't allow the obtainment of such thin products, and the only solution was to get bigger cylinders and then to verify experimentally the hypothesis. In Figure 13 the reader can see the cylinders obtained, with diameter and length of approximately 17 mm and 50 mm respectively; shorter cylinders were used for the experimental validation on the hypothesis of infinite length. In Figure 14, a comparison of two drying curves obtained in the same condition between the longer cylinders and the shorter ones (17 mm of diameter and 40 mm of length). No substantial difference can be appreciated. As a result, the hypothesis of infinite length is retained to be verified for the longer cylinders used for our manipulations. This evidence suggests that, according to the internal cells and fibres structure of cassava, the matter exchange due to drying occurs predominantly radially and not longitudinally.

*Figure 12 Instrument used for the obtainment of cassava cylinders from the roots*

*Figure 13 Cylinder-shaped products*

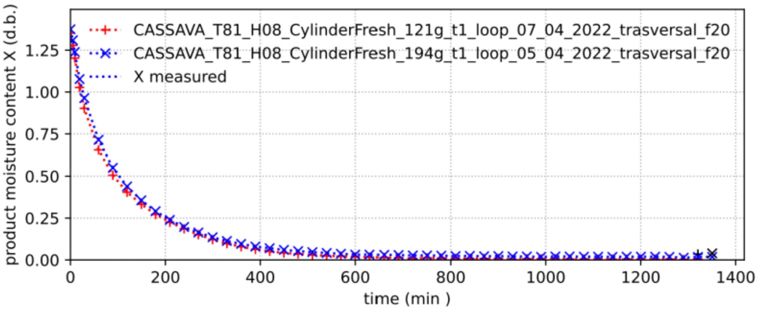

*Figure 14 Comparison between drying curves obtained on cylinders of different length for validation of "infinite length" hypothesis*

### 2.1.1.4. Manufacturing of mash and powder made cylinders

To extend the analysis and to study the effect of the various stages of processing, we decided to produce some cylindric shaped products made of mash and of powder. Additionally, for the latter, two different levels of porosity were investigated by creating powder cylinders with the same dimensions (also equal to the ones of raw cassava cylinders) but using a different quantity of cassava. The mash made cylinders (Figure 15) as well as the higher porosity powder made ones (Figure 16), needed an external structure to stay in the cylindric shape needed for a meaningful comparison with the raw cassava cylinders. The manufacturing of these goods foreseen the placing of the mash or the powder inside the structure which internal dimensions are the same of the raw cassava cylinders. Then, applying a little pressure on the top, the product fills completely the cylindric space of the structure. For the less porous powder made cylinders (Figure 17), instead, no external artefact is needed to stand, and they are produced applying a higher level of pressure. We used a hollow steel cylinder with an internal diameter of 17 mm, and we filled it with powder, pressing it until a length of around 50 mm.

*Figure 15 Mash made cylinders*

Figure 16 High porosity powder made cylinders

Figure 17 Low porosity powder made cylinders

### 2.1.2 Drying procedure

The thermal dying of goods is performed in dryers using a hot air flow that can be perpendicular to the tray (*cross/traversing flow drying*) or can encounter it laterally (*parallel/lateral flow drying*). During the procedure the weight is sampled at different times, with a not constant frequency, varying during the procedure according to the rate of drying. Indeed, in a drying procedure there are usually three phases, characterized by different rates: warm-up phase, a constant rate step and, finally, one last phase at decreasing rate[27] . The frequency of weight sampling is then chosen according to this evidence.

The assumption we made is that the decrease of weight that occurs over time is entirely due to the loss of moisture content in the product. This hypothesis is than validated with a mass balance on the dry matter, made at the end of the process: dry matter content is measured before and after dying keeping some samples in an oven at 100°C for 24 hours. A comparison between dry matter before and after drying showed that mass balance is respected in all the manipulation done, with a maximum difference of around 3%.

Before the start of the drying procedure, the preheating of the equipment is required until the desired conditions of temperature and RH%. Repetitions of the very same experiment is previewed to verify a good repeatability of the results.

The moisture content of the product is measured both before and after drying by leaving some samples in the oven for 24 hours at 100°C and assuming that, at the end, all the water in the product is removed and only remains dry matter. The initial moisture content is then used as a starting point for the calculation of the drying curve; instead, the final one is employed in the as a verification of the reliability of the trial, by comparing the final moisture content calculated and the one measured. In Table 1 the average values for the moisture content before and after drying for the products considered. The measurements are made on each manipulation carried out in the experimental work, so the average values are accompanied by the standard deviation. This latter is not available for the mash, as we have only one measurement.

*Table 1 Initial and final moisture content of different cassava products*

| **Product** | **$X_0$ (d.b.)** | **Std. deviation on $X_0$** | **$X_f$ (d.b.)** | **Std. deviation on $X_f$** |
|---|---|---|---|---|
| Raw cylinders | 1.465 | 0.0199 | 0.0672 | 0.025 |
| Mash | 1.5 | / | 0.0395 | / |
| Powder | 0.760 | 0.0085 | 0.046 | 0.0166 |

### 2.1.2.1 Summary of tests

In Table 2 a summary of the tests made on the above-described products. The reader can find information about the equipment involved, the type of product, the air conditions, the characteristic dimension before and after drying, the initial and final moisture content and the number of times the same experiments was repeated. Repetitions on the same experiments are useful to study s repeatability, in order to validate the procedure employed to conduct the various experiments. Reproducibility tests were also done for validation on more than one pilot dryer.

*Table 2 Summary of the experimental drying manipulations on cassava*

| **Equipment** | **Product** | **Product shape** | **Direction of the air flow** | **$T_{air}$ (°C)** | **RH (%)** | **$v_{air}$ (m/s)** | **Initial characteristic dimension* (mm)** | | **Final characteristic dimension* (mm)** | | **Initial moisture content d.b.** | | **Final moisture content d.b.** | | **# Repetitions** |
|---|---|---|---|---|---|---|---|---|---|---|---|---|---|---|---|
| | | | | | | | **Mean** | **Std dev** | **Mean** | **Std dev** | **Mean** | **Std dev** | **Mean** | **Std dev** | |
| CIRAD Loop dryer | Cassava after defreezing and pressing | Powder | Traversing | 40 | 21 | 1,832 | PSD** | PSD** | PSD** | PSD** | 0,752 | 0,005 | 0,068 | 0,0036 | 3 |
| CIRAD Loop dryer | Cassava after defreezing and pressing | Powder | Traversing | 60 | 8 | 1,832 | PSD** | PSD** | PSD** | PSD | 0,761 | 0,0086 | 0,043 | 0,0026 | 3 |
| CIRAD Loop dryer | Cassava after defreezing and pressing | Powder | Traversing | 80 | 8 | 1,832 | PSD** | PSD** | PSD** | PSD | 0,767 | 0,0125 | 0,03 | 0,0042 | 3 |
| CIRAD Loop dryer | Cassava fresh unpressed | Cylinder | Traversing | 40 | 21 | 1,832 | 17,053 | 0,189 | 13,274 | 0,431 | 1,146 | 0,0082 | 0,089 | 0,018 | 3 |
| CIRAD Loop dryer | Cassava fresh unpressed | Cylinder | Traversing | 60 | 8 | 1,832 | 16,843 | 0,57 | 13,303 | 0,219 | 1,41 | 0,011 | 0,07 | 0,0007 | 3 |
| CIRAD Loop dryer | Cassava fresh unpressed | Cylinder | Traversing | 80 | 8 | 1,832 | 16,986 | 0,242 | 13,073 | 0,11 | 1,39 | 0,032 | 0,023 | 0,016 | 3 |
| CIRAD Loop dryer | Cassava after defreezing and pressing | Powder | Parallel | 40 | 21 | 1,832 | 3,875 | 0,106 | 2,85 | 0,212 | 0,743 | 0,0325 | 0,04 | 0,007 | 2 |
| CIRAD Loop dryer | Cassava after defreezing and pressing | Powder | Parallel | 60 | 8 | 1,832 | 4,28 | / | 2,98 | / | 0,736 | / | 0,054 | / | 1 |

|  |  |  |  |  |  |  |  |  |  |  |  |  |  |  |  |
|---|---|---|---|---|---|---|---|---|---|---|---|---|---|---|---|
| CIRAD Loop dryer | Cassava after defreezing and pressing | Powder | Parallel | 80 | 8 | 1,832 | 3,84 | 0,240 | 3,065 | 0,085 | 0,735 | 0,0014 | 0,029 | 0,0007 | 3 |
| CIRAD Loop dryer | Cassava after defreezing and pressing | Powder | Parallel | 80 | 8 | 1,832 | 8.24 | / | 6.28 | / | 0,719 | / | 0,028 | / | 1 |
| CIRAD Loop dryer | Cassava after defreezing and pressing | Powder | Parallel | 80 | 8 | 1,832 | 14.29 | / | 11.12 | / | 0,7451 | / | 0,033 | / | 1 |
| CIRAD Loop dryer | Cassava fresh unpressed | Cylinder | Parallel | 40 | 21 | 1,832 | 17.02 | / | 14.18 | / | 1,16 | / | 0,09 | / | 1 |
| CIRAD Loop dryer | Cassava fresh | Cylinder | Parallel | 60 | 8 | 1,832 | 17.91 | / | 13.46 | / | 1,372 | / | 0,06 | / | 1 |
| CIRAD Loop dryer | Cassava fresh | Cylinders | Parallel | 80 | 8 | 1,832 | 17.22 | / | 13.40 | / | 1,27 | / | 0,06 | / | 1 |
| CIRAD Loop dryer | Cassava after defreezing and pressing | Cylinder low porosity | Traversing | 60 | 8 | 1,832 | 18 | 0 | 17.425 | 0.149 | 0,69905 | 0.0042 | 0,046155 | 0.0071 | 2 |
| CIRAD Loop dryer | Cassava after defreezing and pressing | Cylinder high porosity | Traversing | 60 | 8 | 1,832 | 18 | 0 | Unavailable | Unavailable | 0,7274 | 0.044 | 0,04562 | 0.005 | 2 |
| CIRAD Loop dryer | Cassava fresh ground | Cylinder MASH | Traversing | 60 | 8 | 1,832 | 18 | / | Unavailable | / | 1,505 | / | 0,04 | / | 1 |
| A.T.A. Loop dryier | Cassava after defreezing and pressing | Powder | Traversing | 60 | 8 | 1 | PSD | PSD** | PSD** | PSD** | 0,797 | 0 | 0.0405 | 0.006 | 2 |
| A.T.A. Loop dryier | Cassava after defreezing and pressing | Powder | Parallel | 60 | 8 | 1 | Unavailable | Unavailable | Unavailable | Unavailable | 0,797 | / | 0.058 | / | 1 |
| A.T.A. Loop dryier | Cassava after defreezing and pressing | Powder | Parallel*** | 60 | 8 | 1 | Unavailable | Unavailable | Unavailable | Unavailable | 0,797<br>0,797<br>0,797<br>0,797 | / | 0.016<br>0.018<br>0.0194<br>0.013 | / | 1 |
| A.T.A. Loop dryier | Cassava after defreezing and pressing | Powder | Parallel*** | 60 | 8 | 0,7 | Unavailable | Unavailable | Unavailable | Unavailable | 0,797<br>0,797<br>0,797<br>0,797 | / | 0,05<br>0.06<br>0.04<br>0.057 | / | 1 |

*The characteristic dimension is different according to the product: For cylinders it corresponds to the diameter, for powder in cross flow is particle size distribution, and for powder in parallel flow is represented by the thickness of the layer (section

** Values from the Particle size distribution (sub-section 2.1.1.2)

*** Four trays on the same rack were put during the trial, then analysed singularly. The objective will be better discussed in the section "Results and discussion" of the present work

### 2.1.3 Drying equipment

The apparatus employed on the purpose are mostly two: the loop dryer in the laboratory of CIRAD and the one from A.T.A.

Approaching the study of drying procedures in pilot equipment, we must notice that the air flow, when encounters the drying chamber, can be still not-completely developed. Instabilities can be due, as an example, to the presence of elbows just before the drying chamber, as happens for both dryers employed in the experimentation. Indeed, into an industrial plant the chamber would have been placed at a minimum distance of 10 pipe diameters from elbows, valves, or items able to modify the dynamic of the fluid. Discrepancies among the kinetics found on different trays could be due to this kind of fluid-dynamic issues and, in order to lower the influence of these factors on our results, we always work on one single tray in our experiments.

#### *2.1.3.1 CIRAD loop dryer*

The CIRAD loop dryer (Figure 18) comprises two drying chambers, one for traversing and one for parallel drying, and it is also constituted by a fan for the air flow movement, a boiler for the handling or the relative humidity of the heating air, and an electric heater for the manipulation of its temperature. A system of valves is foreseen for the inlet of the circulating air and the displacement of the flow during the weight sampling. Moreover, a by-pass pipe running in parallel with the two drying chambers collects the air flow during the weight sampling. The traversing chamber is placed on the right, and it dispose of three consecutive racks. For the latter, the measurement of the weight can be done automatically thanks to a system capable to weight independently the three racks inside. The dryer is connected to a computer with a dedicated software for the setting of the set-point temperature and relative humidity of the air, as well as the type and frequency of the weight detections. At the end of the process, the measurements are stored into two easily downloadable text files, then used to plot the drying curves. For the parallel drying chamber, placed downwards, the weighting is in continuum, but the record of the measurement and the deviation of the air flow must be done manually by the user.

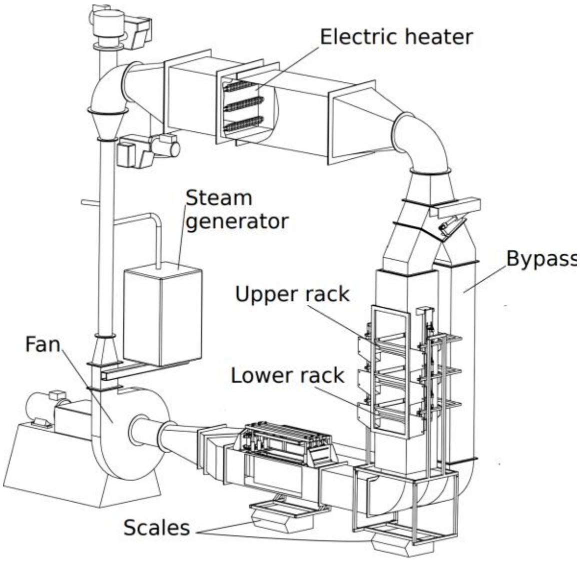

*Figure 18 Schematic of the loop dryer of CIRAD laboratories*

#### *2.1.3.2 CIRAD loop dryer: strengths and limitations*

For our applications, one limitation of this dryer is the minimum reachable velocity of the air, that is around 1.8 m/s, and the limited range of temperatures that can be explored. As a matter of fact, the dryer does not work properly with a set point of temperature below 40°C. Another limitation of the dryer comes out to be a penury of measurements in the first, faster phase of drying. This is due to the procedure of serial weighting of all the racks that takes a minimum of one minute to be completed. The powder shaped product is the one for which this issue is more relevant, by the time it exposes a huge specific surface to the hot air flow, leading to a very fast drying in the first 3-4 minutes of the process. Another aspect that must be considered is the absence of a condenser, so the impossibility to reach the desired relative humidity of the air in some condition of temperature.

Despite of the drawbacks, the dryer proved to mostly satisfy the needs for our applications, and the automatic weighing system is equipped with a balance whose sensibility is sufficient to also detect the minor changes in weight that characterize the last, slower part of the process.

#### *2.1.3.3 A.T.A. loop dryer:*

The interest to investigate the drying of cassava products even at lower values of air velocity led us to make some trials at the A.T.A laboratory loop dryer (Figure 19). This equipment can dry in 3 different ways: traversing, parallel, and in fluidizing bed. It has no boiler and so the humidity of air is manipulated thanks to the different opening percentage of the valves that communicates with the outside environment. The fan can be controlled by setting its rotating speed according to the one required for the experiment; the air can reach velocities also below 1 m/s. Finally, an electric heater is set for the air temperature handling. The dryer is equipped with sensors for the measurement of the temperature and the humidity of the air entering and leaving each chamber, as well as a system for the automatic weight sampling during the parallel drying procedure. On the contrary, in cross flow mode, these measures must be taken manually, opening the drying chamber, removing the tray, and placing it on an external scale. A Pitot-tube system (Figure 20) for the measurement of the pressure-drop, and so of the air velocity, is placed just after the fan and enable to predict the velocity of the gas approaching the chambers. Here, the software assumes that there are no pressure drops in the circuit, despite the presence of valves and elbows. The equipment gives the possibility to choose the fraction of fresh air entering the system, thanks to a system of valves that communicate with the external environment. For the experiments described in this work, the author opted for a 100% replacement: the air running into the equipment is entirely discharged after each loop and replaced with fresh one. In Figure 21 a schematic of the loop dryer in the screen dedicated to the set point establishing, and in Figure 22 and Figure 23 the detail of the traversing and lateral drying chambers respectively.

*Figure 19 Loop dryer of the A.T.A laboratories*

*Figure 20 Pitot-Tube system for the measurement of the pressure drop*

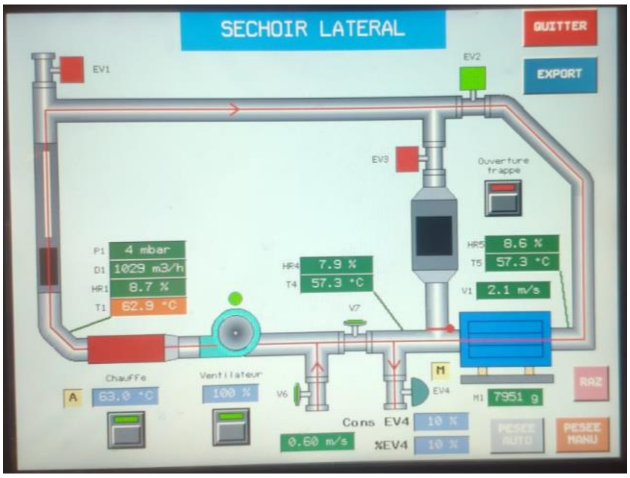

P1 4 mbar
D1 1029 m3/h
HR1 8.7 %
T1 62.9 °C
HR4 7.9 %
T4 57.3 °C
HR5 8.6 %
T5 57.3 °C
V1 2.1 m/s
M1 7951 g
Chauffe 63.0 °C
Ventilateur 100 %
0.60 m/s
Cons EV4 10 %
%EV4 10 %

*Figure 21 Screen of the A.T.A. Dryer for the manipulation of the set-points of the fan, heater and valves*

*Figure 22 Detail of the cross drying chamber of A.T.A.*

*Figure 23 Detail of the parallel drying chamber of A.T.A.*

#### *2.1.3.4 A.T.A. loop dryer: strengths and limitations*

The software controlling the apparatus is capable to store the weight measurements of the trays over time, with a constant frequency chosen by the user. To lower the instability during the weighing procedure, the air flow can be temporarily deviated and there is a lag time to allow the stabilization before each measurement. Unfortunately, it seems not to be possible to synchronize the sampling of the weight and the deviation of the flow, so that in the final record file it is not possible to isolate the measurement made with the deviated flow from the other ones registered all along the trial. Furthermore, the internal balance showed a sensibility below the one required for our scopes: an external balance and manual measurements resulted to be necessary both for perpendicular and parallel flow drying tests. As mentioned, an advantage of the second dryer is that it allows to work at a lower air velocity, and it can be also accessed by external sensors for the verification of the air characteristics in points of interest (e.g. before and after the parallel drying chamber).

### 2.1.4 Air properties and characterization in the equipment

Both dryers dispose of sensors for the measure of the temperature, the relative humidity, and the velocity of the air. The reliability of the measures was tested with external sensors as is better discussed in Annex 1.

In the study of the behaviour of a product subjected to drying procedures it’s very important to properly characterize the drying air. The water vapor carried out from the surface of the product forms a mixture with the incoming air in which the components can be considered separately: this is the subject of *psychrometry.* In the following sub-sections, a list of the psychrometric properties of air with a relevance in the drying domain are discussed.

#### *2.1.4.1 Absolute and relative humidity*

The absolute humidity is the amount of water vapor contained in air, and it is expressed as a mass ratio between water vapor ($m_V$) and dry gas ($m_G$).

$$H = \frac{m_V}{m_G}$$

This is a "dry basis" definition, as the denominator presents only the mass of dry gas and not the total mass of air. Scientifically, this kind of definition is preferred also for the product moisture content, replacing the mass of the dry gas with the mass of dry product, as the denominator remains constant during drying, thus its derivation leads to easier equations.

The relative humidity is instead defined as the ratio between the absolute humidity and the saturation one ($H_S$), the point at which the air is fully charged in humidity and cannot host more:

$$RH = \frac{H}{H_S} = \frac{P_v}{P_v^{sat}}$$

#### *2.1.4.2 Density*

The total pressure and number of moles (subscript T) in the mixture are given respectively by the summation of the pressure and moles of dry gas (subscript G) and water vapor (subscript V):

$$P_T = P_G + P_V$$

$$n_T = n_G + n_V$$

The density is than calculated thanks to the ideal gas equation as follows

$$\rho = \frac{m_T}{V} = \frac{P_T(n_G + n_V)}{RT}$$

As visible, the density of air is strongly related to the relative humidity and the temperature.

#### *2.1.4.3 Enthalpy*

Into a drying process, the heat exchange is one the main phenomena that occurs. In this perspective, is important to measure the amount of heat energy of the air-vapor mixture, so its enthalpy, with respect to some reference conditions. Those last, for what regards food drying are usually considered to be the following: gas liquid state at 0°C for dry air and liquid state water at 0°C for water vapor. The reason behind this choice lies in the fact that we expect air to remain in the gas state but water to change its phase from liquid to vapor. The enthalpy can be finally calculated as follows:

$$h = m_a[c_aT + H(c_vT + \lambda_0)]$$

where $m_a$ is the mass of air, $c_a$ th specific heat of dry air, $c_v$ the water vapor one, and $\lambda_0$ the latent heat of evaporation evaluated at 0°C. The value commonly adopted for these properties are the following:

$$c_a = 1.0 \left[\frac{kJ}{kg \cdot K}\right]$$

$$c_v = 1.87 \left[\frac{kJ}{kg * K}\right]$$

$$\lambda_0 = 2501 \left[\frac{kJ}{kg}\right]$$

Three different terms can be distinguished in the equation: the sensible heat term for dry air ($m_a c_a T$), the sensible heat term for water vapor $(m_a H c_v T)$ and the latent evaporation hear term $(m_a H \lambda_0)$.

It is important to stress that during drying the enthalpy of the air and the products remains constant, as the latent heat of evaporation for products moisture content is supplied by heat convection from air.

### 2.1.5 Measurement of the convective coefficient in parallel flow

For the scope of the present work, it is also useful to determine experimentally the value of the convective coefficient *h*, in the case of parallel drying on a slab of ground cassava. To obtain such value, we used an aluminium plate on which center a hole is drilled for the insertion of a temperature sensor. The aluminium plate is then subjected to hot air in the same conditions of the cassava products that we aim to simulate, while the sensor detect its temperature along the procedure and another one is set for the ongoing air temperature measurement. Getting in this way the evolution of the plate and air temperature over time, and imposing a simple energy balance, is then possible to derive a value for the convective coefficient as follows:

$$\mathrm{m} \cdot c_p \cdot \frac{dT}{dt} = h \cdot A \cdot (T_a - T)$$

where *m* is the mass of the plate (kg), $c_p$ is the heat capacity at constant pressure of aluminium ( $\frac{J}{Kg \cdot °C}$) and *A* is the surface exposed to the air flux ($m^2$), $T_a$ is the temperature of the air and $T$ the plate one.

To integrate and solve the balance, we need a function that can approximate the trend over time of the difference between air and product temperatures. The graph in Figure 24 shows this difference over time, and a linear and exponential approximation of the latter.

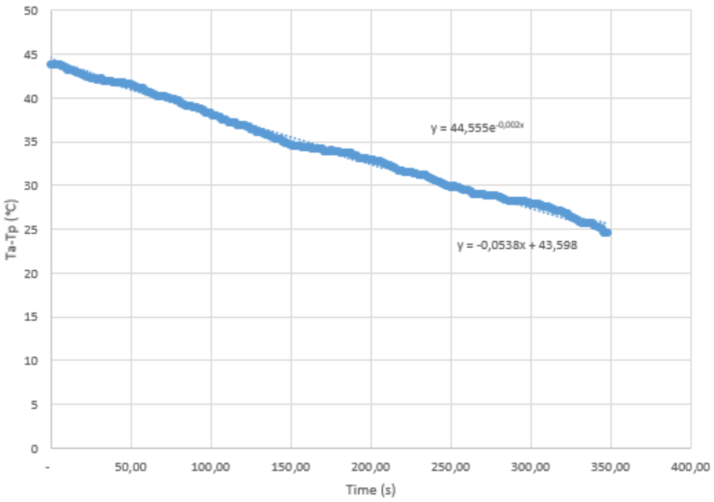

*Figure 24 Trend over time of the difference of temperature between the air and the Aluminium plate*

Solving the integral we obtain a value of 17.86 and 19.84 $\frac{W}{m^2 * K}$ respectively with exponential and linear approximation. Another possibility is to consider the temperature of the air constant and to solve the integral simply by separation of variables: this method leads to a value of 15.48 $\frac{W}{m^2 * K}$. Finally, as a reliable value for *h* we can use an average between the three: 17.72 $\frac{W}{m^2 * K}$.

## 2.1.6 Characterization of the products

In the present section an overview of the geometrical and structural characteristics of our products and the way they were measured. In particular, the density and porosity measurements at the pycnometer, the granulometry made on powder and the evaluation of the shrinkage following drying.

### 2.1.6.1 Measure of the density and porosity of the products

The density of the powder and of the raw cylinders has been measured thanks to a pycnometer at helium (Figure 25). With the measure of the density and the perfect law gas is then possible to deduce porosity. Let us start with some definitions:

$$\rho_{app} = \frac{m_{product}}{V_{dry\ matter} + V_{water} + V_{pores}}$$

$$\rho_t = \frac{m_{product}}{V_{dry\ matter} + V_{water}}$$

$$\varepsilon = \frac{V_{pores}}{V_{dry\ matter} + V_{water} + V_{pores}} = 1 - \frac{\rho_{app}}{\rho_t}$$

where $\rho_{app}$ is the apparent density, $\rho_t$ is the “true” density accounting only for the non-void part of the product, and $\varepsilon$ is the porosity.

The principles of the density and porosity measurement at the pycnometer are the following:

1. The sample of product is weighted and placed into a small recipient of known volume

2. The recipient is hermetically closed and then filled with a known quantity of Helium, at a known pressure of reference.
3. The gas pressure in the recipient is measured
4. Using the perfect gas law, the volume occupied by the gas is calculated. Here the volume we consider is the one that is not occupied by the sample and the pores with a diameter greater than the one of the Helium molecules ($d_{He}$ = 256 · $10^{-12}$ m).
5. The volume of the sample is deduced as follows: $V_{\text{sample}} = V_{dry\ matter} + V_{water} + V_{\ pore<dHe}$.
   To solve this equation and obtain the volume of the pores with a diameter smaller than the one of the Helium molecules, a two-step procedure is needed. As a first step, we want to measure the density of the dry matter of cassava powder. To do so, powder is ground very finely, in order to minimize the porosity, then weighted. The pycnometer will then provide the volume value of our sample ($V_{dry\ matter}$), from which we can also derive the density of the dry matter. In the second step, the pycnometer is used to determine the volume of a sample of cassava powder ($V_{\text{sample}}$). The volume of water ($V_{water}$) is known from the moisture content measurement, around 0.044 w.b. for after drying powder, and the known density of liquid water, 998 kg/m$^3$.

   With the values calculated, the two densities and the porosity are then easily deduced. The results about powder and raw cylinders are shown in Table 3, where the data about the dry matter denisity calculated with the finely ground cassava is also present. Each measurement is being conducted in duplicate.

*Figure 25 Pycnometer at helium for the measure of the powder and raw cylinder density*

*Table 3 Density and porosity measured for powder and raw cylinders at pycnometer*

| **Product** | **True Density** | **Porosity** |
|---|---|---|
| Powder grinded | 1479 +/- 8 [kg/m$^3$] | 0% |
| Raw cylinders | 1090 +/- 17 [kg/m$^3$] | 43% |
| Powder | 1300 +/- 12 [kg/m$^3$] | 72% |

The value found for the powder density is consistent with the one that can be found in the work of Escobar[25], 1565 kg/m$^3$, nevertheless the measurements at the pycnometer can be affected by the moisture content of the products as the water can pass into the gas. In our case the moisture content was very low, as the manipulations were done on dried powder and cylinders, so we can consider the flux of water in Helium negligible.

However, different authors[28][29][30] have delt with the subject of determining the particle density according to the moisture content of the cassava. In Figure 26 a graph representing the particle density with respect to the moisture content for different cassava-based products is shown.

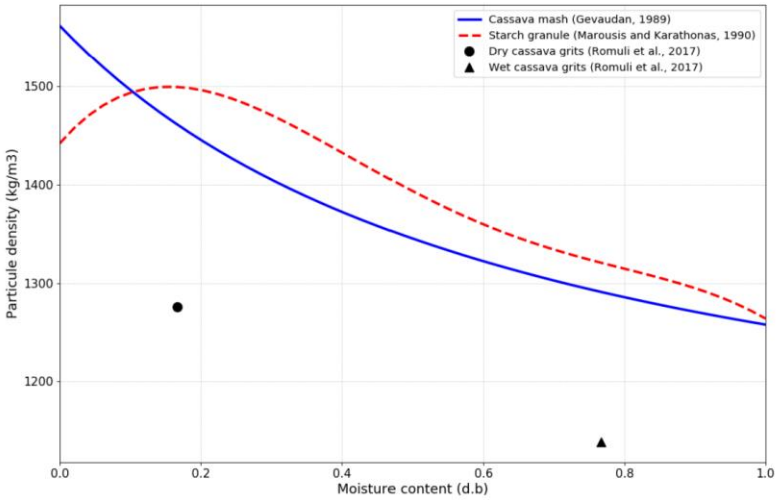

*Figure 26 Cassava products particle density according to the moisture content. Study on cassava mash*[28]*, starch granules*[30] *and cassava grits*[29]

### 2.1.6.2 Particle size distribution

To evaluate the dimension of the particles in the powder, granulometry and image analysis were combined and applied on the dried powder. Granulometry was performed on a sample of powder by passing it through sieves in series. The passage sections of the various sieves are gradually smaller and of known size. A vibration helps the smaller particles pass through the sieves until the one whose mesh size allows them to be retained. In subsequent data processing, the characteristic size of the particles is assumed to be intermediate between the passage section of the previous sieve and the one on which the particles are effectively retained. The addiction of image analysis comes from the need to characterize the bigger particles dimension, all retained in the larger mesh of the available sieves (diameter bigger than 4.18 mm), but with different characteristic length among them. Thus, a picture of the particles was taken with a camera fixed perpendicularly to the product and with a good lighting (Figure 27), and the dimensional analysis was performed with the software ImageJ.

*Figure 27 Photo of the bigger particles subjected to image analysis-based granulometry*

The software is able to evaluate the external surface area and the perimeter of the particles in the image, from which is possible to derive the characteristic length by considering a perfect sphere with the same surface area of the one of the particles. A sphericity factor S is also found in order to evaluate the quality of the approximation of the particles to perfect spheres in modelling.

$$S = 4 \cdot \pi \cdot \frac{Area}{(Perimeter)^2}$$

The value of S goes from 0 (very bad sphere approximation) to 1 (correspondence to a perfect sphere) and in our case the value was: 0,64. We can consider the particle analysed with image analysis to be a good approximation of perfect spheres.

In Figure 28 and Figure 29 the result of the sieve granulometry made on particles with diameter in the range 0.025-4.18 mm.

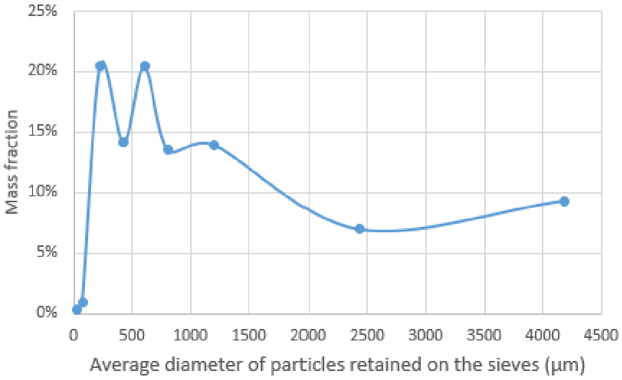

*Figure 28 Particle size distribution from sieve granulometry on particles with diameter in the range 0.25-4.18 mm*

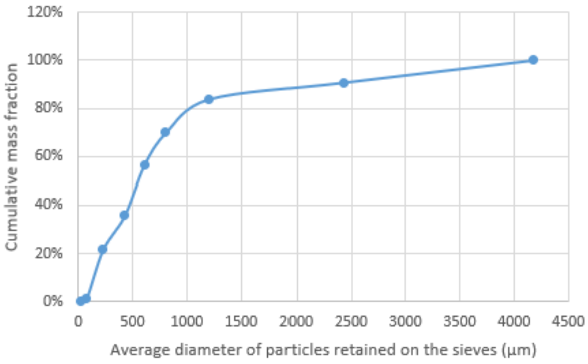

*Figure 29 Cumulative frequency trend with respect to average particle diameter. Particles from sieve granulometry with diameter in the range 0.25-4.18 mm*

The combination of the two techniques requires some clarifications: the granulometry made with sieves gives the mass fraction of particles with the radius in a certain range of values, the image analysis provides instead the numeric fraction. The two can be combined thanks to calculation of the product density (see section 2.1.3.2) and the value of the volume deriving from the diameter we consider for the class of particles. With this information, we can easily calculate the mass of each particle belonging to each class, so mass and numeric fraction can be easily interchanged. In Figure 30 the results of the granulometry made on the bigger particles with image analysis technique.

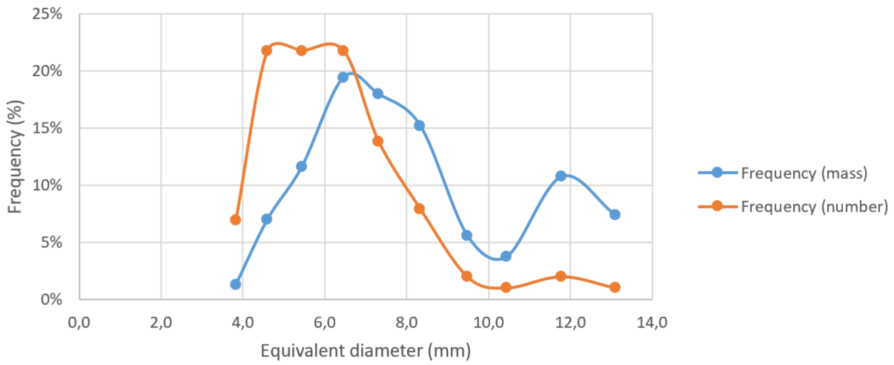

*Figure 30 Particle size distribution from granulometry performed by image analysis on particles with diameter bigger than 4.18 mm*

The overall particle size distribution is shown in Figure 31, while Figure 32 shows the trend of the cumulative frequency with respect to the particle average diameter. The decision to perform the analysis on dry powder comes from the evidence that it is more representative of the product subjected to drying with respect to the not dried one. Performing granulometry on high moisture containing particles, indeed, requires doing it in aspersion of water, that tends to disband the clusters. What experienced in all the trials is instead the presence of agglomerated particles at the end of the drying procedure. The average and median diameter resulted to be respectively of 1.639 mm and 0.589 mm.

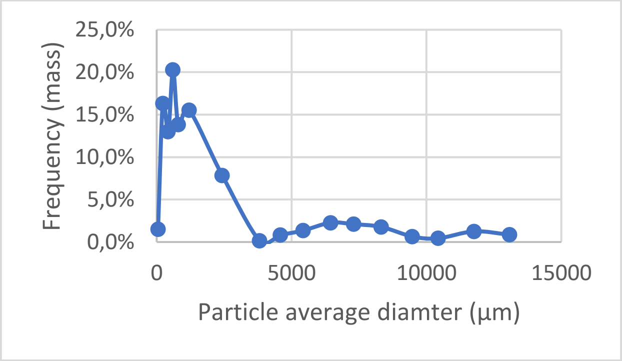

*Figure 31 Particle size distribution for dried powder*

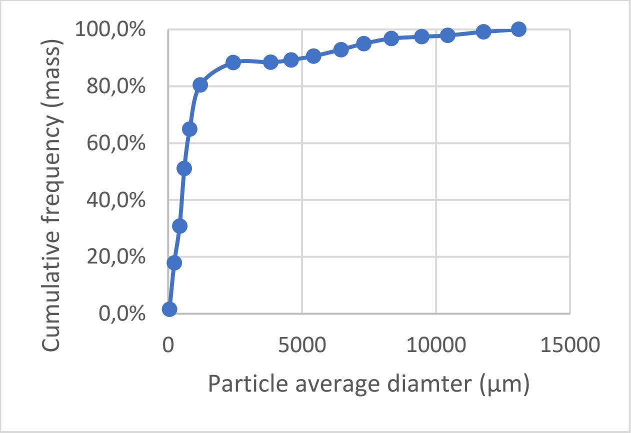

*Figure 32 Cumulative frequency trend with respect to average particle diameter for dried powder*

Still, granulometry on Cassava mash was performed in an earlier phase of the project[16] leading to a $d_{50}$ of 0.704 mm. This result is than being compared with the works conducted by Escobar[25] and Gévaudan[28].The former found a $d_{50}$ for fresh mash of 1,196 mm while 1,272 mm for *gari*, while the latter a $d_{50}$ between 0.590 – 0.660 mm for the cassava mash and between 0.630 – 0.691 µm for *gari.*

### 2.1.6.3 Evaluation of the shrinkage

To characterize the product is also important to consider the initial dimension and the potential shrinking during the drying. In order to access such information, two different procedures are being developed for cylinders and powder.

As discussed, cylinder of different length in the range of interest showed negligible differences in the drying kinetic, allowing us to assume true the approximation of infinite length cylinders and to consider only the radial variation in the analysis. Moreover, the drying of cylinders led to a final product with no more a prefect cylindrical shape, but they take on a slightly convex form leading to different values of diameter, depending on the position along the length on which the measurement is done. The best way to access an average value for the diameter proved to be the following: the measure of the length is made with a calliper, and then the volume of the cylinder is measured with the variation of the volume of a known quantity of oil into a graduated Becher. Therefore, with the values of volume and length, the equivalent diameter is easily calculated. In Table 4, the average among the values of the dimensions and the shrinkage for raw cylinders employed in our manipulations

*Table 4 Dimensions and shrinkage of raw cylinders*

| Dimension | Before drying | After drying | Shrinkage |
|---|---|---|---|
| Diameter | 16,96 [mm] | 13,288 [mm] | 21,65 % |
| Length | 49,94 [mm] | 38,38 [mm] | 23,14 % |
| Volume | 45111,4 [mm$^3$] | 21279,8 [mm$^3$] | 52,82 % |

A different system is instead used for the dimensional characterization of the powder-shaped products. We can consider a double identity for this kind of product: one at the particle level and one at the level of the layer. For the former, as discussed in sub-section 2.1.4.2, a combination of granulometry and image analysis led to the particle size distribution and to the described values for the particles average and median diameters. Unfortunately, granulometry performed on the products undried seems not to offer comparable measurements, being different the way in which granulometry is performed on wet and dry powders. The shrinkage at the particle level is so not easily definable. What we can effectively access is the thickness of the layer, but a direct measurement with a calliper proved to be failing and inaccurate. Instead, a more reliable way to indirectly measure it is the following: a sample of the cassava is put into a small known volume can, so it fills the recipient to the brim. The net weight of the cassava inside is then noted and a proportion will lead to a value for the average thickness in the tray of the dryer, since the surface on which the powder is distributed is known. The experimental work involved trials at different powder layer depths, on which an average value of 14,55% was measured for the thickness shrinkage.

## 2.2 Modelling of cassava products drying

The model developed finds its roots in the principles of matter and energy transfer in high moisture content food subjected to convective drying. In these processes both convective and diffusive mass transfer occurs, leading to a loss of moisture content in the product until the equilibrium value with the hot drying air. In the following sub-sections, a brief overview of the principles just mentioned and a description of the model, with the main differential equations and their solution method, are presented . The properties of the products, useful for the application of the model on the case of cassava, are obtained both from the experimental characterization of the product discussed in the previous sections of the present work, from literature, and from parameter identification methods applied on the experimental drying curves.

### 2.2.1 Principles of convective food drying

In the process of food drying heat and moisture transfer occur simultaneously since the former is transferred from the hot air to the surface, then moving inside the material, and the latter consist of a diffusion toward the surface of the aliment, before to evaporate in the external environment. The two processes are driven by two different forces: the temperature difference for heat transfer and the local gradient of moisture concentration (or partial pressure of water vapor) for the mass transfer. Once the surface of the is dried by the hot air flow, a difference in the moisture content occurs with the interior of the product, and water diffuses from higher moisture content areas to lesser containing ones. Concurrently, the external surface temperature of the product is higher than the temperature of the interior part, thus a temperature difference is created. Is thus clear that the two mechanisms occur in opposite directions. The heat moves from the hot air to product surface by convection, it increases the energy of the water molecules on the surface allowing the evaporation, that in turn removes heat as latent heat. The water within the product must reach the surface by diffusion, and by doing it encounters two resistances: the surface of the products acts like a barrier for the heat supply, and the thickness of the boundary layer also concurs in limiting diffusion.

In our experimentation we obtained drying curves, with different rates depending on many factors (e.g. surface exposed, cell structure, thickness). Each drying curve shows different phases, each of which is governed by some controlling heat and mass transfer mechanisms, characterized by a particular trend for the drying rate. Generally, in the first phase of food drying, the product is not in equilibrium with the air, and a steady state is still not reached. This is known as the “warm-up” phase, at the end of which thermal and moisture equilibration finally arises. Due to the difference in time in which the two are reached, there could be some anomalies in the first part of the kinetic curve (e.g. an increase of the moisture content in the first part, possibly due to condensation of air humidity on the surface of a cold product). The second phase is at constant rate: moisture is available on the surface of the products and removed continuously by convection. [31] The last phase is at falling rate, and it is characterized by a depleted surface moisture and the internal moisture diffusion is the controlling mechanism. As a matter of fact, additionally the mentioned resistances at the diffusion, in this phase the internal moisture content of the product is also diminishing, lowering the local concentration gradient representing the driving force for mass transfer. [32]

The Fick’s first law of diffusion governs the diffusion mechanism:

$$\frac{1}{\rho}\frac{\mathrm{d}m}{\mathrm{d}t} = -DA\frac{dM}{dx}$$

Where $\rho$ is the density, *D* the diffusivity, *A* the area, *M* the moisture content d.b, and *x* the distance.

The Fourier law summarize instead the heat exchange:

$$\dot{Q} = -kA\frac{dT}{dx}$$

where $k$ is the heat conductivity. The solution of these two equations is the basis to build most of the drying models commonly used.

### 2.2.2 Limiting transfer phenomena evaluation: the Biot numbers

The need to investigate the relative weight of internal and surface mass and heat transfer is needed to properly choose the modelling way. A common method to evaluate the relative importance of the various thermal and matter transfer mechanisms is the calculation of the thermal and matter Biot numbers.

We calculate the thermal Biot number as:

$$Bi_{th} = \frac{h \cdot L_c}{k}$$

where $h$ is the convective coefficient, $L_c$ is the characteristic length of the material, and $k$ the thermal conductivity. If the value of $Bi_{th}$ is lower than 1 we can assume that the conductive mechanism is negligible with respect to the convective one. The characteristic length is usually the ratio between volume and surface of the product.

The value of the convective coefficient has been directly investigated only in the case of the powder in parallel flow (section 2.1.5) and is deduced by the Nusselt and Reynolds correlation in all the other cases.

For the Chilton-Colburn analogy we have:

$$h = \frac{Nu \cdot \lambda_a}{L_{eq}}$$

$$Re = \frac{\rho_a \cdot v_a \cdot L_{eq}}{v_a}$$

$$Pr = \frac{Cp_a \cdot v_a \cdot \rho_a}{\lambda_a}$$

In the case of cylinder:

$$Nu = \frac{0.3 \cdot \left(0.62 \cdot Re^{0.5} \cdot Pr^{\frac{1}{3}}\right)}{\left(1 + \left(0.4 / Pr^{\frac{2}{3}}\right)\right)^{\frac{1}{4}} \cdot \left(1 + \left(Re / 282\right)^{\frac{5}{8}}\right)^{\frac{4}{5}}}$$

In the case of powder in traversing mode we have instead:

$$Nu = 0.5 \cdot \sqrt{Re} + 0.2 \cdot Re^{\frac{2}{3}} \cdot Pr^{\frac{1}{3}}$$

where the suffix $a$ is referred to the air characteristics, in particular $\lambda_a$ is the conductivity $\left(\frac{W}{m\cdot K}\right)$ $v_a$ is the velocity (m/s) $Cp_a$ is the heat capacity $\left(\frac{J}{kg\cdot K}\right)$ at constant pressure $\upsilon_a$ is the cinematic viscosity $\left(\frac{m^2}{s}\right)$ and $\rho_a$ the density $\left(\frac{kg}{m^3}\right)$. $L_{eq}$ is the equilibrium length (m), corresponding in this case to the diameter of the cylinder, and to the following expression:

$$L_{eq} = \frac{D_{eq} \cdot \varepsilon}{(1-\varepsilon)}$$

$$D_{eq} = {}^{6}\!\Big/\!\frac{S}{V}$$

where $\varepsilon$ is the porosity of the bed, $S$ the surface of the spheres ($m^2$) and $V$ the volume ($m^3$).

Finally, the choice of a value for the thermal conductivity for cassava will be further discussed (section 2.2.4.2) and comes from consideration on the applicability of general models based on the composition and on experimental data from the literature.

The matter Biot number represents instead a way to investigate the relative weight between external convective mass transfer phenomena and internal diffusive ones.

$$Bi_{mat} = \frac{D_{eff} \cdot L_c}{k_{mat}}$$

where $D_{eff}$ is the effective diffusion coefficient $\left(\frac{m^2}{s}\right)$ and $k_{mat}$ $\left(\frac{m}{s}\right)$ is the mass transfer coefficient.

The research of a value for the diffusion coefficient for cassava products represents one of the main goals of the present work. As it will better discussed in section 2.2.4.4, parameter identification was applied to experimental drying kinetics with the aim to study diffusivity in cassava products since literature data gives a wide range of possible values for the diffusion coefficient, broader than what expected for an intrinsic property of the same medium. In order to calculate the Biot number, we did a hypothesis on $D_{eff}$, trusting to compare it with the outcomes of the identification and repeat the calculations.

The mass transfer coefficient $k_{mat}$ is analogous to the $h$ of the heat transfer domain, and a link between the two is possible in different ways. In the present work we consider the Lewis correlation[33]:

$$k_{mat} = \frac{h}{\rho_a \cdot c_{p_{AH}} \cdot Le^{\frac{2}{3}}}$$

where $Le$ is the Lewis number and $c_{p_{AH}}$ is the specific heat at constant pressure for humid air.

Table 5 shows the results for the calculation of the Biot numbers for the different products we consider

*Table 5 Thermal and matter Biot numbers for the different cassava products*

| | Powder in traversing flow drying | Cylinder | Powder in parallel flow drying |
|---|---|---|---|
| **BI_th** | 0.236 | 1.378 | 0.164 |
| **Bi_mat** | 5.27E+03 | 6.29E+04 | 3.86E+04 |

From the results we noticed that for powder shaped product transfer convective phenomena are mostly the controlling ones with respect to the conductive ones, since $Bi_{th}$ is lower than one. This is not entirely applicable to the case of cylinders. The $Bi_{mat}$ shows values >100 meaning both convective and diffusive mechanisms must be considered in the model[34].

### 2.2.3 The drying model

The model we use was developed by C. Lambert et al[24] in a frame of creating a generic convective drying simulator for solid food particles. These kinds of models are usually validated using experimental data using a bottom-up or top-down approach. In the first case, empirical equations with no generic extrapolation capabilities are used. The top-down approach leads to a model with a potential compatibility with different kind of food products and drying conditions. The main requirement in this case are the food properties. In this perspective, the work of C. Lambert et al represents an attempt to obtain the most general possible method for modelling air dying of food using classical modelling approach. In the following sub-sections we show a description of the possible modelling approaches, the main equations involved in the model we used, the description of how it was applied to the case of cassava products and the way all the properties of the latter are predicted.

#### *2.2.3.1 Modelling approaches*

To build a simulator for food drying processes we have some categories of modelling approaches that can be explored: *black box models*, *simplified white box models* and *sophisticated white box models*.

The *black box models* are usually static, and then unable to properly simulate complex dynamic processes with important variations of temperature and moisture content and based on fitting experimental data with curves. Zero-dimensional transfer is only described by one variable (product moisture content), and a sufficiently wide range of applicability is only reached with a huge amount of experimental work, because the extrapolation possibility is heavily limited. On the other hand, these models do not require challenging laboratory measurement of food properties and enhanced coding abilities.

In the *simplified white box models* a dynamic simulation is possible by solving the ordinary and partial differential equations involved. The latter usually come from the heat and mass transfer description starting from the Fick and Fourier laws. The simplified characteristic is referred to the geometry of the products that are retained ideal (perfect spheres, or infinite cylinders or slabs) with no shrinkage during drying. Moisture content and temperature are the two product variables (sometimes also pressure variation is considered) describe the one-dimensional transfer. The thermophysical properties of the products must be determined precisely with laboratory work, literature research and/or identification based on experimental studies. These kinds of models have usually a good extrapolation capability and resulted to be the best choice for the scope of this work.

The *sophisticated white box models* are an extension of the simplified one to 2D/3D transfer and considering non-ideal shrinking geometries for the products. This is paid with high computational cost, the impossibility to simulate a whole dryer but only some parts, need for numerical identification on many food properties that cannot be directly accessed, and accumulation of prediction error.

### *2.2.3.2 Model main hypothesis*

The model is built on the following assumptions:

1. The product has uniform and isotropic properties with heat and mass transfer occurring only in radial direction
2. Ideal geometry of infinite cylinder, infinite slab or spheres is assumed: shrinkage and swelling are considered to be negligible
3. Heat transfer by conduction between particle is neglected
4. Thermal expansion coefficient is neglected
5. Evaporation occurs only on the surface of the particles, as well as mass and heat convection
6. Heat conduction and liquid water diffusion occurs instead within the particle

The model was developed for both thin layer and deep bed drying, where the latter is seen as a succession of thin layers in which transfer phenomena occurs between air and product after each layer. In this case, heat and mass balance are needed for the air after each layer crossed[35]. In our case, we only consider thin layer behaviour, as the property of air crossing the product in the dryer do not seem to be modified.

### *2.2.3.3 Mass and heat balances*

The following balances are written for particles perfectly spherical with mass and heat transfer occurring only radially. The complete description is given by the work of Romdhana et al. [36], and has been generalized to different geometries by C. Lambert et al [24].

Combining the Fick law and the principle of conservation of mass, considering spherical symmetry, the mass transfer is described by the following partial differential equation in spherical coordinates:

$$\frac{\partial X}{\partial t} = \frac{1}{r^2}\frac{\partial}{\partial r}\left(r^2 D_{eff}\frac{\partial X}{\partial r}\right)$$

where *X* is the moisture content, r is the radial position, $D_{eff}$ the effective water diffusion coefficient ($m^2s^{-1}$) and *t* the elapsed time.

Nevertheless, to completely describe the moisture transfer we need two boundary conditions respectively at the centre and at the surface of the spherical particle. In particular we have no mass transfer at the centre (r =0) because of the symmetry hypothesis:

$$\left(\rho_{dm} D_{eff}\frac{\partial X}{\partial r}\right) = 0 \qquad when \;\; r = 0$$

where $\rho_{dm}$ is the density of the dry matter (kg $m^{-3}$)

At the surface (*r* = *R*) the boundary condition is given by the continuity by the moisture diffusion and the mass flux density on the surface $\dot{m}$ (kg $s^{-1}m^{-2}$):

$$\left(\rho_{dm} D_{eff}\frac{\partial X}{\partial r}\right) = \dot{m} \qquad when \;\; r = R$$

For the heat transfer the most common approach consist in considering conductive heat transfer inside the particle subjected to drying. The heat transfer is governed by the Fourier law:

$$\frac{\partial\left(\rho C_p T\right)}{\partial t} = \frac{1}{r^2}\frac{\partial}{\partial r}\left(r^2 \lambda \frac{\partial X}{\partial r}\right)$$

Where $C_p$ is the specific heat capacity (J kg$^{-1}$ K$^{-1}$), $\lambda$ is the thermal conductivity (W m$^{-2}$ K$^{-1}$)

In our work we neglect shrinkage and consequently the density of dry matter remains constant, and the mass diffusivity is only function of moisture content and temperature. Nevertheless, is important to notice that the transport properties may change according to the variation of the geometry in the case of shrinkage, puffing, crystallization or glass transition. Indeed, these phenomena lead to a series of consequences of which a non-exhaustive list of examples is the following: moisture diffusivity lowering, particles tend to have less surface area and so to decrease the rate of moisture removal by convection, volume reduction with consequent change of dry matter density, deformation of the shape of the product and need for simulation of moving surfaces.

Neglecting chemical reactions and shrinkage we can write:

$$\rho C_p = \rho_{dm}(Cp_{dm} + XCp_w)$$

where the subscripts *dm* and *w* are referred respectively to dry matter and water.

Additionally, similarly to what we have seen for mass transfer, the boundary conditions are set at the surface and at the centre of the particle. At the surface (r = R) the heat transfer occurs driven by the temperature difference and the evaporation rate. At the centre (r = 0) adiabatic conditions are due to the symmetry.

$$\left(-\lambda \frac{\partial T}{dr}\right) = 0 \qquad when\, r = 0$$

$$\left(-\lambda \frac{\partial T}{dr}\right) = h(T - T_\infty) + \dot{m}(\Delta H_v + Cp_v T) \qquad when\, r = R$$

where *h* is the convection heat transfer coefficient (W m$^{-2}$ K$^{-1}$) and $\Delta H_v$is the latent heat of evaporation of water (J kg$^{-1}$).

### 2.2.3.4 Evaporation rate

The evaporation on the surface of the particles depends on the difference of moisture content between the air and the surface of the product, and on the mass transfer coefficient k (m s$^{-1}$).

$$\dot{m} = k(C_{r=R} - C_\infty)$$

where $C_{r=R}$ and $C_\infty$ are respectively the moisture concentration (kg m$^{-3}$) on the surface of the particle and in the drying air.

If we consider an ideal behaviour for gasses, the water concentration can be written as follows:

$$C = P_v \frac{M}{RT} = \frac{M}{R}\frac{P_v}{P_v^{sat}}\frac{P_v^{sat}}{T}$$

Here the dependence of the concentration is on the pressure of water vapor $P_v$ (Pa), the temperature, the constant of ideal gasses and the and the water vapor partial pressure at saturation.

We define the water activity of the product in the region near to the surface, and the relative humidity of air as follows:

$$a_w = \frac{P_{v,r=R}}{P_{v,r=R}^{sat}}$$

$$RH = \frac{P_{v,\infty}}{P_{v,\infty}^{sat}}$$

and from this definition we have an equation for the mass transfer dependent on temperature, saturated vapor pressure of water, water activity and relative humidity:

$$\dot{m} = k\frac{M}{R}\left(a_w\frac{P_{v,r=R}^{sat}}{T_{r=R}} - RH\frac{P_{v,\infty}^{sat}}{T_\infty}\right)$$

At this point, we only need to find a connection between the heat and mass transfer coefficients, and the most commonly used method to relate the two is the Chilton-Colburn's analogy[37] for which mass transfer coefficient can be approximated with the following value:

$$k = \frac{h}{1000}$$

where *h* is the convective heat transfer coefficient.

### *2.2.3.5 Extending the validity of the equations*

In order to expand the validity of the previous balances, made on a spherical geometry, to others ideal geometries (e.g. infinite cylinders), in the work of Lambert et al[24] there is a slight modification of the balances with the inclusion of the shape factor *n* equal to 1 or 2 respectively for cylindrical and spherical shape. Moreover, the authors included the spatial variable z representing the position along the height of the bed so to consider exchanges and transfers on the two directions.

From the Fourier and Fick laws, the mass and heat balances lead in this case at the following equations:

$$\left(\frac{\partial X_t^{r,z}}{\partial t}\right) = \frac{1}{r^n}\frac{\partial}{\partial r}\left(r^n D_{eff}\frac{\partial X_t^{r,z}}{\partial r}\right)$$

$$\left(\frac{\partial Tp_t^{r,z}}{\partial t}\right) = \frac{1}{\rho_{dm}\left(Cp_{dm} + X_t^{r,z}Cp_w\right)r^n}\frac{\partial}{\partial r}\left(r^n\lambda_{eff}\frac{\partial Tp_t^{r,z}}{\partial r}\right)$$

To solve these equations we need some boundary conditions:

1. Moisture content assumed uniform within the particle: $\left(\frac{\partial X_t^{0,z}}{\partial r}\right) = 0$
2. Temperature assumed uniform within the particle: $\left(\frac{\partial Tp_t^{0,z}}{\partial r}\right) = 0$
3. $\rho_{dm}\left(\frac{\partial X_t^{R,z}}{\partial r}\right) = \dot{m} = k\frac{M_w}{R}\left(\frac{a_w P_v^{sat}\left(Tp_t^{R,Z}\right)}{Tp_t^{R,z}} - \frac{RHPv^{sat}(Ta_t^z)}{Ta_t^z}\right)$
4. $\lambda_{eff}\left(\frac{\partial Tp_t^{R,z}}{\partial r}\right) = h\left(Tp_t^{R,z} - Ta_t^z\right) - \dot{m}\,\Delta H_v\left(Tp_t^{R,z}\right)$

In the equations $M_w$ is the molar mass of water and Ta is the temperature of the air.

In the case of deep bed drying balances of heat and matter on the air are also needed. Nevertheless, we only consider the case of thin layer, in which the air does not change its characteristics passing through the product. Consequently, for our scope, is not necessary to detail the balances on the air.

#### 2.2.3.6 The finite volume numerical solution of the equations

The heat and mass balance seen, in order to be solved, must be discretized in some ways. The most common ways of discretizing differential equations are finite difference, finite elements, and finite volume methods[38]. When thermo-physical properties of the material changes during the procedure, finite volume method proved to be adequate. In our application, moisture diffusivity as well as thermal conductivity is subjected to variation in time, and so we used the finite volume method of discretization, of which main passages for a spherical geometry are briefly shown in this paragraph according to the work of Romdhana et al.[36]

We define a network of *N* control volumes $CV_i$ (Figure 33), each of which is characterized by a nodal value at the centre, and two points identified by geographical subscription *e* (east) and *w* (west), useful to define the mass and heat exchanging surface of the control volume. The radius of the spheres is discretized in *N*-2 compartments of size Δ*r* and two compartments of size Δ*r*/2. From this, the discretization step is defined as follows:

$$\Delta \mathrm{r} = \frac{R}{N-1}$$

Each control volume is identified by the radius $r_{ci}$ and the east and west edges $r_{i,e}$ and $r_{i,w}$, defined as follows

$$r_{ci} = (i-1)\Delta r$$

$$r_{i,e} = r_{ci} + \frac{\Delta r}{2}$$

$$r_{i,w} = r_{ci} - \frac{\Delta r}{2}$$

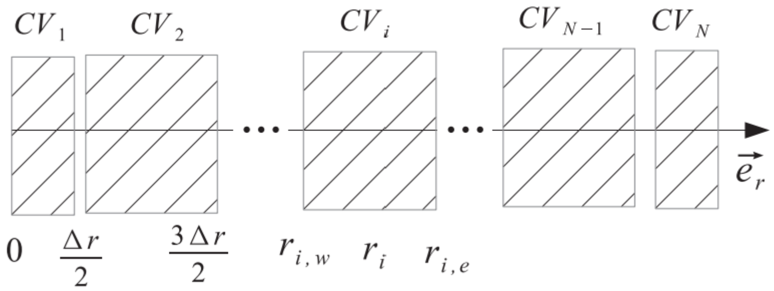

*Figure 33 Scheme of finite volume discretization volume. Romdhana et al*[36]

Integrating the conservation law to obtain the average temperature and moisture content on the control volume, leads to the following expressions:

$$\int_{r_{i,w}}^{r_{i,e}} \frac{\partial X}{\partial t} 4\pi r^2 dr = \int_{r_{i,w}}^{r_{i,e}} \frac{1}{r^2}\frac{\partial}{\partial r}\left(r^2 D \frac{\partial X}{\partial r}\right) 4\pi r^2 dr$$

$$\int_{r_{i,w}}^{r_{i,e}} \frac{\partial(\rho CpT)}{\partial t} 4\pi r^2 dr = \int_{r_{i,w}}^{r_{i,e}} \frac{1}{r^2}\frac{\partial}{\partial r}\left(r^2\lambda\frac{\partial X}{\partial r}\right) 4\pi r^2 dr$$

If we consider the moisture content and the term $\rho CpT$ constant in a control volume, we can simplify the accumulation term:

$$\frac{\partial X_i}{\partial t} = \frac{3}{r_{i,e}^3 - r_{i,w}^3}\left[r_{ci}^2 D\frac{\partial X_i}{\partial r}\right]_w^e$$

$$\frac{\partial T_i}{\partial t} = \frac{3}{r_{i,e}^3 - r_{i,w}^3}\frac{1}{(\rho Cp)_i}\left[r_{ci}^2 \lambda_i\frac{\partial T_i}{\partial r}\right]_w^e$$

Temperature and moisture content gradients at the control volume faces are calculated thanks to a linear approximation of the flux. Thanks to this, temperature and moisture content gradients can be calculated by solving $\frac{\partial X}{\partial r}$ and $\frac{\partial T}{\partial t}$ then by evaluating the result at the neighbour nodes:

$$\left.\frac{\partial T_i}{\partial r}\right|_e = \frac{T_{i+1} - T_i}{\Delta r}$$

$$\left.\frac{\partial T_i}{\partial r}\right|_w = \frac{T_i - T_{i-1}}{\Delta r}$$

$$\left.\frac{\partial X_i}{\partial r}\right|_e = \frac{X_{i+1} - X_i}{\Delta r}$$

$$\left.\frac{\partial X_i}{\partial r}\right|_w = \frac{X_i - X_{i-1}}{\Delta r}$$

A geometrical average between nodal points is used to calculate the transfer properties in the control volume. For thermal conductivity and moisture diffusivity we have:

$$D_{i,w} = (D_{i-1}D_i)^{\frac{1}{2}}$$

$$\lambda_{i,w} = (\lambda_{i-1}\lambda_i)^{\frac{1}{2}}$$

$$D_{i,e} = (D_{i+1}D_i)^{\frac{1}{2}}$$

$$\lambda_{i,w} = (\lambda_{i+1}\lambda_i)^{\frac{1}{2}}$$

Finally, applying the boundary conditions at nodal points *r* = 0 and *r = R* we obtain a system of 2*N* first order differential equations:

For *i* = 1

$$\frac{\partial X_1}{\partial t} = \frac{6}{\Delta r^2} D_{1,e}(X_2 - X_1)$$

$$\frac{\partial T_1}{\partial t} = \frac{1}{(\rho Cp)_1}\frac{6}{\Delta r^2}\lambda_{1,e}(T_2 - T_1)$$

For *i = 2…N-1*

$$\frac{\partial X_i}{\partial t} = \frac{3}{r_{i,e}^3 - r_{i,w}^3}\left(r_{i,e}^2 D_{i,e}\frac{X_{i+1} - X_i}{\Delta r} - r_{i,e}^2 D_{i,e}\frac{X_i - X_{i-1}}{\Delta r}\right)$$

$$\frac{\partial T_i}{\partial t} = \frac{1}{(\rho Cp)_i}\frac{3}{r_{i,e}^3 - r_{i,w}^3}\left(r_{i,e}^2 \lambda_{i,e}\frac{T_{i+1} - T_i}{\Delta r} - r_{i,e}^2 \lambda_{i,e}\frac{T_i - T_{i-1}}{\Delta r}\right)$$

For *i = N*

$$\frac{\partial X_N}{\partial t} = \frac{-3}{R^3 - \left(R - \frac{\Delta r}{2}\right)^3}\left(R^2\frac{\dot{m}}{\rho_{dm}} + \left(R - \frac{\Delta r}{2}\right)^2 D_{N,w}\frac{X_N - X_{N-1}}{\Delta r}\right)$$

$$\frac{\partial T_N}{\partial t} = \frac{1}{(\rho Cp)_N}\frac{-3}{R^3 - \left(R - \frac{\Delta r}{2}\right)^3}\left(R^2(h(T_N - T_\infty) - \dot{m}(\Delta H_v + Cp_v T_N) \ldots \right.$$
$$\left. + \left(R - \frac{\Delta r}{2}\right)^2 \lambda_{N,w}\frac{T_N - T_{N-1}}{\Delta r}\right)$$

### 2.2.4 Estimation of thermo-hydro properties of Cassava necessary for modelling

The geometrical characterization of the products, seen in section 2.1.4, can be easily determined with some laboratory measurements with callipers, sieves or by using image analysis; density and porosity are simply investigated using a pycnometer. Nevertheless, to apply the model to the case of cassava, we need to investigate the thermo-hydro properties of the latter that are required, and it is possible to mostly derive it from literature. They are mostly dependent on state variables like temperature and composition, and this latter can be obtained from U.S. Department of Agriculture and the CIQUAL Nutrient Database for Standard Reference[39]. We can distinguish between predictive and empirical models for the estimation of these properties, with an obvious difference in the extrapolation suitability between the two: empirical models are limited to specific products and operating conditions[24].

However, for the moisture diffusion coefficient, it was necessary to investigate it with an experimental work combined with identification procedures as no method is available for a priori prediction of this property for solid foods. In the following sub-sections, a description of the properties concerned, and their values chosen for modelling, is given.

#### *2.2.4.1 Heat capacity*

The heat capacity (Cp) is dependent on temperature and composition of the product, but most of the literature neglect the dependency of the former[40][41]. Choi and Okos[42] developed an equation for Cp dependent on its composition:

$$c_p = 4.180 \cdot X + 1.711 \cdot x_{protein} + 1.929 \cdot x_{fat} + 1.547 \cdot x_{carbohydrate} + 0.908 \cdot x_{ash}$$

where *X* is the wet basis moisture content, and *x* is the product composition (w.b).

Another generic model is developed by Heldman and Sight[43] and includes the following equation for heat capacity:

$$c_p = 4.180 \cdot X + 1.5949 \cdot x_{protein} + 1.675 \cdot x_{fat} + 1.424 \cdot x_{carbohydrate} + 1.8378 \cdot x_{ash}$$

Other authors measured cassava heat capacity at different moisture content, neglecting the influence of the temperature. It is the case of Njie[40] and Ademiluyi et al [44] that fitted the measurement with a linear equation:

$$c_p = 4.180 \cdot X + a$$

Finally, Gevaudan[28] measured heat capacity on anhydrous cassava roots cause of the influence of gelatinization on the measure, then adding the heat capacity of pure water.

The main and more reliable values for the heat capacity resulted to be the following:

- 1.50 [kJ·kg$^{-1}$·K$^{-1}$] from an average between the measure of Njie and the two generic models, with respect to which there is less than 8% error.
- 1.22 [kJ·kg$^{-1}$·K$^{-1}$] representing a mean value Ademiluyi and Gevaudan measurements.

This second value seems to be consistent since anhydrous cassava is mainly composed by starch, whose heat capacity is 1.2 [kJ·kg$^{-1}$·K$^{-1}$]. Nevertheless, in the model we used the first value, more suitable for moisture containing cassava according to the authors cited. This value can be reasonably used for all the cassava varieties.

### *2.2.4.2 Thermal conductivity*

Conductivity is mostly influenced by the moisture content of the product and temperature dependence is often neglected. Choi and Okos[42] and Sweat[45] proposed generic equations for food conductivity based on its composition:

$$k = 0.628 \cdot X + 0.21 \cdot x_{protein} + 0.10 \cdot x_{fat} + 0.24 \cdot x_{carbohydrate} + 0.37 \cdot x_{ash}$$

$$k = 0.58 \cdot X + 0.155 \cdot x_{protein} + 0.16 \cdot x_{fat} + 0.25 \cdot x_{carbohydrate} + 0.135 \cdot x_{ash}$$

Heat conductivity is not easily measurable on porous medium. In spite of this, Gevaudan [28] used impulsive and continuous heat sources to measure it respectively on 50% w.b. and 52% cassava mash a different porosities. The measure can be satisfactorily approximated with the value from the generic equations only for lower porosity values, otherwise the relative difference is very high. Njie[40] measured conductivity with DSC technique, concluding Sweat model to well predict the value of the thermal conductivity only below a moisture content of 60% w.b. Negligible effect of variety composition differences resulted from the application of the two equations.

Cassava conductivity can be compared with the one calculated for starch granules with a good correspondence, according to the work of Drouzas et al [46], when the moisture content is between 0 and 40%. At very low moisture content modifications in density and porosity occur, leading to a strong decrease of the conductivity.

To obtain a value for *k*, what is usually done is to distinguish two situations: if the thermal conductivity has no strong influence, a value of *k* = 0.22 [W· m$^{-1}$· K$^{-1}$] is acceptable, in the conductivity is instead relevant, we can use the value found for starch granules by Drouzas et al. In our application, on the basis of the composition, a value of 0.4 [W· m$^{-1}$· K$^{-1}$] was chosen

### *2.2.4.3 Sorption phenomena*

Product stability in drying procedures is strongly related to water activity and behavior of the product in water sorption and desorption[47][48]. For this reason, for cassava drying process modelling it is also required to define the water sorption isotherm, in order to have a relation between the moisture content and the water activity in the product at the equilibrium. In this, it comes to our aid the work of Van der Werf et al.[49], a literature review aimed at the attainment of the most generic possible temperature dependent model by fitting all the adsorption and desorption data reviewed. An equation for heat sorption is then deduced from the global model. The validity range of the model found is 25 – 90 °C for temperature and 0.05 – 0.93 for water activity.

The main results are the following:

- Cassava variety and level of transformation have an unclear influence on sorption. However, gelatinization and the adding of oil affects hygroscopicity.
- No relevant hysteresis is detected between sorption and desorption
- Weak hygroscopic modifications with temperature

The equation of sorption/desorption isotherm and heat of sorption/desorption are the following:

$$X = \left(\frac{\exp(-0.0142998 \cdot T_K)}{-\log(a_w)}\right)^{1/1.83388}$$

$$L_p = 7.0903 \cdot X^{-1.792} + L_v$$

where $a_w$ is the water activity, $X$ the moisture content dry basis, $T_K$ the temperature (K), $L_p$ the cassava heat of sorption (kJ·kg$^{-1}$), $L_v$ the latent heat of vaporization of free water (kJ·kg$^{-1}$). The corresponding isotherm and generic heat of sorption curves are shown in Figure 34 Sorption/desorption isotherm of cassava from the fitting work of van der Werf et al[49]Figure 34 and Figure 35.

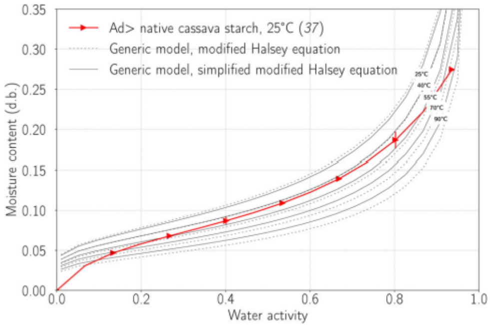

*Figure 34 Sorption/desorption isotherm of cassava from the fitting work of van der Werf et al*[49]

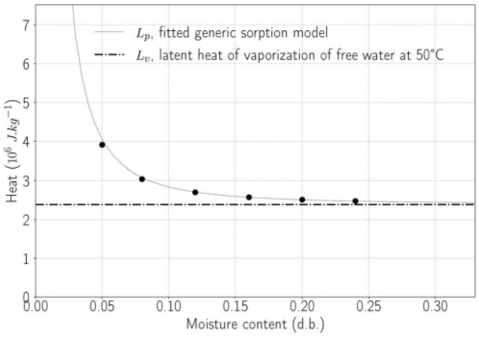

*Figure 35 Heat of sorption of cassava compared to heat of vaporization of free water*[49]

### *2.2.4.4 Diffusion coefficient*

Moisture content of cassava moves from the internal part of the cassava product toward the surface thanks to diffusion mechanism. Water moves through macroscopic medium (cassava dry matter) by mean of molecular agitation until equilibrium is reached[50]. To characterize diffusivity we need diffusion coefficient, an intrinsic property of the material dependent mostly on moisture content, structure of the product's cells and temperature[51]. During drying procedure, the structure of the food can change, facilitating or worsening the diffusion of water. As an example, the modification of starch grain structure during drying, increases diffusivity by creating channels in which the movement of water is facilitated[52].

Due to the need of control of a large set of parameters, a direct measurement of the diffusion coefficient is difficult to be implemented, but a simpler way, using the experimental drying curves and deducing the value for the diffusion coefficient from the Fick law, is possible and is the technique used by many authors in literature. The values of the effective diffusion coefficient obtained in this way are not dependent on moisture content and porosity. In Table 6 a list of the values found by different authors for the diffusion coefficient of some cassava derived products, detailing the initial moisture content, the air temperature and the drying equipment employed.

*Table 6 Cassava products effective moisture diffusivity*

| **Product** | **$D_{eff}$ ($m^2 \cdot s^{-1}$)** | **Initial moisture (% w.b.)** | **Air T (°C)** | **Drying equipment** | **Reference** |
|---|---|---|---|---|---|
| Casava flour | $1.74 \cdot 10^{-10}$ | 45 | 140 | Conductive rotatory dryer | Sanni et al. [22] |
| Gari | $4.51 \cdot 10^{-10}$ | 45 | 200 | Conductive rotatory dryer | Sanni et al. [22] |
| Fermented ground cassava | $1.32–3.52 \cdot 10^{-9}$ | * | 115-230 | Bench rotatory dryer | Ademiluyi et al[41] |
| Cassava chips | $2.43–4.52 \cdot 10^{-11}$ | 82 | 60-80 | Tunnel dryer | Stephen Ajala et al. [53] |
| Cassava chips | $7.31\text{-}8.06 \cdot 10^{-7}$ | 13 | 60 | Hot air tray dryer | T.Tunde-Akintunde et al[54] |

| | | | | | |
|---|---|---|---|---|---|
| Cassava chips | 3-30 $\cdot 10^{-11}$ | ** | 55 | Convective tunnel dryer | Lopez-Ortiz et al. [55] |
| Cassava pellets | 1.4-2.3 $\cdot 10^{-9}$ | 76-78 | 66-81 | Convective tray dryer | Onyemazuwa et al.[56] |
| Cassava chips | 1.57-2.15 $\cdot 10^{-9}$ | ** | 40-70 | Cabinet dryer | Chavez-Méndez et al.[57] |

* Pressed cassava pulp had around 45% moisture content w.b

** Cassava root moisture content around 60-65% w.b

Discrepancies in a wide range of values between the various data are visible. Panagiotu et al. reviewed 1773 food product diffusivity, stating that the values found were in the range $10^{-12} - 10^{-6}$ [$m^2 \cdot s^{-1}$] with a large majority between $10^{-8} - 10^{-11}$[$m^2 \cdot s^{-1}$]. Most of the values shown in Table 5 are consistent with the range predicted. Nevertheless, the difference between the values found in the data reviewed is huge, considering the common medium, whilst allowing some difference due to the structure of the product (we expect cassava chips or pellets to have a different diffusivity with respect to mashed of gelatinized cassava). This notwithstanding, no precise correlation between the product structure and the values found for the coefficient can be highlighted. A possible reason for the evidence of the wide range of $D_{eff}$ found for the same medium, can be ascribed to the different experimental condition of drying equipment, air temperature and initial moisture content, or, more likely, to different analysis methods.

The result is an overall unreliability of the data from literature, and the need to identify the diffusion coefficient, preferably in the range $10^{-9} - 10^{-11}$[$m^2 \cdot s^{-1}$], with data fitting and optimization based our experimental work. In order to do so, parameter optimization was conducted on a temperature dependent equation for the diffusion coefficient. As a matter of fact, the dependency on porosity was not taken into account for thin layer simulations, and the dependency on the product moisture content, initially considered, proved to be feeble. As a result, the optimization was made on the parameters a and b of the following equation

$$D_{eff}(T) = a \cdot \exp\left(-\frac{b}{T_p}\right)$$

where $T_p$ is the temperature of product (°C)

The equation is a modified version the one proposed by Zogzas et al.[58] for granular starch, that also contains the dependency on moisture content, resulting in a three-parameter equation:

$$D_{eff}(X,T) = a \cdot \exp(b \cdot X) \cdot \exp\left(-\frac{c}{T_p}\right)$$

where $a = 5.321 \cdot 10^{-6}, b = 1.511$ and $c = 2848.5$ when $0.05<X<5.0$ and $298<T<413$ at atmospheric pressure.

As the dependency on the moisture content didn't really prove to have a huge influence on the outcomes, we decided to remove this dependency in favor of slender computational calculations requiring, 2-parameter equation. The identification method used in the present work for the parameters of the previously mentioned equations is the Nelder-Mead one, of which is given a basic insight in the following section.

### 2.2.5 The Nelder-Mead optimization method

The Nelder-Mead algorithm[59], originally conceived by Nelder and Mead in 1965 is a widely used method for multidimensional unconstrained optimization (treated in the best-seller *Numerical Recipes*[60] and in *Matlab* [61]). The methods revealed to be suitable for parameter estimation also in problems with non-smooth functions, typical in chemistry and medicine. A detailed description of the method is outside from the scope of the present work and only a basic description of the main optimization steps is reported [62]. The interested reader is invited to consult the literature, of which is provided a starting point, for a deeper insight.

The method belongs to the so called "Direct search methods"[63] and is based on a simplex in $R^n$ with $n+1$ vertices identified with the points $x_0,\ldots x_n$. To each point corresponds a function evaluation $f_j := f(x_j)$ for $j=0,\ldots,n$. The initial simplex is usually constructed around the al point $x_0$ and it can have two standard shapes: right-angled at x0 and $x_j = x0+h_je_j$ where $h_j$ is the step size in the direction of the vector $e_j$ in $R^n$, or a regular simplex with all the edges with the same length [62][64].

At each iteration of the method, three steps are subsequentially performed:

1. Ordering: setting of $h,s,l$ indices so that $f_h = max_j f_j$, $f_s = max_{j\neq h} f_j$ and $f_l = min_{j\neq h} fj$
2. Centroid calculation: $c = \frac{1}{n}\sum_{j\neq h} \mathrm{h}(x_j)$.
3. Transformations of the current simplex by computing a new one using reflection, expansion, or contraction with respect to the line connecting $x_h$ and c with the aim to substitute $x_h$ with a better point. If a new accepted point is found, then it replaces $x_h$, otherwise the simplex "shrinks" in the direction of $x_l$.

The transformation step is controlled by parameter $\alpha$, $\beta$, $\gamma$ and $\delta$ respectively for reflection, contraction, expansion and shrinkage. These parameters are subjected to constraints: $\alpha > 0$, $0 < \beta < 1$, $\gamma > 1$ $\alpha > \delta$ $0 < \delta < 1$. According to this, some standard values are widely used for these parameters:

$\alpha$ = 1 $\beta$ = ½, $\gamma$ = 2 $\delta$ = ½, with some variations[65].

The procedure described is iterative and it stops when one of the following conditions is reached:

- Domain convergence: the simplex becomes small enough that the vertices overcome a certain minimum distance
- Function value convergence: the functions evaluations are close enough
- Non-convergence if the number of iterations exceeds a certain value set by the user[62]

### 2.2.3 Data processing

#### *2.2.3.1 Minimization procedure – definition of parameter j*

The model with the Nelder-Mead minimization method were implemented on Python in order to obtain the simulated curves. The minimization procedure was aimed to find the parameters for the temperature dependent equation for the effective diffusion coefficient, and it is an iterative procedure initialized with two parameters taken from the work of Zogzas et al.[58] and relative to starch. The initial value for the *a* and *b* parameter are:

$$a = 5.321\mathrm{e}-6\ [m^2/s] \quad b = 2848.5\ [\mathrm{K}]$$

To avoid numerical inconsistencies, cause of the huge difference on the order of magnitude between the two parameters, they are passed to the function in the form of logarithm.

The minimization is done the j parameter, expressing the relative differences between the experimental and the simulated curve, expressed as follows:

$$j = \frac{(X_{simu} - X_{exp})}{X_{exp} \cdot N_p}$$

where $X_{simu}$ is the moisture content of the points of the simulated curve, $X_{exp}$ are the ones of the experimental drying curve, and $N_p$ is the number of points of the experimental curve. The latter was included to take into account the fact that not all the curves have the same number of points. The iterations continue until tolerances are reached for the value of j or the maximum number of iterations is exceeded. The default tolerance of the Nelder-Mead method when implemented on Python, maintained for our applications, is 0.0001 both for domain and function value convergence. The imposed value for the maximum number of iterations was instead 200.

#### 2.2.3.2 Experimental basis for identification of $D_{eff}$

To be applied, the model requires information about other product's properties like heat capacity and thermal conductivity, as well as its geometrical characterization. The latter is easier and more precise when is done on cylindric shaped products with respect to the others since it can be obtained by direct measurement of length and diameter. On the contrary, the measure of the thickness of the powder layer must be done indirectly (Section 2.1.6.3 Evaluation of the shrinkage), and the particle size distribution of the spheres is obtained by granulometry (Section 2.1.6.2). For this reason, for a first identification of the diffusion coefficient, we relied on the experimental kinetics obtained on raw cassava cylinders.

As rasping and mechanical dewatering by pressing seems to have negligible effect on diffusivity of water in the product (Section 3.1.1.3), what expected is to find the same value for the diffusion coefficient for all the various products at different level of processing. Based on this, the value of the diffusion coefficient identified on raw cylinders is applied to powder in cross and parallel flow. As a further confirm of the found values, the identification was also done basing drying curves obtained on powder in parallel flow. For the final validation, a computer with high computational power was employed to identify the parameters of the effective diffusion coefficient equation on all the available kinetics of powder and cylinders, in all the conditions, at the same time.

#### 2.2.3.3 Error bar

In the Result and Discussion Section, drying kinetics will be presented both to analyse the behaviour of cassava in drying and for the modelling and identification part. The experimental curves will be characterized by an error bar: it represents the standard deviation between the points of the drying curves obtained in the same conditions as repetitions. The standard deviation was calculated on the values of the moisture content at several time steps. A trend for the standard deviation with respect to moisture content $\sigma = f(X)$ was then achieved: a linear behaviour was found for both powder and cylinders

### 2.2.3.4 Modelling the behaviour of a population of spheres having a wide range of particle sizes

Powder dried in cross flow behaves differently from the one dried in lateral flow, and they can't be modelled in the same way. As it will be better discussed in the section "Result and Discussion" of this work, the former can be treated as a population of independent spheres, while the latter is better approximated by a slab of porous material. Here we focus on the first case and how a population of spheres with different sizes can be treated in the modelling phase, being the simulated curves strongly dependent on the chosen value for the radius.

From granulometry we obtained several classes of particle, each in a range of sizes and characterized by a mass fraction with respect to the total. Thus, the simulations are made with each value of particle size, obtaining a set of simulated drying curves each corresponding to a different radius for the particles. Ponderation of the kinetics of each particle size is then done by the mass proportion, basing on the mass fraction of each class, given by the particle size distribution. Lastly, the final kinetic is obtained by summing the pondered ones. This way is proved to better approximate the experimental drying curve with respect to the application of an average or median diameter on one single simulation. In Figure36 an example of simulated ($D_{eff}$ optimized) and experimental curve. The various grey curves (increasingly darker with the lower radius) visible in the image are the kinetics obtained with each value of the diameter obtained by granulometry. The blue curve is the final one, obtained with the technique just described.

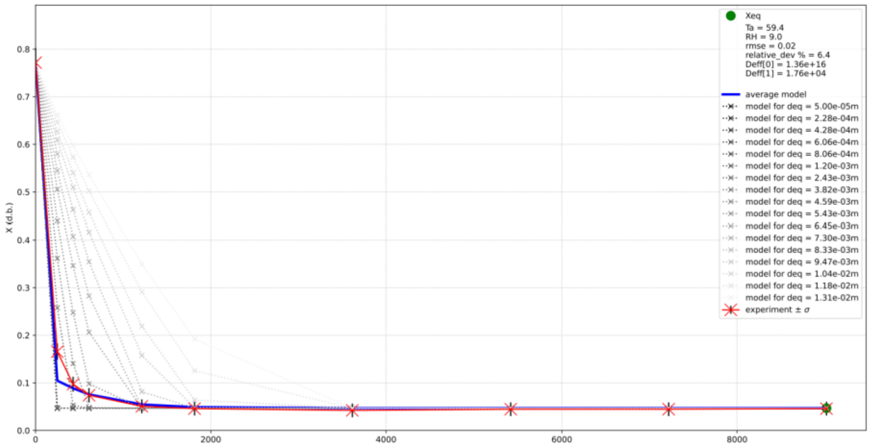

*Figure36 Simulated drying curve obtained by ponderation and sum of the kinetics simulated with every radius from granulometry*

## 2.2.4 Fourier's Abacus

To further confirm the reliability of the outcomes of the identification, a comparison with the values found for the diffusion coefficient in the Abacus graph (Figure 37)[66] can be done. This graph is conceived for the heat diffusion but is easily convertible to matter diffusion replacing temperatures with moisture content on the ordinate axis. In the graph we can see three curves representing different ideal geometries: cylindrical, spherical, and of infinite slab. On the abscissa axis we have instead an expression including a characteristic dimension (thickness of the slab or diameter for cylinder and sphere), time and diffusion coefficient.

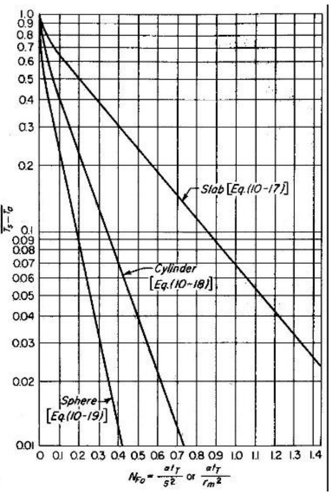

*Figure 37 Average temperature during unsteady state heating or cooling of a large slab, an infinitely cylinder or a sphere*[66]

Using the values of moisture content and elapsed time taken from the drying kinetics, and the dimension of diameter or thickness characterizing the various products, it was possible to derivate a value for the diffusion coefficient. In the following sub-sections, a deeper explanation of the outcomes from identification of the diffusion coefficient and the application of the latter to the different geometries and on products at various level of processing. Identification was also performed basing on the kinetics of powder in parallel flow, modelling it as a porous slab instead of independent spheres. Finally, thanks to the use of a computer with a stronger computing power, identification was done on all the geometries at the same time. The values of the parameters identified, and the diffusion coefficient ranges explored, are discussed and compared between each other and with the values from the Abacus graph.

# 3 Results and Discussion

## 3.1 Experimental analysis of cassava products drying

The experimental work led to the attainment of some kinetic data that are presented and commented here. As previously mentioned, the trials were carried out in traversing and parallel mode, in all cases accompanied by the characterization of the product and of the air flow.

### 3.1.1 Analysis of the results and repeatability/reproducibility tests

As a first step, is important to validate the procedure used for the experiments on the pilot equipment. This is done by repeating the experiment in the same conditions in the same equipment, testing its repeatability, then transferring it on a different equipment to test its reproducibility. The outcomes are encouraging and seem to validate the procedure used. In the following sub-sections, the obtained drying curves are commented and analysed, and some considerations about repeatability and reproducibility of the experiments are given.

#### *3.1.1.1 Cross flow drying – powder*

The repeatability test on powder in traversing flow drying was made by repeating the same experiment three times. The velocity of the air was around 1.83 m/s for all the trials and temperature and relative humidity of the air tested were respectively 40°C and 21%, 60°C and 8% and 80°C and 8%. The quantity of powder in the rack is 125 g, corresponding to an initial average thickness of the product layer of approximately 4 mm (see Table 2 in section 2.1.2). The results are shown in Figure 38, Figure 39, and Figure 40, where the two graphs represent respectively the kinetic of drying (product dry basis moisture content on the Y axis and time on the X axis), and the rate of drying $\left({}^{dX}/_{dt}\right)$ with respect to the moisture content of the product. The same structure of representations is maintained for the description of all the manipulations presented in this section.

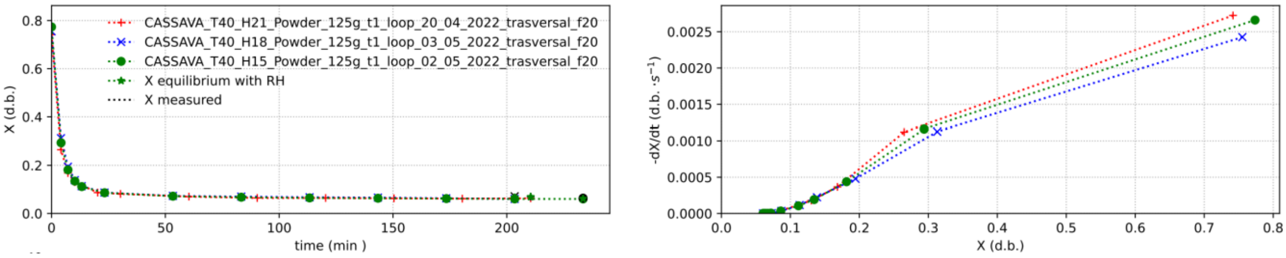

*Figure 38 Repeatability test on powder in traversing mode. T=40°C HR = 21% v = 1.83 m/s*

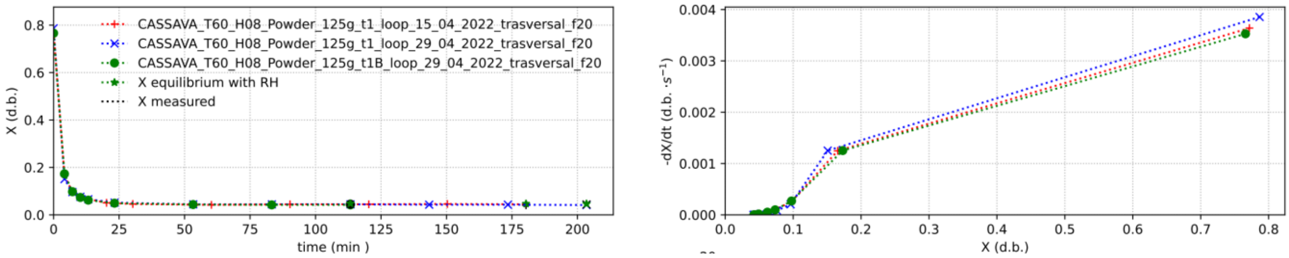

*Figure 39 Repeatability test on powder in traversing mode. T=60°C HR = 8% v = 1.832 m/s*

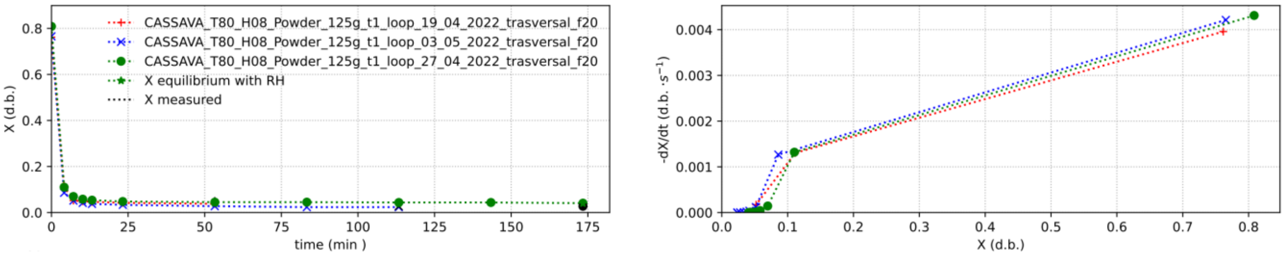

*Figure 40 Repeatability test on powder in traversing mode. T=80°C HR = 8% v = 1.832 m/s*

As visible, for the three air conditions the procedure allowed to obtain a good repeatability of the results. The shape of the curves shows that the first phase of drying is absent, so no "warm up" phase is visible in these trials. On the contrary, a fast initial decrease of moisture content is found in all the conditions, although being more relevant with the increase of the air temperature. The kinetic curves are calculated starting from the initial measured moisture content, and the graphs also show the measured end-point moisture content, to be compared with the calculated one as a validation: the two coincide for all the tests. The equilibrium point calculated with the sorption isotherms according to the relative humidity of the air is also shown in the graphs, and what we can see is that, mostly, the drying reaches the equilibrium point at the end of the process. The graph representing the drying rate with respect to the moisture content must be read from right to left: the first point on the right represents the starting point of the curves. The rate has a decreasing trend with different slops: the drying of the product is initially very fast when convective mechanism is more relevant, and then decreases at lower values of moisture content where diffusion is instead the limiting phenomena. The reason behind this evidence, and the limitation imposed to diffusion by the structure of the aliment and the diminishing of the internal concentration gradient, are better discussed in section 2.2.1 of this Thesis. The equilibrium value for the moisture content is achieved at different times depending on the drying air conditions: at 40°C is roughly reached after 125 minutes, decreasing to around 50 minutes at 60°C and 25 minutes at 80°C. The difference in the drying rate according to the air conditions is better appreciable in the second graph in Figure 41.

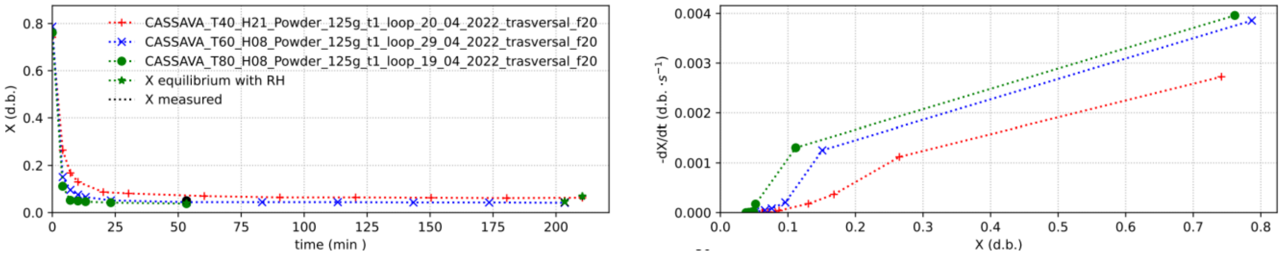

*Figure 41 Comparison between kinetics on powder in cross flow drying in different air conditions: T=40 HR=21% (red curve),T=60 HR=8% (Blue curve),T=80 HR=8% (green curve)*

To test reproducibility, some trials were done using the drying equipment of A.T.A laboratories on powder in cross flow. Figure 42 shows two trials made in cross flow on 130 grams of mechanically pressed product, with the temperature set at 60°C, and the relative humidity at 8%. The only difference is the air velocity: in the A.T.A dryer was set at 1 m/s, instead for the CIRAD loop dryer we have 1.832 m/s as minimum value. The initial thickness of the layer of cassava on the tray is around 4 mm.

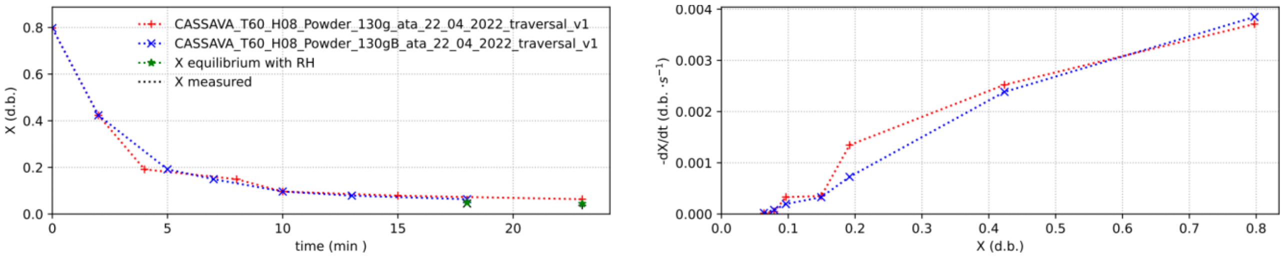

*Figure 42: Repeatability test A.T.A. dryer: kinetic and drying rate, traversing, T 60°C, HR 8%, 130 g, 1m/s*

Figure 43 shows on the same graph the drying curves obtained from both the trials made with CIRAD and A.T.A equipment in the same conditions of T and RH.

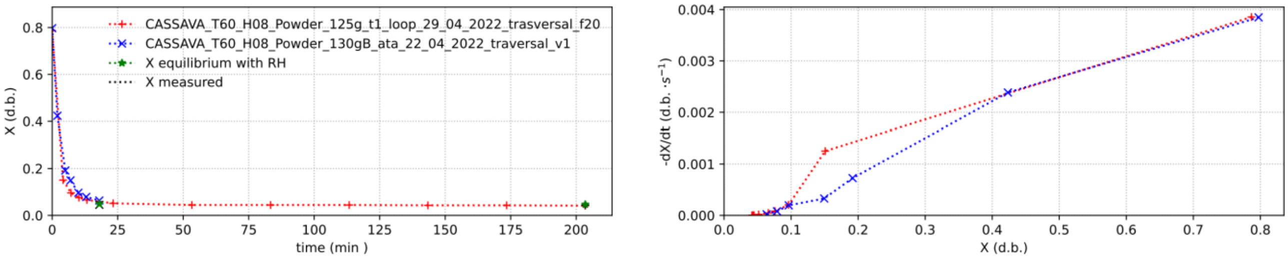

*Figure 43: Comparison between kinetics obtained from A.T.A (blue curve). and CIRAD (red curve) dryers in traversing mode on powder*

As we can notice, the red curve representing the manipulation on A.T.A. dryer stops just when a critical value for the moisture content of the product is roughly reached. Nevertheless, the two curves show a very similar shape, despite the difference in the air velocity. There could be many reasons behind this evidence: we can venture that, in this range, the velocity of air does not significantly affect the drying rate, but it is also worth noting that there are only a few measurements in the first, fast phase of the process. A larger number of experimental points could lead to a more precise and reliable curve but, unfortunately, for the powder-shaped products, it results to be very difficult to sample the weight of the product in the first phase, without affecting the drying process. The air flow in the chamber can also be not uniform, as well as the measurement of the air velocity can have some uncertainty.

From what is visible in the graph, the reproducibility of the experiment is well reached, since a similar shape for the drying curve and the drying rate for the two experiments conducted on the two pilots is shown.

#### 3.1.1.2 Cross flow drying – raw cylinders

Drying procedures applied on cylinders in cross drying were also triplicate for each air conditions. As for powder, the three set-point temperatures for the experiments were 40°C, 60°C and 80°C, with a relative humidity of 21% for the 40°C trials and of 8% for the others. The reason of this difference lies on the limited relative humidity values that can be explored by the equipment at lower temperatures, since no condenser is installed. Figure 44, Figure 45, and Figure 46 show the graphs with the results of the various trials made on raw cylinders, confirming a good repeatability of the experiments since the various drying curves almost overlap. No reproducibility test is available since no trial is being made on cylinders on another pilot.

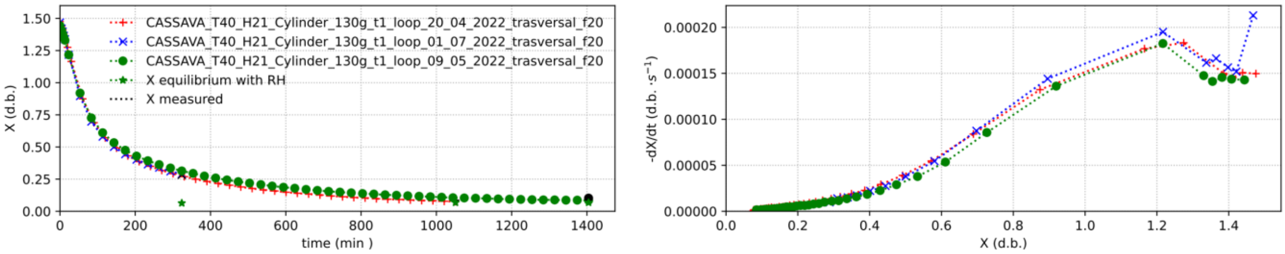

*Figure 44: Repeatability test on raw cassava cylinders in cross flow. T=40°C HR = 21% v = 1.832 m/s*

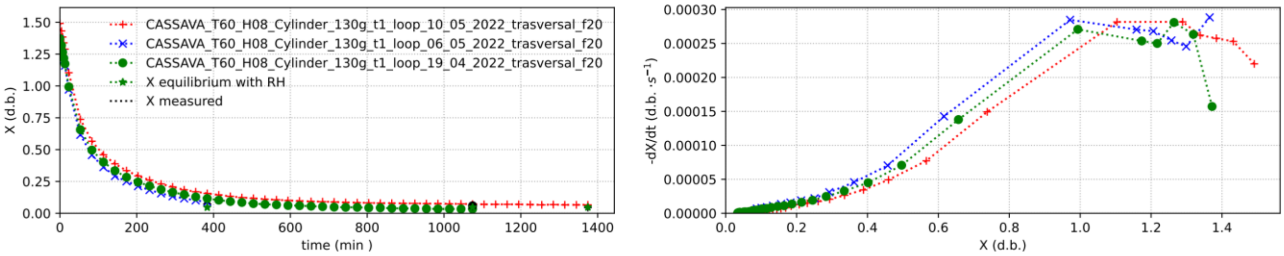

*Figure 45 Repeatability test on raw cassava cylinders in cross flow. T=60°C HR = 8% v = 1.832 m/s*

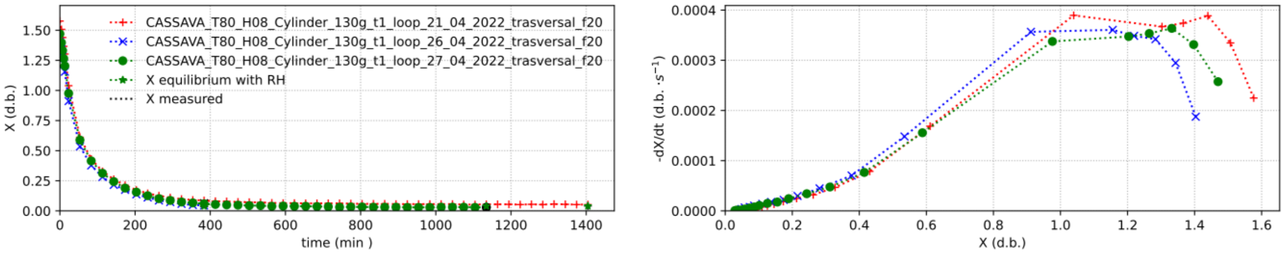

*Figure 46 Repeatability test on raw cassava cylinders in cross flow. T=80°C HR = 8% v = 1.832 m/s*

As it can be noticed, the starting value of the moisture content here is higher than the one we had with powder, since here we used a raw product coming directly from the cassava root; on the contrary, the powder results from grounding and then pressing raw cassava, so the moisture content is lowered. The drying kinetic is much slower than the case of powder and the “warm-up” phase is here visible, especially in the drying rate graph, in which the decreasing trend with different slopes we already saw for powder, is now preceded by an increasing and an about constant one. The same behaviour is noted for most of the trials made.

Cylinders expose a smaller surface area to the hot air flow with respect to powder, and the distance that the moisture must cover diffusing from the bulk toward the surface, where it is removed by convection, is higher. This explains the difference in the time needed to reach an equilibrium value for the moisture content and the reason behind the fact that the drying rate is one order of magnitude smaller than the one characterizing the ground and pressed product. The mechanisms occurring during the first phase of drying are usually difficult to describe precisely because of the large number of contingencies that can occur. This is the reason why this part of the curve is usually not modelled[32]. In our case, a possible reason can reside on the high value of initial moisture content that leads to the need to warm up a large quantity of water. Sensible heat moves from the hot air to the product, increasing the temperature of the water before reaching the equilibrium evaporation rate.

Again, air temperature and relative humidity heavily influence the drying behaviour of cassava in drying, modifying the shape of the curve and the speed at which a critical value for the moisture content is finally reached. In Figure 47, three trials at different air characteristics are shown on the same graph, and the relative curves of drying rates.

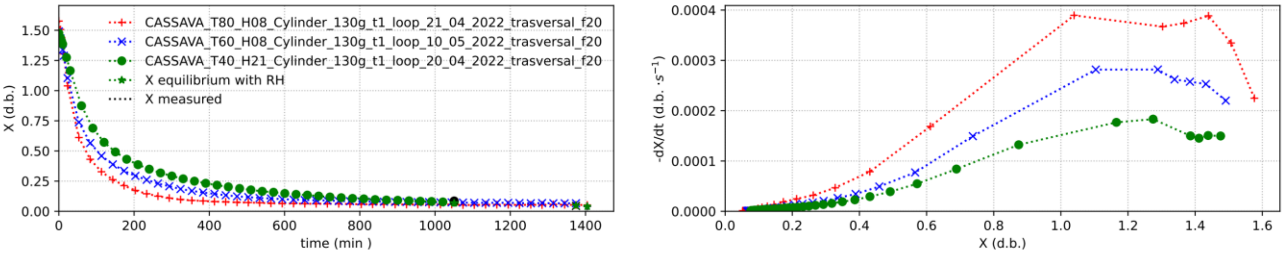

*Figure 47 Comparison between kinetics on raw cassava cylinders in cross flow drying in different air conditions: T=40 HR=21% (green curve), T=60 HR=8% (blue curve), T=80 HR=8% (red curve)*

### 3.1.1.3 Cross flow drying - powder and mash made cylinders

The willingness to have an idea of how the level of processing influences the cassava behaviour in drying led us to subdue also powder made cylinders, and mash made ones, to thermal dewatering. The effect of porosity is also being investigated since powder-made cylinders at two different levels of porosity were available (see section 2.1.1.4). The same dimensions of the raw cassava cylinders were kept in order to have a meaningful comparison between the various cylindric-shaped products, and the conditions of the hot air stream were 60°C of temperature, a relative humidity of 8%, and a velocity of 1.832 m/s. In Figure 48 the graphs referring to the mash made cylinders drying kinetic and rate, and in Figure 49 for the two powder made ones at different porosities (trials repeated twice). As we can see the starting moisture content for the two kind of products is different as the mash is not pressed, and its moisture content is close to the one of raw cassava (only little losses can be due to the procedure of root grinding). In order to account for this difference and still compare all the cylindric-shaped products, the graph referring the drying curve in Figure 50 has, on the vertical axis, the moisture content divided by the value of the initial one for each curve. In this way the starting point is the same for all and a comparison on the shape of the curve can be easily done. In the graph it is also included the curve referring to the raw cassava cylinders dried in the same conditions as the other products.

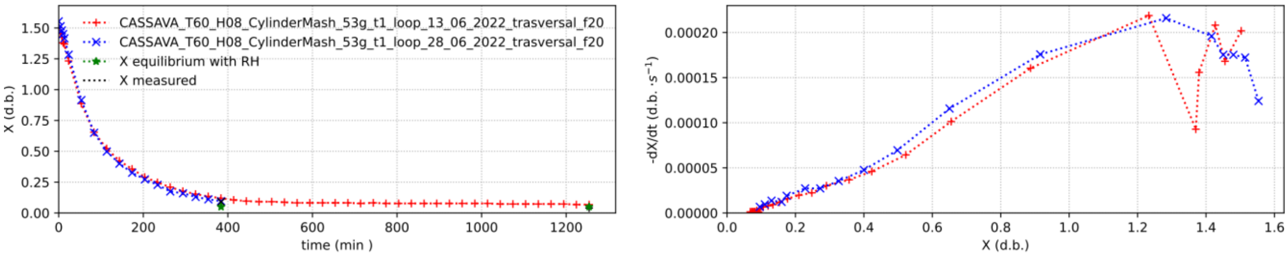

*Figure 48 Repeatability test on cassava mash made cylinders in traversing mode. T=60°C HR = 8% v = 1.832 m/s*

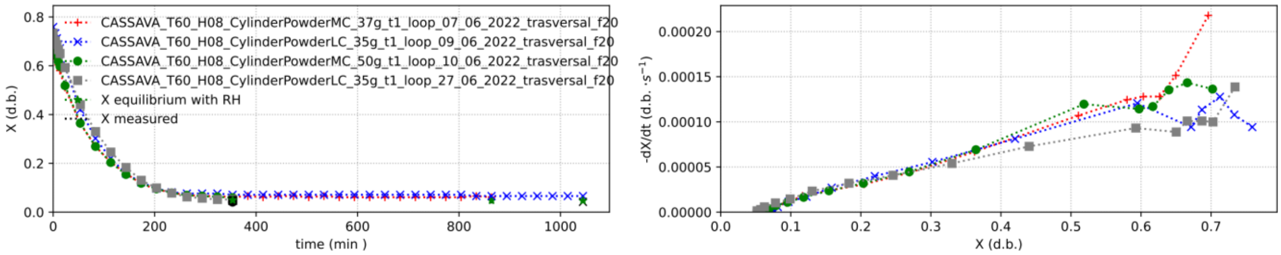

*Figure 49 Comparison between trials on cassava powder made cylinders of different porosities, in traversing mode. T=60°C HR = 8% v = 1.832 m/. High porosity cylinders (blue and grey curves) and low porosity (red and green curves)*

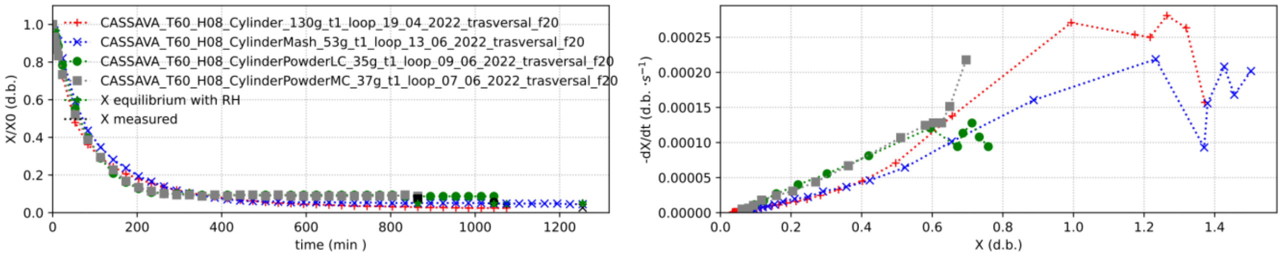

*Figure 50 Comparison of all cylindric products: red curve for raw cylinders, blue curve for mash made ones, green curve for high porosity powder made cylinders, grey curve for low porosity powder made ones.*

It is possible to highlight a good repeatability of the experiments also in this case, whether concerning the two trials on mash, the two on low porosity powder made cylinders(blue and green curve in the graphs of Figure 50) and the two on highly porous ones (red and grey curves in the graphs of Figure 50). The samples had all the same initial shape, length, and dimeter. Volumetric shrinkage occurred in raw cassava cylinders as discussed in section 2.1.4.4, almost no shrinkage occurred instead for the powder made low porosity cylinders. For the other two kinds of products, it was not possible to evaluate the shrinkage because of the fact that, once the external structure was removed, they lose their structure, and no measures of length or diameter could be done.

The interesting result of the comparison shown in the left graph of Figure 50 consists in the fact that almost no differences are detectable between the drying curves. So, the various levels of processing seem to have negligible influence on the shape of the curve. Moreover, also the effect of porosity seems to be negligible, as the drying rate curves overlap for most of the drying process. There are no clear reasons behind this evidence, that seems to suggest us that the cellular structure of the products has slight influence on the behaviour of cassava products in drying, and consequently on diffusivity. Nevertheless, some hypothesis can be done. The different processing level passing from root to mash and then to powder changes the internal structure of fibres and cells of the product. Initial moisture content also changes among the various products, having an effect, although minor, on the internal moisture transfer mechanisms. Surfaces evaporation of water is instead dependent on the condition of the air approaching the surface and the surface itself. The external container used on the highly porous cylinders and the mash made ones influences the air flow since it has to pass through the grid of the item before reaching the product: the section of passage changes and the velocity varies alongside with a variation of the aerodynamics around the cylinders. A combination of these and other factors can be hypotized as possible reasons behind the obtained results. Nevertheless, a deeper study of the various effects can be conducted, so to better explain the absence of significative differences among the trials. As only contribution to this scope, a study of diffusivity is done and described in section 3.2 of this Thesis, verifying if the same value for diffusivity can lead to a good prediction of the experimental curves of differently processed cassava products.

### 3.1.1.4 Parallel flow drying - powder

Parallel flow drying was applied to cassava powder in both pieces of equipment considered in this work. Experiments were repeated to assure repeatability under different air conditions, and different values of air velocity were also tested to investigate its effect.

At first, we consider the drying kinetics obtained employing the CIRAD loop dryer. As usual, drying rates at 40 °C, 60°C and 80 °C were investigated, with a relative humidity of the air of respectively 21%, 8% and 8%. The velocity of the air is the minimum value available for this equipment, namely 1.83 m/s. The product was put on a rack suspended on a scale that measured the weight in continuum; the weight is sampled by the user after the air deviation, with an opportune frequency. The quantity of powder on the tray assured an average thickness of the layer of around 4 mm. The repeatability tests are shown in Figure 51 for the 40°C, 21% RH trial, in Figure 53 for the 80°C, 8% RH one, and in Figure 52 the only one trial made at 60°C, 8% RH.

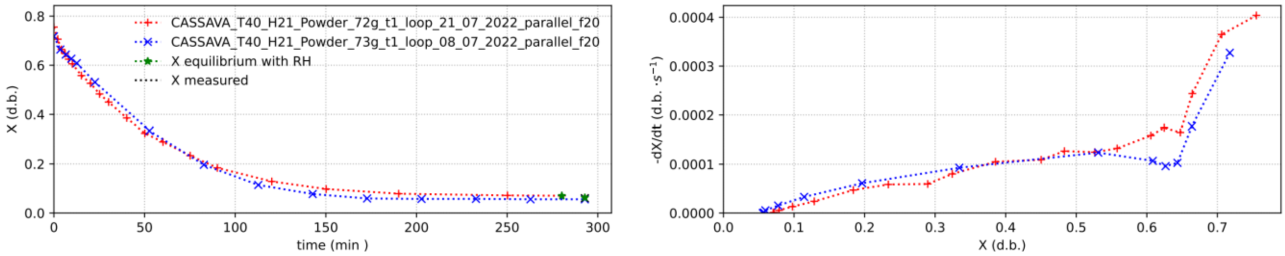

*Figure 51 Repeatability test on cassava powder in lateral drying. T=40°C HR = 21% v = 1.832 m/s*

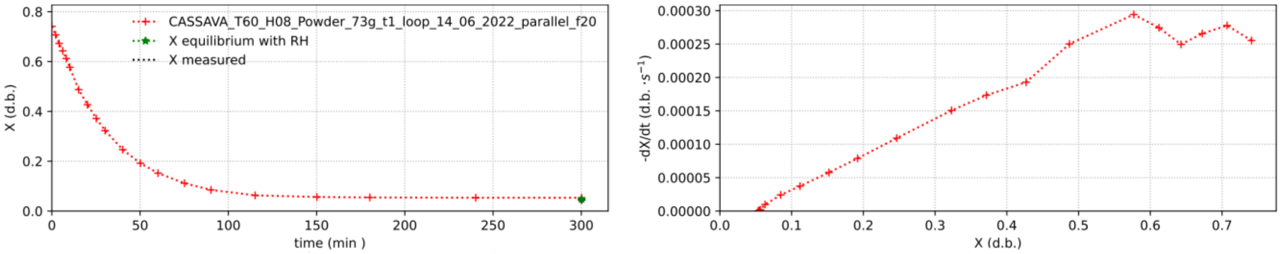

*Figure 52 Cassava powder in lateral drying. T=60°C HR = 8% v = 1.832 m/s*

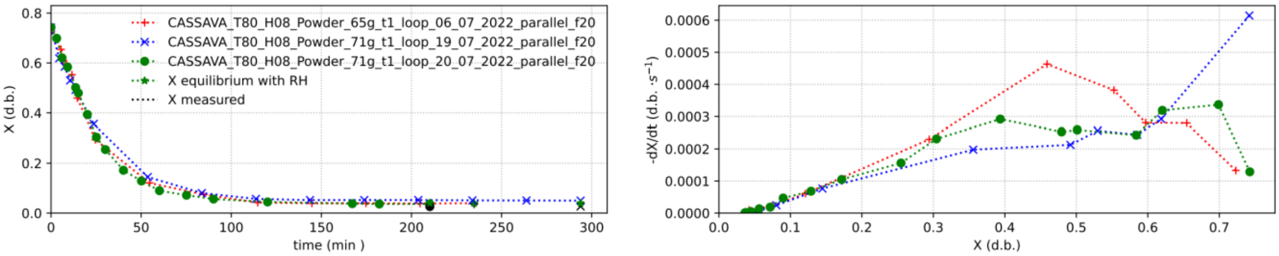

*Figure 53 Repeatability test on cassava powder in lateral drying. T=80°C HR = 8% v = 1.832 m/s*

In the trials for which we have repetitions we can see the a good repeatability is reached. Little discrepancies in the initial part of the drying rate curve are visible for the 80°C trials, still not sufficient to invalidate the test: the procedure employed can be considered valid also in parallel drying of powder.

In Figure 54 we can see a comparison between the outcomes from drying made in the same temperature and humidity conditions, in different pilot dryers. The only difference between the two experiments was the air velocity: 1,83 m/s for the CIRAD dryer and 1 m/s for the A.T.A one. There is a huge difference in the quantity of cassava processed: 195 g in A.T.A. dryer and only 73 g in the CIRAD one. The focus, indeed, is to compare two experiments characterized by the same thickness of the powder layer on the rack; hence the different quantity is directly linked to the different surface of the tray on which the powder is placed.

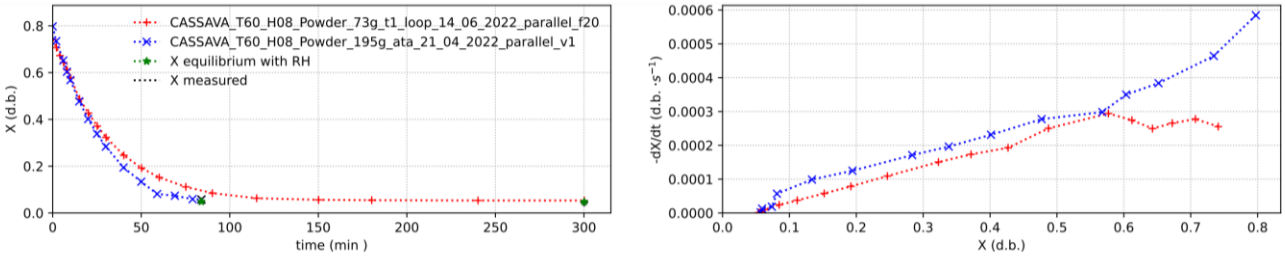

*Figure 54 Comparison between trials in lateral drying on powder made on different pilot dryers. T = 60 °C HR = 8%*

The two curves show some discrepancies after the first 20 minutes of drying: the essay conducted in CIRAD exhibits a slightly slower rate and a critical value for the moisture content is reached after around 130 minutes of drying, much more with respect to the 80 minutes needed in the A.T.A. dryer. Moreover, in the drying rate graph the red curve is placed in a lower position. This is in contrast with what we expected since an increased value of the air velocity is normally connected to a faster drying. Nevertheless, as previously mentioned, pilot equipment like the ones used in this experimental work are characterized by irregularities in the air flow due to the presence of elbows and valves in the vicinity of the drying chamber: it is therefore possible that the velocity near the product does not have the same value measured upstream and downstream the chamber, and aerodynamic can also vary according to the equipment and the height at with the rack is placed inside the chamber. This fact can explain the differences we observe in the two drying rates obtained in the two pilots.

Other trials were conducted using A.T.A pilot dryer, with the objective to investigate repeatability and the effect of air velocity, since low values of the latter are achievable with this equipment. For this reason, an experimentation was done in parallel flow drying using 4 different trays, divided into two pairs placed in series (see the scheme in Figure 55) on the same rack. Since the trays had different distances from the air inlet, the idea was to look for differences in the drying rate that could be addressed to a change in relative humidity of the air while passing from trays 1 and 2, before reaching trays 3 and 4.

*Figure 55 Scheme of the position of the trays and direction of the air flow*

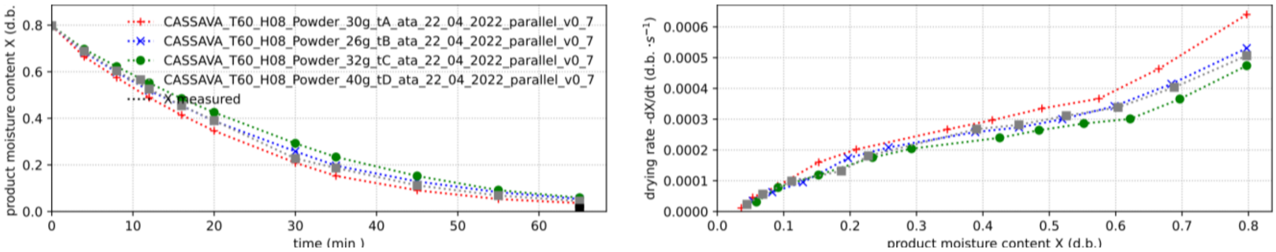

*Figure 56 Kinetic and rate of drying for parallel drying, T 60°C, HR 08%, 0.7 m/s, different trays.*

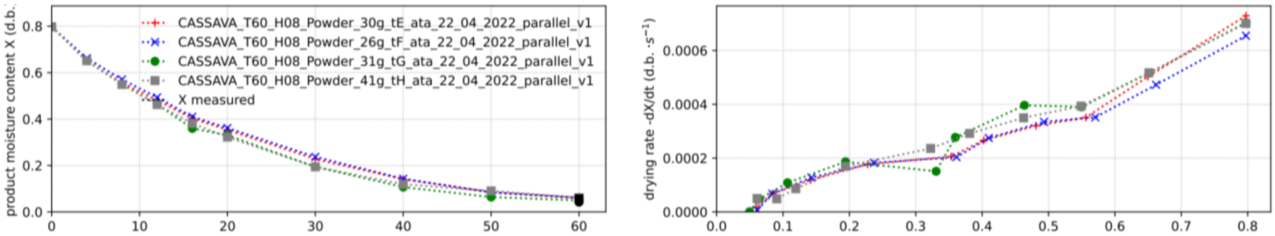

*Figure 57 Kinetic and rate of drying for parallel drying, T 60°C, HR 08%, 1 m/s, different trays. Tray 1 (red), tray 2 (blue), tray 3 (green) and tray 4 (grey)*

From the outcomes, no significative differences can be addressed to a change in the air characteristics. Both trials were made at 60°C and at 8% of relative humidity and only the air velocity set point was different between the two: In Figure 56 the velocity of the air for the represented kinetics is set on 0.7 m/s and instead in Figure 57 is 1 m/s. However, both velocities do not seem to be high enough to allow a residence time sufficient to significatively modify the composition of the gas and, consequently, the drying rate. The slight differences among the various curves, visible especially in the case of the lowest air speed, can be better due to some instability of the flow in the chamber.

The main conclusion we can take is that since modifications of the air characteristics are negligible, "thin layer" approximation for the product can be done in modelling.

#### 3.1.1.5 Parallel flow drying – raw cylinders

Lateral drying was also applied on raw cylinders in the CIRAD laboratories. No repeatability or reproducibility test is available since only one trial for each air condition was carried out. The outcomes are shown in Figure 58, Figure 59 and Figure 60, with a comparison of the three in Figure 61, where the moisture content of the left graph is normalized with respect to the initial value for a better comparison.

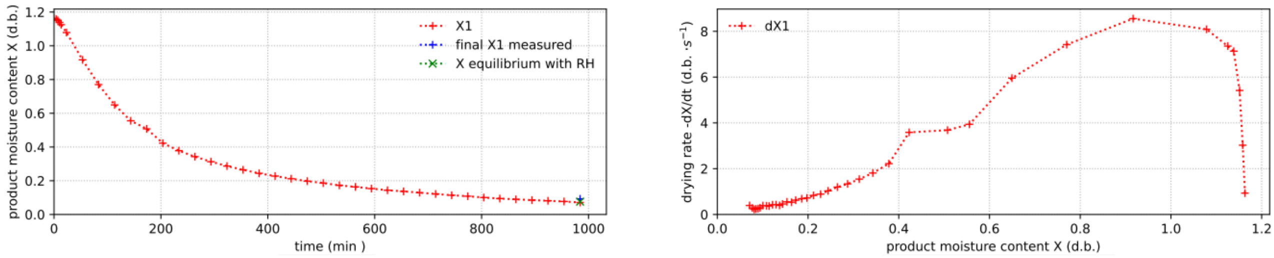

*Figure 58 Raw cassava cylinders in lateral drying. T=40°C HR = 21% v = 1.832 m/s*

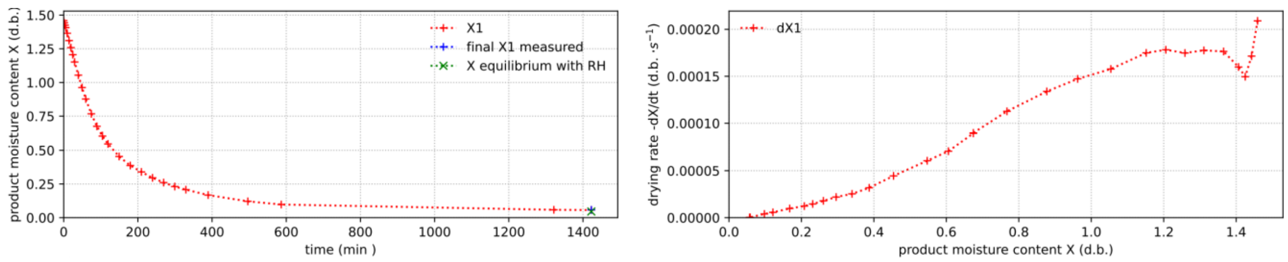

*Figure 59 Raw cassava cylinders in lateral drying. T=60°C HR = 8% v = 1.832 m/s*

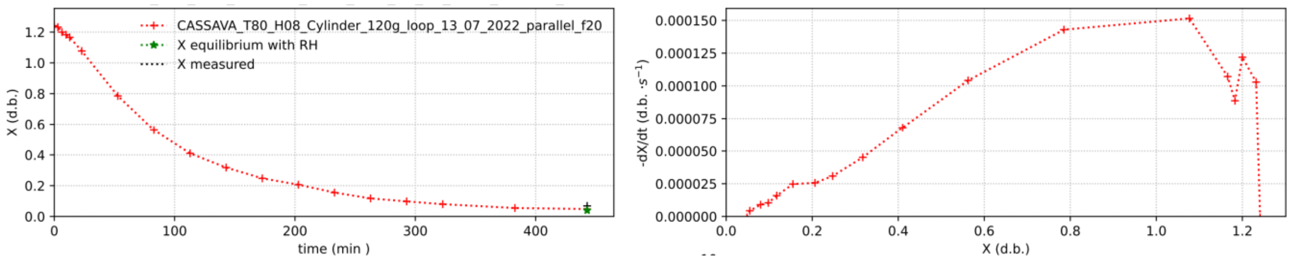

*Figure 60 Raw cassava cylinders in lateral drying. T=80°C HR = 8% v = 1.832 m/s*

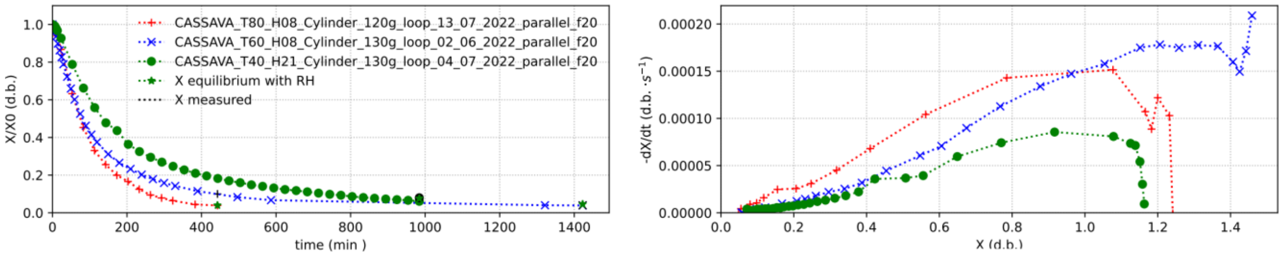

*Figure 61 Comparison of kinetics and drying rates from trials on raw cassava cylinders in lateral drying. T = 40°C HR = 21% (green curve), T = 60°C HR = 8% (blue curve), T = 80°C HR = 8% (red curve)*

The drying rate curve shows in this case, especially for the trials at 40 °C and 80°C, a first increasing trend, followed by an almost constant one and a last decreasing part. This reflects the complete theoretical drying rate curve that also includes the “warm-up” phase. The constant part of the curve is representative of the phase in which the surface evaporation occurs with the same velocity needed for the moisture to reach the surface and “refill” it. The decreasing phase is usually linked to the fact that diffusion is even more limited by physical barriers and diminution of the concentration gradient. The drying curve coming from the experiment at 60°C is closer to the one at 80°C with respect to the one at 40°C in the first part, where convection is the limiting phenomena.

### 3.1.1.6 Parallel and cross flow drying – comparing kinetics

What follows is a comparison between parallel and cross drying conducted in the same conditions on the CIRAD pilot dryer. The curves already seen singularly in the previous sub-sections are now represented on the same graph to enable some considerations to be done on the differences between the two drying methods. Figure 62, Figure 63 and Figure 64 are referred to powder, while Figure 65, Figure 66 and Figure 67 are referred to raw cylinders, with the air characteristics already seen and repeated in the figures caption.

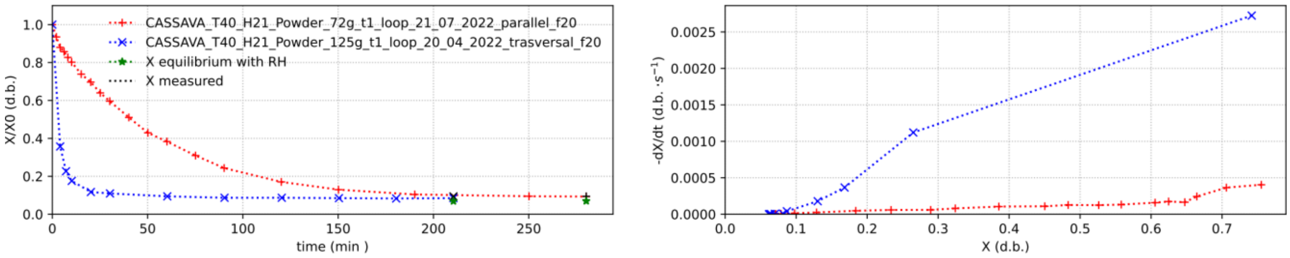

*Figure 62 Kinetic and drying rate comparison between parallel (red curves) and cross (blue curves) drying on cassava powder. T = 40°C HR = 21%*

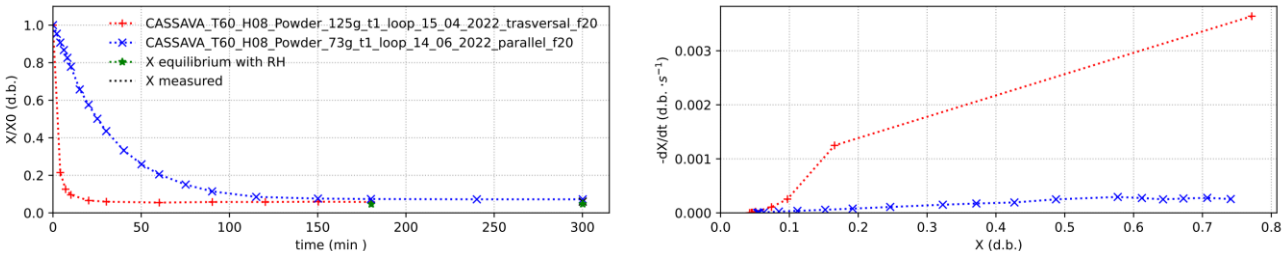

*Figure 63 Kinetic and drying rate comparison between parallel (red curves) and cross (blue curves) drying on cassava powder. T = 60°C HR = 8%*

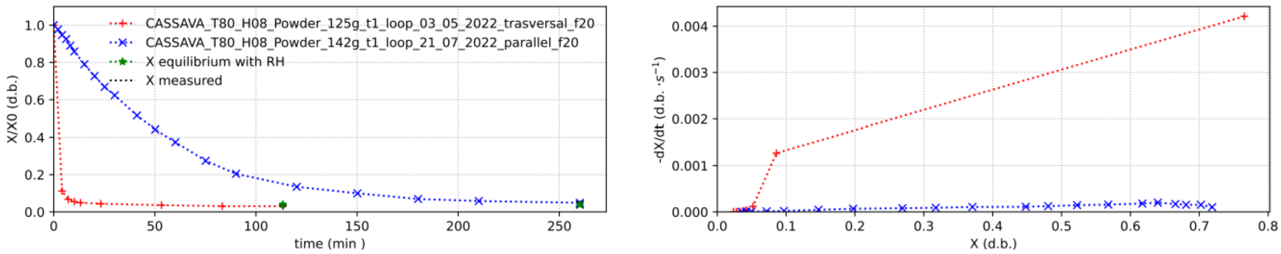

*Figure 64 Kinetic and drying rate comparison between parallel (red curves) and cross (blue curves) drying on cassava powder. T = 80°C HR = 8%*

Considering the powder, what stands out is the big difference between the two methods in terms of drying rate. The same considerations can be done for every air condition. In the right graphs, where $^{dX}/_{dt}$ is plotted with respect to the moisture content on dry basis, a difference of around one order of magnitude is calculated between the drying rates in lateral and traversing mode. This is reflected also is the left graphs, where the reader can see that the time needed for the moisture content to reach the equilibrium value in the trials in cross flow, even if is slightly different according to the temperature of the trial, it remains by far lower with respect to the one needed in lateral drying. The surface exposed directly to the air flow is higher is the case of cross flow and this enables a faster evaporation on the surface: this is visible in the initial part of the drying curves, driven by convection, with a very steep slope especially at higher temperatures. Indeed, the air in this case is forced to cross the layer of powder, whose particles are then surrounded by the hot gas. In the case of lateral drying, instead, air laps the external faces of the layer, creating a sort of preferential path that avoids the pressure drop due to the crossing, and so going mainly around the layer rather than crossing it. Therefore, in the case of parallel flow, the geometry of the product is better approximated by a porous slab undergoing drying, with respect to spheres as it is done for the traversing case. This difference will be exploited in the modelling phase and in the identification of the diffusion coefficient as will be better discussed in the following sections.

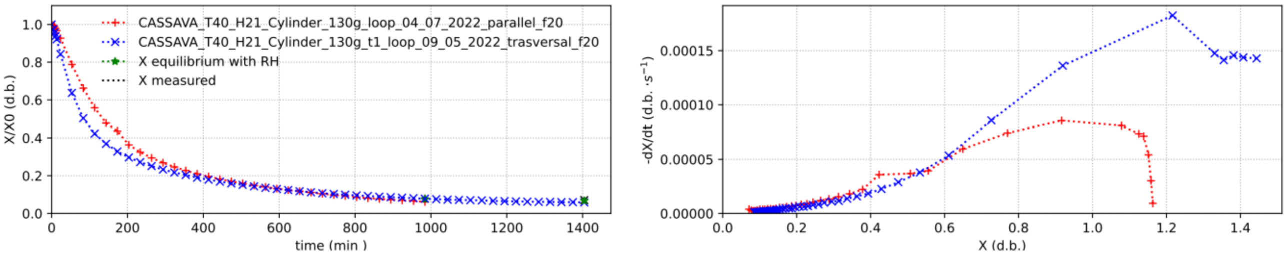

*Figure 65 Kinetic and drying rate comparison between parallel (blue curves) and cross (red curves) drying on cassava raw cylinders. T = 40°C HR = 21%*

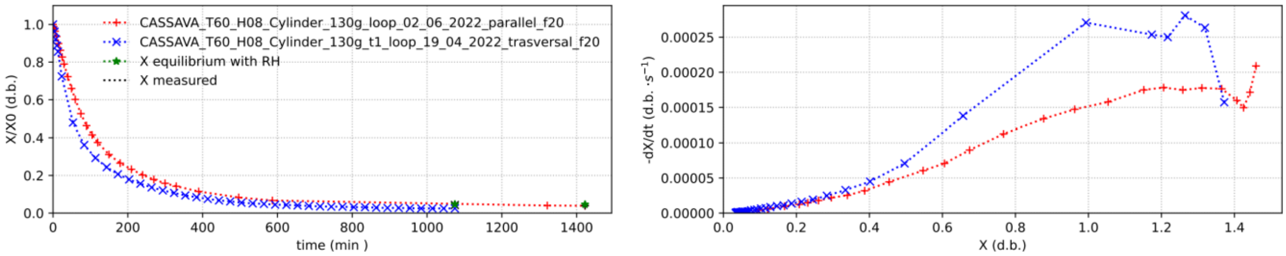

*Figure 66 Kinetic and drying rate comparison between parallel (blue curves) and cross (red curves) drying on cassava raw cylinders. T = 60°C HR = 8%*

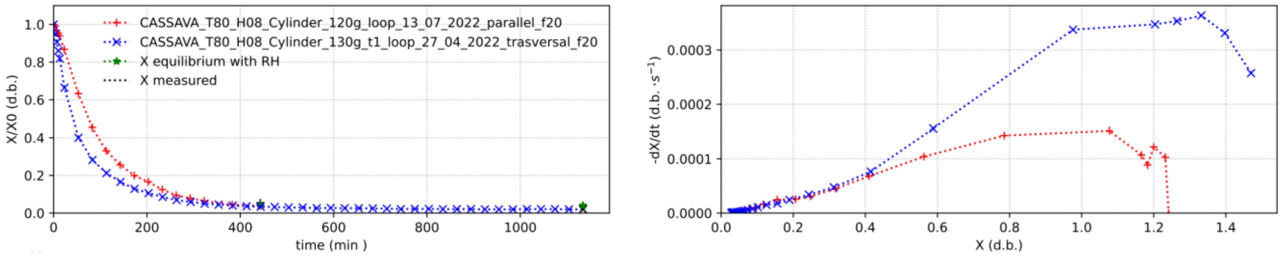

*Figure 67 Kinetic and drying rate comparison between parallel (blue curves) and cross (red curves) drying on cassava raw cylinders. T = 40°C HR = 21%*

Differences between the two drying methods are instead less pronounced in the case of raw cassava cylinders. In this case, indeed, the surface exposed does not present many differences and the discrepancies we can observe between the two methods can be better due to the aerodynamic inside the two different traversing and lateral drying chambers.

## 3.2 Modelling of cassava products drying

As mentioned in the "Materials and methods" section, in order to apply the model, it is necessary to better define diffusivity, as the wide range of values for the diffusion coefficient found in the literature does not allow to rely on a precise one for our products. The experimental work led to the obtainment of the drying parameters was described in Section 3.1 of this Thesis, and most of them are now used to identify the diffusion coefficient with the Nelder-Mead minimization method. The identification procedure is applied on the parameters $a$ and $b$ of the following, temperature dependent, equation for the diffusion coefficient:

$$D_{eff}(T) = a \cdot \exp\left(-\frac{b}{T_p}\right)$$

### 3.2.1 Identification diffusion coefficient parameters – Cylinders

The identification was conducted using three experimental drying curves regarding raw cassava cylinders drying at three different temperatures in cross flow. In Figure 68, the red curve represents the experimental drying curve, while the blue curve is calculated with the optimized values for the parameters of the diffusion coefficient equation. On the experimental points of the red curve are also present the error bars, representing the deviation between the various repetitions of the experiment under the same conditions. From right to left we have respectively the fit with a trial at 40°C, 60°C and 80°C, and the optimization is done on the three drying curves at the same time, in order to determine a temperature dependent *D<sub>eff</sub>* function that fits all. The correspondence between the simulated and the experimental curve appears acceptable, with a standard deviation between the points of the two curves respectively of 9%, 8.1% and 7.4% for the 40°C, 60°C and 80°C tests. Moreover, as visible, the simulated curve remains mostly inside the error bar range.

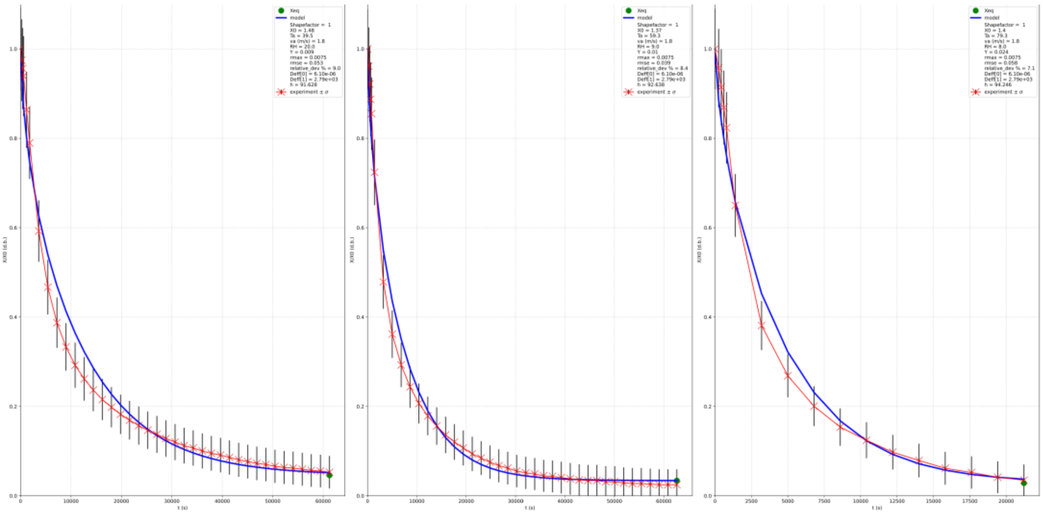

*Figure 68 Simulated and experimental curve for raw cylinders kinetic in cross flow at (from left to right) 40°C, 60°C and 80°C*

The identified parameters for the temperature dependent equation for the effective diffusion coefficient are:

$a = 0.00610\ [m^2/s]\ ;\ b = 2790\ [K]$

According to these values the resulting equation is represented in Figure 69, where the graph shows the $D_{eff}$ trend with respect to the temperature. The curve is slightly increasing and goes from a value of $0.6 \cdot 10^{-9}$ to $2.2 \cdot 10^{-9}$ $\left[\frac{m^2}{s}\right]$. These values are slightly lower with what is found for ideal cylinders in the Abacus graph relying on a trial made on raw cylinders at 60°C (Table 7), but still in agreement for what regards the order of magnitude.

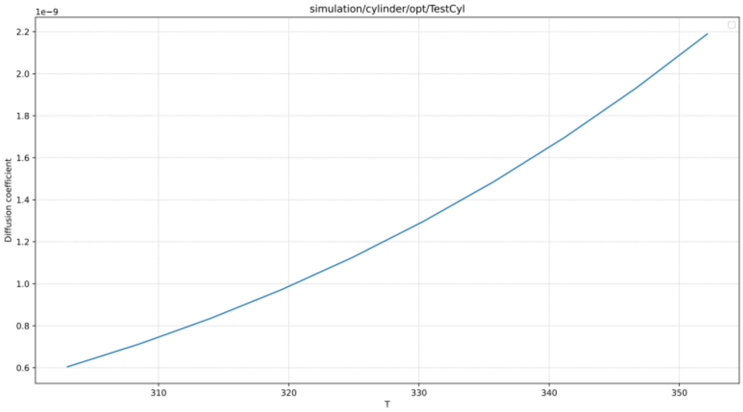

*Figure 69 $D_{eff}$ vs T graph. Parameters identified on raw cylinders drying curves in cross flow*

*Table 7 $D_{eff}$ from Abacus graph for infinite cylinders. Data relying on a kinetic at 60°C in cross flow*

| Moisture content | $^{X_{ini}-X}/_{X_{ini}-X_{fin}}$ | $N_{F0}$ | Time [min] | Diam [m] | $D_{eff}$ $[^{m^2}/_s]$ |
|---|---|---|---|---|---|
| 0,3 | 0,193788 | 0,218734 | 173,6 | 0,016 | 5,37595E-09 |
| 0,2 | 0,119415 | 0,320438 | 243,2 | 0,016 | 5,62172E-09 |
| 0,1 | 0,045041 | 0,398 | 351,2 | 0,016 | 4,83523E-09 |

#### *3.2.1.1 Parameters identified on raw cylinders applied on powder in cross flow*

The parameters identified with the cylinders were then applied to the powder in cross flow drying curves, to verify if the correspondent simulated curve is also able to satisfactory simulate the experimental drying curve of the spherical product in cross flow drying. As mentioned, the trials made on spheres are repeated three times for each temperature investigated. In Figure 70 we have indeed nine drying curves, disposed in three levels: on the first raw we have the three available drying curves at 40°C, on the second the ones at 60°C and on the last one at 80°C. It is suddenly visible that the blue simulated curve is a good approximation of the experimental one in all the cases, with a range of relative deviation going from 12.6% till 14.7% for the experiments at 40°C, from 8.2% till 10.7% for the ones at 60°C and form 6% to 15.3% for the 80°C ones. The particle size distribution gives the geometry information about the population of spheres of different sizes needed to develop the simulated curves. The method used to derive these latter is described in section 2.2.6.

Even if the internal structure of the cells changes going from raw cylinders to powder, the diffusion coefficient found by minimization based on the drying curves of raw cassava led to simulated drying curves that also fits the rasped and dewatered product experimental kinetics. In Table 8, the values found on the Abacus graph for powder at 60°C are shown. The found values are in agreement with the one from the simulation, and mostly inside the range.

*Table 8 Deff from Abacus graph for spheres. Data relying on a kinetic at 60°C in cross flow*

| **Moisture content** | $X_{ini} - X / X_{ini} - X_{fin}$ | **N$_{F0}$** | **Time [min]** | **Diam [m]** | **D$_{eff}$ $[m^2/s]$** |
|---|---|---|---|---|---|
| 0,3 | 0,339441 | 0,0582 | 4,3085 | 0,0033 | 2,45173E-09 |
| 0,2 | 0,201904 | 0,1144 | 5,9042 | 0,0033 | 3,51675E-09 |
| 0,1 | 0,064366 | 0,2321 | 25,3191 | 0,0033 | 1,66381E-09 |

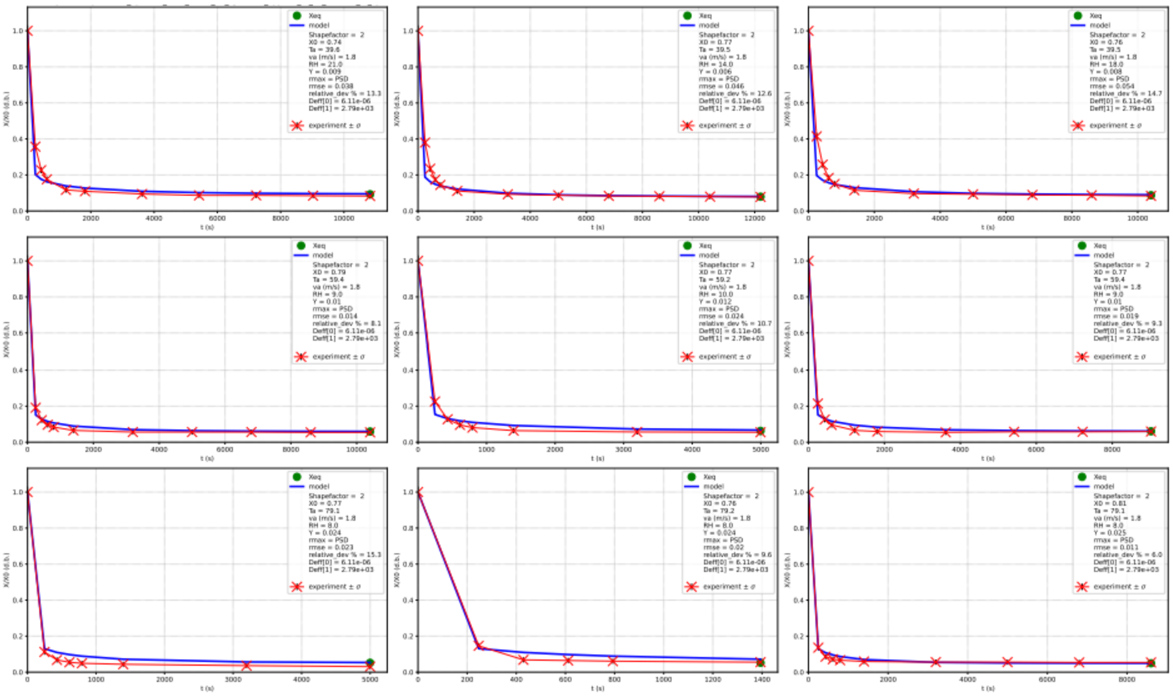

*Figure 70 D$_{eff}$ from identification on cylinders applied on all the kinetics of cassava powder in cross flow at 3 different temperatures*

### 3.2.1.2 Parameters identified on raw cylinders applied on powder/mash made cylinders

The application of the same parameters was then done on the available trials on mash and powder made cylinders at different porosities. The objective was to verify if the same values of the diffusion coefficient, identified on the raw product, can led to simulated drying curves able to well predict the behaviour in drying of the same medium at different processing levels. In Figure 71 the outcomes of the simulations relative respectively, from left to right, to mash made cylinders, to powder made higher porous (HP) ones, and powder made less porous (LP), in cross flow at 60°C.

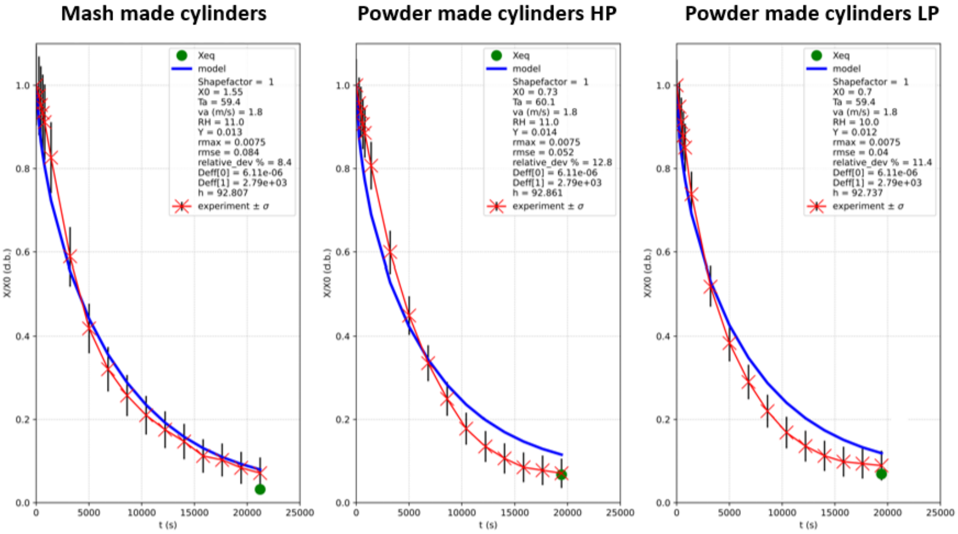

*Figure 71 $D_{eff}$ from identification on cylinders applied on the kinetics of cassava mash cylinder, powder made high and low porosity in cross flow at 60°C*

From the outcomes we can see that the best fit is obtained with the cassava mash, with a standard deviation of 8.4%. The best fit is obtained in the case of mash made cylinders, since the simulated curve remains inside the error bar range. This is not surprising since the mash product, even if ground, keeps a structure more similar to the raw cassava with respect to the powder, that also underwent mechanical dewatering. Nevertheless, the experimental drying curves of powder made cylinders are also predicted with an acceptable accuracy, with relative deviation values of 12.8 % and 11.4 % respectively for higher and lower porous cylinders.

#### 3.2.1.3 Parameters identified on raw cylinders applied on powder in parallel flow

The effective diffusion coefficient obtained with parameter identification procedure on raw cassava cylinders in cross flow kinetics, is now used to simulate the drying curve of cassava powder in parallel flow. As mentioned in sub-section 3.1.1.6 , in this case the best way is to simulate the product as a slab instead of independent spheres: the particle size distribution is no more taken into account, but the only characteristic dimension considered is the thickness of the layer. For the latter, the value chosen was a mean between the initial and final thickness of the layer, since a certain percentage of shrinkage occurs in drying. Moreover, for the convective heat transfer coefficient, direct measurement of air and metal sheet temperatures was performed in these conditions, in order to derive *h* from an energy balance (Section 2.1.5). So, unlike previous cases, the convective coefficient is not calculated using adimensional correlations (Section 2.2.2) but is fixed to a value of 17,72 $\frac{W}{m^2 * K}$. In addition, the ability of the identified values of the effective diffusion coefficient to well predict drying rate at different thickness of the layer was investigated, since experiments with a thickness of around 4 mm, 7 mm and 13 mm were obtained on the CIRAD loop dryer. The comparison between the simulated and experimental curves is shown in the following graphs. The trials to which they are referred are the ones described in sub-section 3.1.1.4, and specifically in Figure 72 the two trials at 40°C, in Figure 73 the only available trial at 60°C, in Figure 74 the three trials at 80°C. In addition, Figure 75 shows the trials with a thicker layer of product, respectively around 7 mm on the left graph and 13 on the right one, both dried at 80°C. The relative deviation between the points of the experimental and simulated curve are respectively: 2.9 % and 6.3 % for the two trials at 40°C, 1.7% for the trial at 60°C, 9.1%, 8.2% and

7.1% for the trials at 80°C and 4 mm thickness of the product, 2.7% and 2.9% for the two trials at 80°C with 7 mm and 13 mm thickness respectively.

As can be noticed, the simulation in these cases can predict with a good approximation all the drying curves obtained in parallel flow on powder. This evidence can be arguable since internal structure and porosity of the product are different between raw cylinders and cassava powder. Nevertheless, since diffusivity is an intrinsic property of the product, is not surprising that for the same medium, the same function for the diffusion coefficient identified on one geometry and level of processing, can be successfully applied to all the other cases. Still, as their porosity is quite different and not taken into account in the diffusivity definition, nor in the model, it may have an influence.

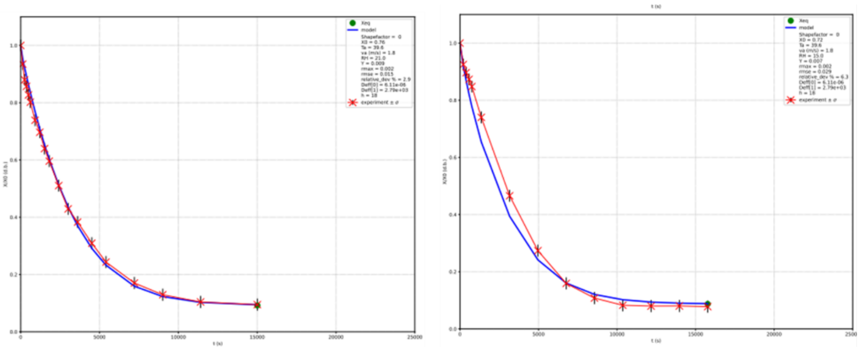

*Figure 72 $D_{eff}$ from identification on cylinders applied on the kinetics on powder parallel flow at 40°C. Comparison between experimental curve (red) and simulated one (blue).*

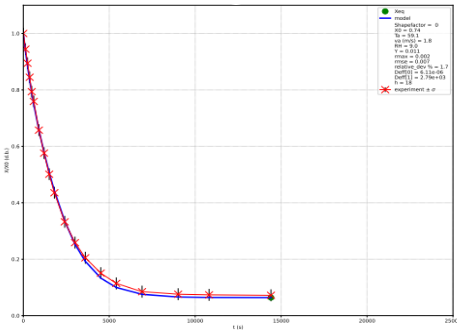

*Figure 73 $D_{eff}$ from identification on cylinders applied on the kinetics on powder parallel flow at 60°C. Comparison between experimental curve (red) and simulated one (blue).*

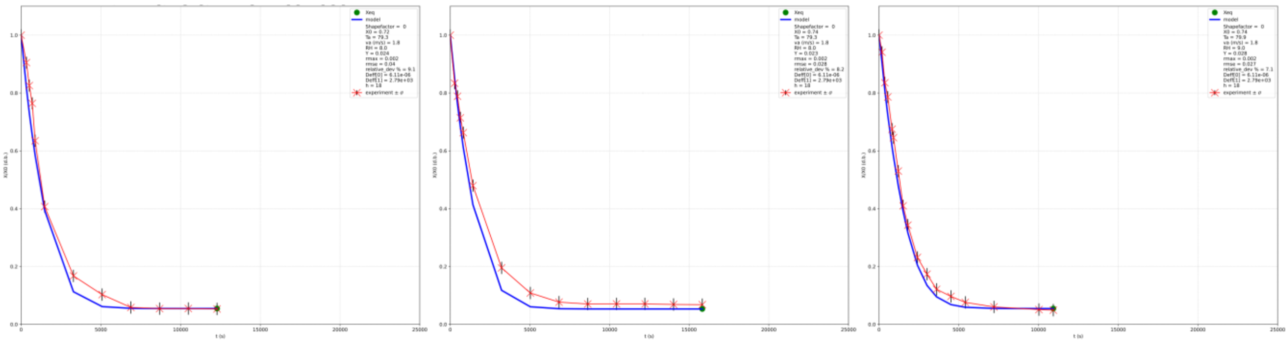

*Figure 74 $D_{eff}$ from identification on cylinders applied on the kinetics on powder parallel flow at 80°C. Comparison between experimental curve (red) and simulated one (blue).*

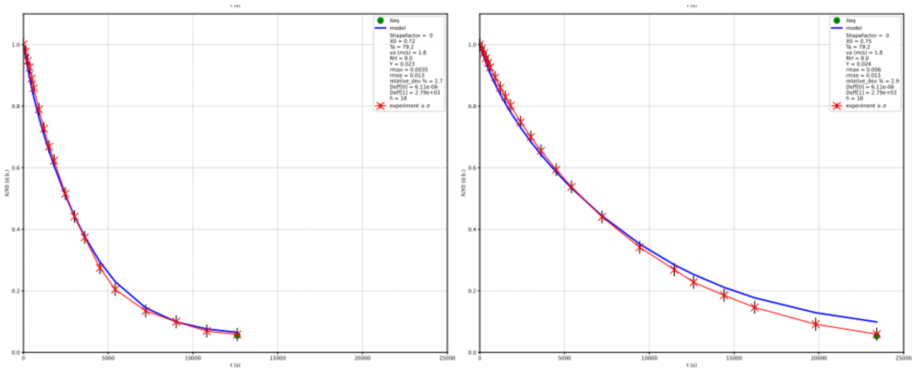

*Figure 75 $D_{eff}$ from identification on cylinders applied on the kinetics on powder parallel flow at 80°C. Average thickness of 7 mm (left graph) and 13 mm (right graph). Comparison between experimental curve (red) and simulated one (blue).*

### 3.2.2 Identification of diffusion coefficient parameters – Slab

Identification procedure is here based on the experimental drying curves regarding powder in parallel flow. New values of the parameters for the $D_{eff}$ equation are found by parameter identification and from this, a new curve for the temperature dependent effective diffusion coefficient is obtained for comparative purposes with the one already available from the identification on raw cylinders. The identification in this case was done using all the available drying curves of powder in parallel flow. In Figure 76 the 40°C experiments (two repetitions), in Figure 77 the 60°C one (one repetition), in Figure 78 the 80°C one (three repetitions), and in Figure 79 the 80°C ones at 7 mm and 13 mm thickness respectively. The relative deviations for the two trials at 40 °C are respectively 4.4% and 5.7%, 2.5% for the one at 60°C, 8%,7.2% and 5.5% for the three at 80°C and 4 mm thickness, and 2.9% for the last two at different product layer thicknesses.

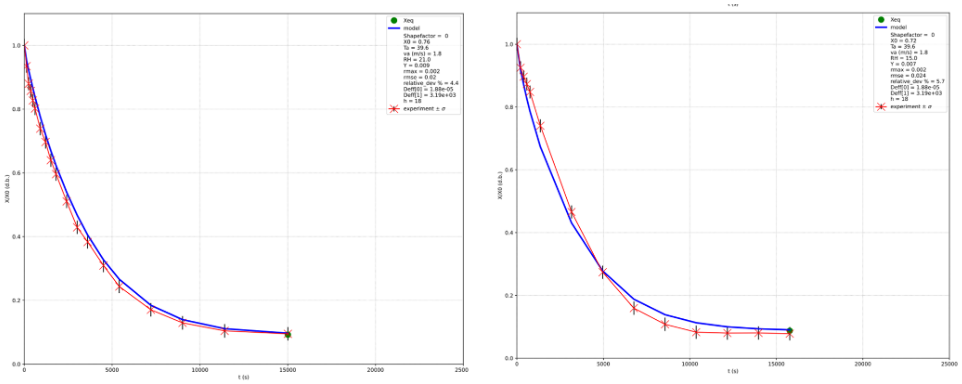

*Figure 76 Simulated and experimental kinetics for powder in parallel flow at 40°C, 4 mm thickness. Comparison between experimental curve (red) and simulated one (blue).*

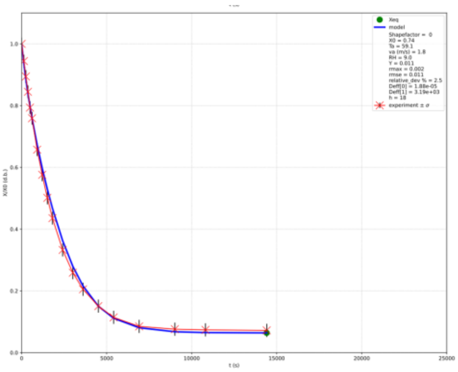

*Figure 77 Simulated and experimental kinetics for powder in parallel flow at 60°C, 4 mm thickness. Comparison between experimental curve (red) and simulated one (blue).*

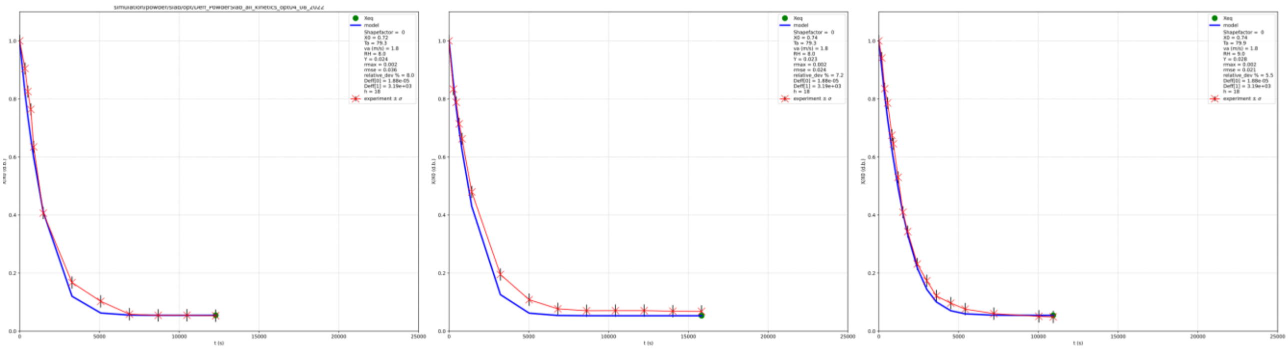

*Figure 78 Simulated and experimental curve for powder in parallel flow at 80°C, 4 mm thickness. Comparison between experimental curve (red) and simulated one (blue).*

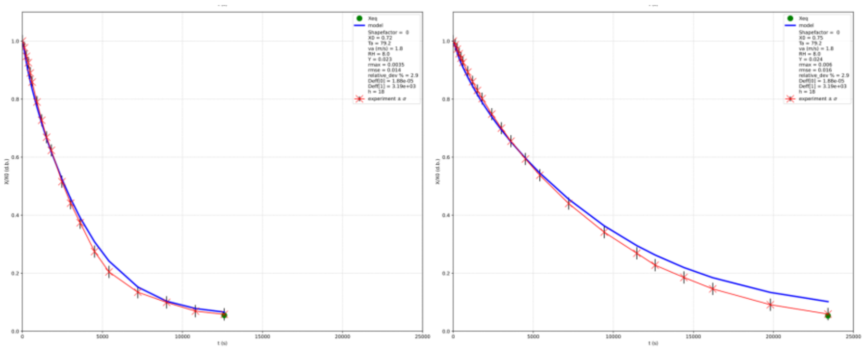

*Figure 79 Simulated and experimental curve for powder in parallel flow at 80°C, 7 mm (left graph) and 13 mm(right graph). Comparison between experimental curve (red) and simulated one (blue).*

The new parameter identified are:

$a = 0.0000188\ [m^2/s]\ ;\ b = 3190\ [K]$

The resulting equation has the shape visible in the graph of Figure 80, with a range of values for the diffusion coefficient going from $0.5 \cdot 10^{-9}$ to $2.2 \cdot 10^{-9}\ [m^2/s]$. In Table 9, Table 10 and Table 11 the diffusion coefficient found on the Abacus graph relying from experimental curves at 80°C and respectively with 4 mm, 7 mm and 13 mm of product layer thickness.

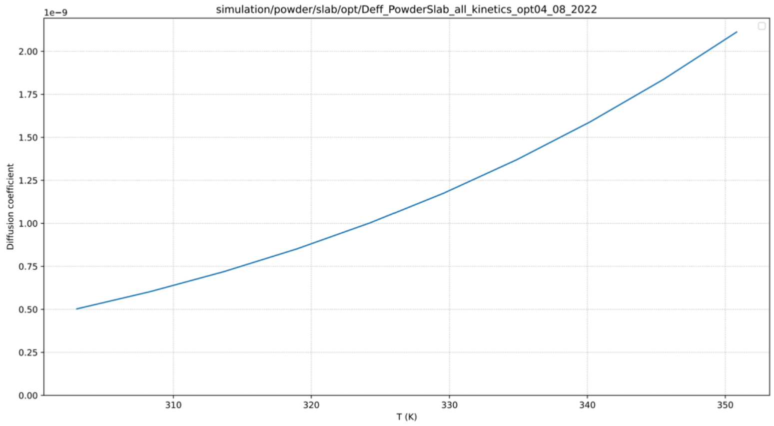

*Figure 80 Deff vs T graph. Parameters identified on powder drying curves in parallel flow*

*Table 9 $D_{eff}$ from Abacus graph for slab. Data relying on a kinetic at 80°C in parallel flow with 4 mm of product layer thickness*

| **Moisture content** | $^{X_{ini}-X}/_{X_{ini}-X_{fin}}$ | **$N_{F0}$** | **Time [min]** | **Thickness [m]** | **$D_{eff}$ $[{m^2}/{s}]$** |
|---|---|---|---|---|---|
| 0,3 | 0,378531 | 0,3177 | 25,331 | 0,004 | 3,34452E-09 |
| 0,2 | 0,237288 | 0,5044 | 36,424 | 0,004 | 3,6928E-09 |
| 0,1 | 0,096045 | 0,866 | 57,45 | 0,004 | 4,01973E-09 |

*Table 10 $D_{eff}$ from Abacus graph for slab. Data relying on a kinetic at 80°C in parallel flow with 7 mm of product layer thickness*

| **Moisture content** | $^{X_{ini}-X}/_{X_{ini}-X_{fin}}$ | **$N_{F0}$** | **Time [min]** | **Thickness [m]** | **$D_{eff}$ $[{m^2}/{s}]$** |
|---|---|---|---|---|---|
| 0,3 | 0,384615 | 0,3034 | 55,27 | 0,007 | 4,48302E-09 |
| 0,2 | 0,244755 | 0,4929 | 77,85 | 0,007 | 5,17065E-09 |
| 0,1 | 0,104895 | 0,83 | 111,81 | 0,007 | 6,06237E-09 |

*Table 11 $D_{eff}$ from Abacus graph for slab. Data relying on a kinetic at 80°C in parallel flow with 13 mm of product layer thickness*

| **Moisture content** | $^{X_{ini}-X}/_{X_{ini}-X_{fin}}$ | **$N_{F0}$** | **Time [min]** | **Thickness [m]** | **$D_{eff}$ $[{m^2}/{s}]$** |
|---|---|---|---|---|---|
| 0,3 | 0,375877 | 0,3177 | 132,11 | 0,013 | 6,77356E-09 |
| 0,2 | 0,237288 | 0,5044 | 191,24 | 0,013 | 7,42902E-09 |
| 0,1 | 0,096045 | 0,866 | 290,51 | 0,013 | 8,39638E-09 |

As it can be noticed, the differences between the values obtained with the identification on cylinders and slab are very feeble, and both are able to well predict the experimental drying curves at the various air conditions and layer thicknesses. The same order of magnitude is found in the values of $D_{eff}$ obtained from the Abacus graph. From what visible comparing the values obtained with the graph, slightly increasing values are found with the increase of the thickness, and a feeble decreasing trend with the moisture content. Effectively, Figure 79 shows, especially for the thicker thickness of the product layer, a slightly slower kinetic with respect to the experimental one, so is reasonable to assume that slightly higher values for diffusivity are needed in this case to achieve a perfect fit. Nevertheless, these results are encouraging because, as we expected, we found similar values for the diffusion coefficient although identifying it on two different cassava derived products. This evidence found reason in the fact that diffusivity is an intrinsic property of the medium and cannot heavily differ with the level of processing. Moreover, diffusivity can also be influenced by the porosity of the medium. Analysing different products with different levels of porosity and finding out a good fit of experimental and simulated curves with the same diffusion coefficient set of values, is reasonable to assume that porosity has negligible effect, and its dependency in not taken into account advisedly.

### 3.2.2 Parameter identification for diffusion coefficient – All processing levels

As a last, definitive, confirm of the identified values for the effective diffusion coefficient, the identification is now made on all the geometries, at various level of processing, at the same time. In this case we used the minimization protocol on all the kinetics made on various cassava products, at different air conditions, and with different quantity of products. In the following figures, the graph with the results of the simulation: red curves are the experimental ones, while the blue ones are the simulated. In particular, in Figure 81 we have three drying curves of powder in cross flow at 40°C, in Figure 82 at 60°C, and in Figure 83 at 80°C. Figure 84 shows instead the case of cylinders in cross flow at 40°C with 3 repetitions, Figure 85 at 60°C, and Figure 86 at 80°C. Finally, for powder in parallel flow, Figure 87 shows the drying curves for the two repetitions of the trial at 40°C,Figure 88 the one at 60°C, and Figure 89 the three at 80°C. For quite all the trials that regards powder, the thickness was around 4 mm. Figure 90 shows instead the simulated and experimental curves of the two trials with increased thickness, used in parallel flow: 7 mm in the left graph and 13 in the right one.

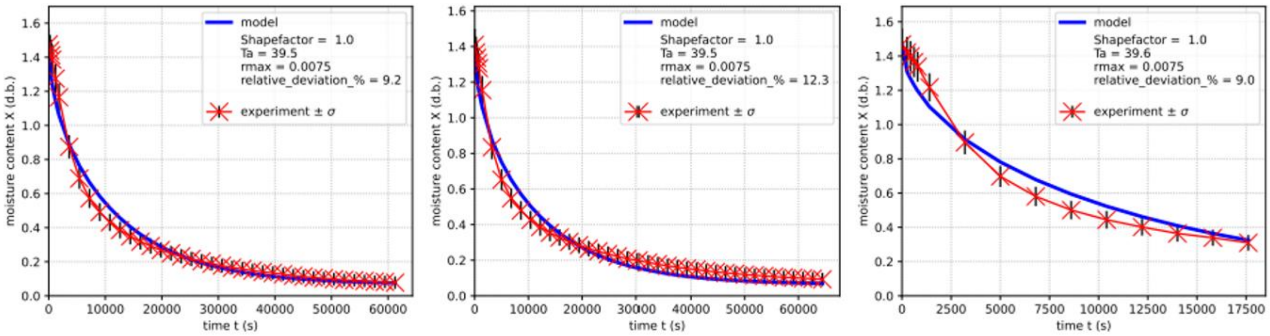

*Figure 81 Simulated (blue) and experimental (red) curve for raw cassava cylinders in cross flow at 40°C*

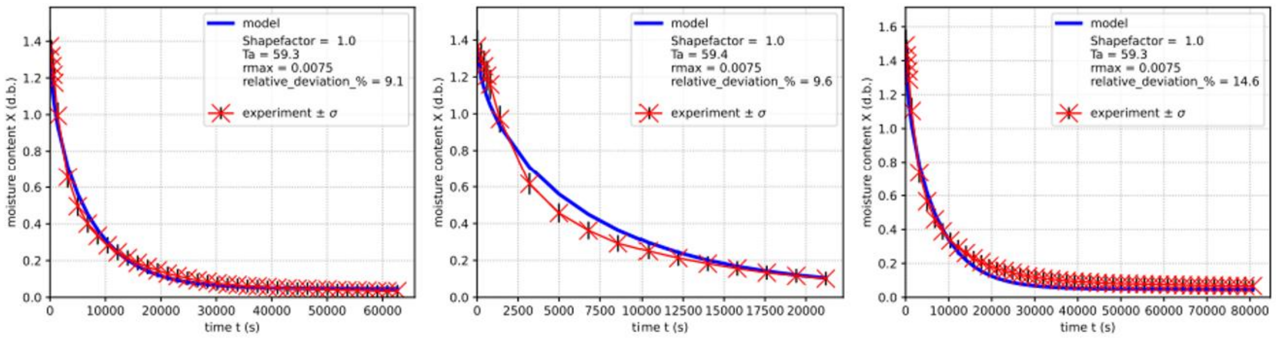

*Figure 82 Simulated (blue) and experimental (red) curve for raw cassava cylinders in cross flow at 60°C*

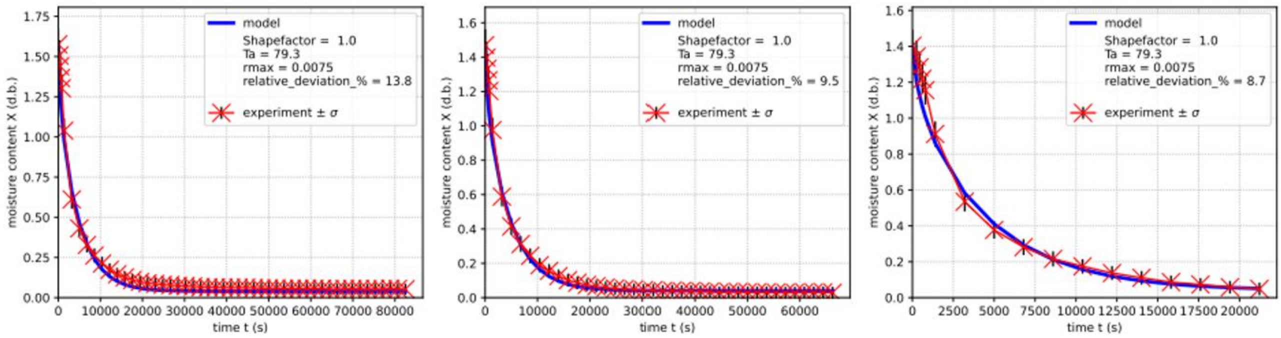

*Figure 83 Simulated (blue) and experimental (red) curve for raw cassava cylinders in cross flow at 80°C*

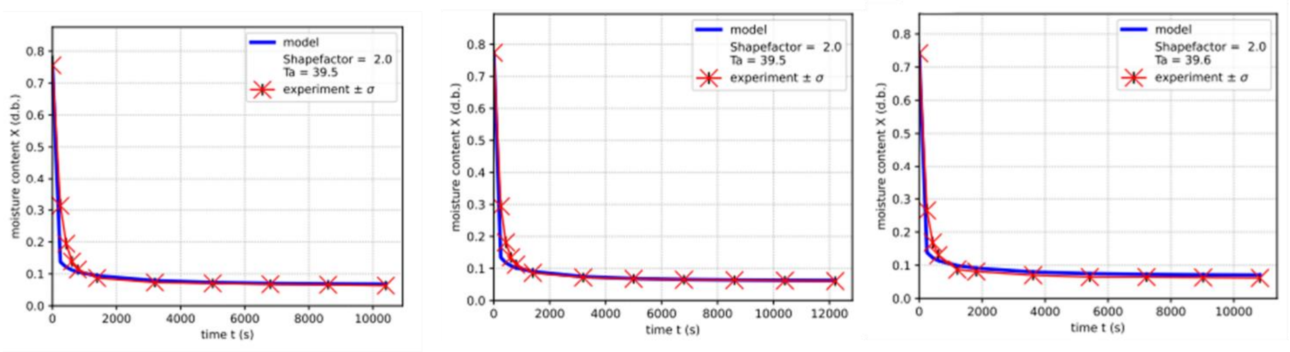

*Figure 84 Simulated (blue) and experimental (red) curve for cassava powder in cross flow at 40°C*

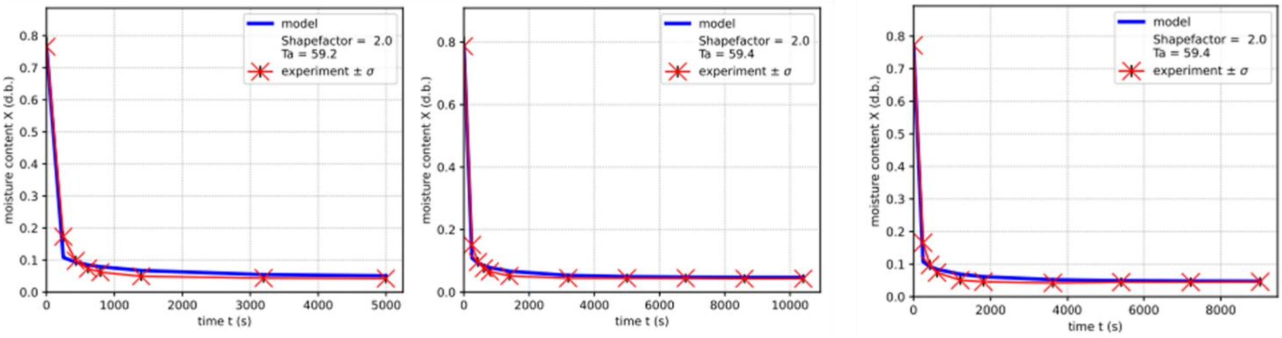

*Figure 85 Simulated (blue) and experimental (red) curve for cassava powder in cross flow at 60°C*

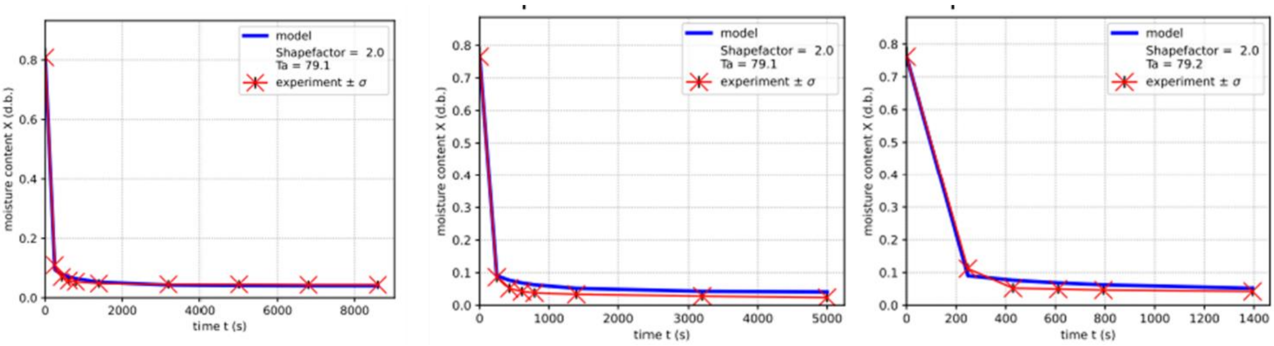

*Figure 86 Simulated (blue) and experimental (red) curve for cassava powder in cross flow at 80°C*

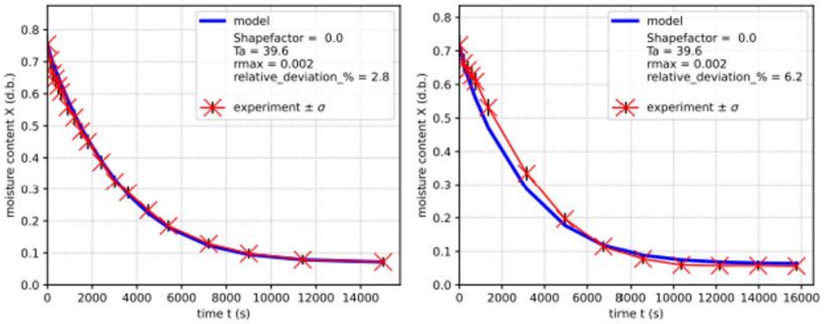

*Figure 87 Simulated (blue) and experimental (red) curve for cassava powder in parallel flow at 40°C*

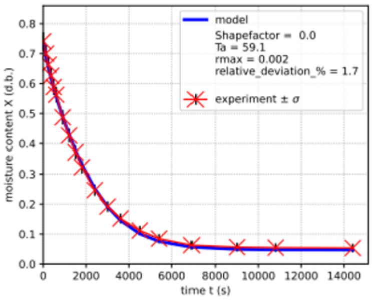

*Figure 88 Simulated (blue) and experimental (red) curve for cassava powder in parallel flow at 60°C*

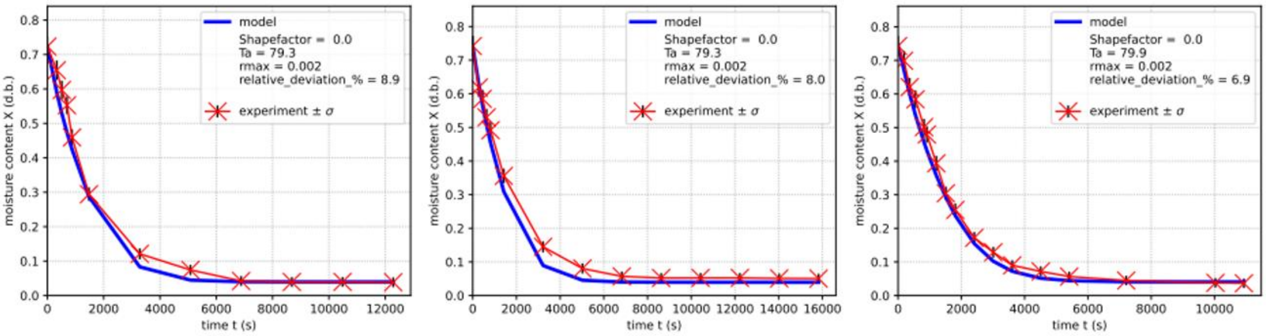

*Figure 89 Simulated (blue) and experimental (red) curve for cassava powder in parallel flow at 80°C*

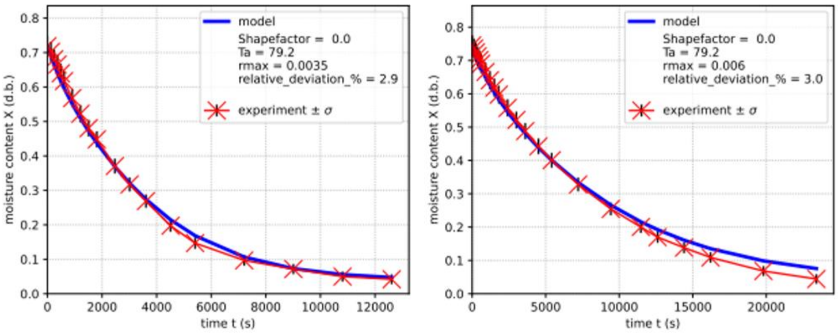

*Figure 90 Simulated (blue) and experimental (red) curve for cassava powder in parallel flow at 80°C, 7 mm (left graph) and 13 mm (right graph) thickness*

The values for the parameters of the effective diffusion coefficient are in this case:

$a = 0.00000633\ [m^2/s]\ ;\ b = 2813.07\ [K]$

The resulting expression for the diffusion coefficient leads to values ranging from 0,42$\cdot\ 10^{-9}$ to 2,2$\cdot\ 10^{-9}\ [m^2/s]$ as visible in Figure 91. As can be easily notices, also in this last identification we obtained similar values for diffusivity with respect to the previous cases. This can be seen as a further validation of the reliability of the results. Last, the graph in Figure 92 is a comparison between the functions for the temperature dependent diffusion coefficient obtained and shown in the present and previous sections by identification on raw cylinders, powder slab in parallel flow, and all kinetics at the same time. The range of relative deviation for 1.7% to 14.6%

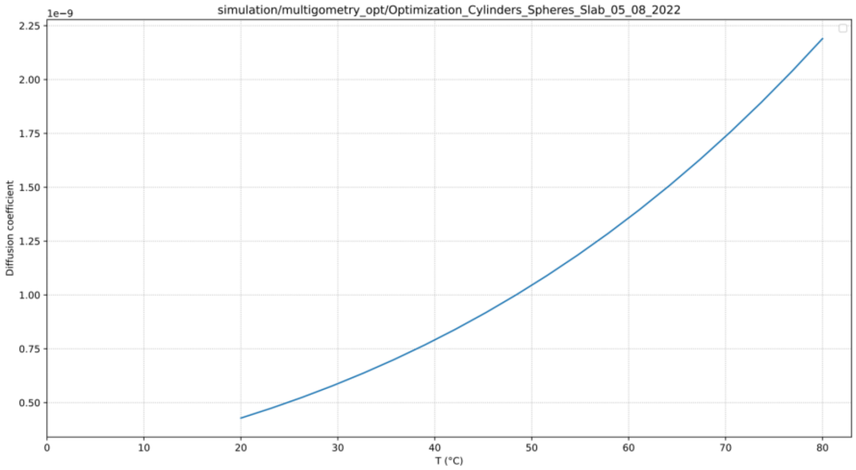

*Figure 91 $D_{eff}$ vs T graph. Parameters identified on all kinetics*

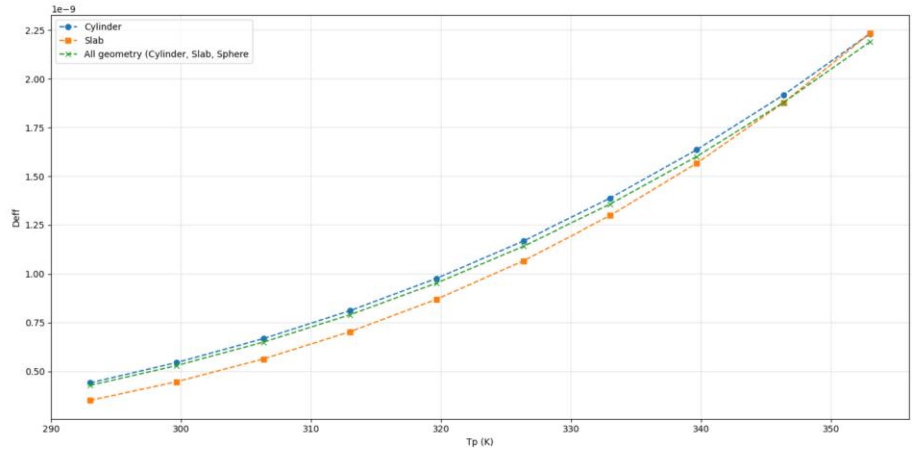

*Figure 92 $D_{eff}$ vs T graph. Comparison between curves.*

# 4 Conclusions and perspective

In this Thesis, the study of cassava derived products undergoing drying is investigated experimentally. Then, an existing convective and diffusive model[24] was applied to the case of cassava.

## 4.1 Experimental analysis of cassava drying

A multitude of products derived from cassava roots is analysed from the manufacturing procedure to the geometrical and structural characterization, to the behaviour in drying. Such products were: cylinders obtained directly from cassava roots by cutting, mash derived from grinding of roots, and powder obtained by mechanical pressing of the mash. The objective was to investigate the effect of the various processing steps on the characteristics of the aliment, and on its drying curve. In this perspective, an attempt to align the geometry was done, by shaping also mash and powder in a cylindric form. Nevertheless, for what regards powder, many experiments were conducted with the product disposed on the tray as a layer. The interest in such disposition comes from the fact that this kind of product is generally employed for the production of cassava floor in sub-tropical countries, and an analysis of its behaviour in drying benefits the perspective of efficiency enhancement and sale-up of drying processes conducted traditionally nowadays.

Two different pilot dying equipment were used to conduct the experiments, and the products were dried through convection of hot air. For the latter, several conditions of temperature, relative humidity, velocity, and flow direction were investigated according to the strength and limitation of each apparatus. Most of the trials were conducted in the CIRAD laboratory using the loop drier in the following air conditions: 40°C and 21% of relative humidity, 60 °C, 8% and 80°C, 8%. According to the relative position between products and air flow direction, we studied both parallel drying (air flow encounters the products laterally) and cross flow drying (air flow cross the layer of product). The limitation of the CIRAD loop dryer was principally the minimum reachable air velocity, that was around 1.8 m/s. This brought us to do some trials using the A.T.A loop dryer, where lower values for the air velocity could be reached.

As a result of the experimentations, drying and drying rate curves were derived from the various test, detailed in section 3.1 of the present work. As main conclusions I dutiful to underline the following:

1. The crossflow drying is much faster than parallel one, especially when applied to powder.
2. The various level of processing seems to have a negligible impact on the drying behaviour of equally shaped products.

Referring to the first conclusion, a further study of the energy requirement will give more information and scale-up perspective of this kind of procedure, that is shown to be an easier and faster way of drying cassava powder with respect to parallel flow. In this context, a first step can be a study of the air velocity since it has a strong influence both on drying procedure and on energy consumption. For what regards the temperature, a balance can be done on the energy expenditure to increase the air temperature and the gain in term of increased drying rate.

Regarding the second main conclusion, it will be useful to deepen the study in order to understand the external factors that influenced the outcomes. A deeper knowledge can also be a starting point to investigate the usefulness and the level of the mechanical dewatering procedures, usually applied in casava treatments before thermal drying. Again, a comparison of the various energy consumption plays a key role in the definition of the most efficient path to follow.

In general, some experiments on a bigger scale dryer, combined with an estimation of the energy requirement, can be a first useful step to further verify the behaviour of the products in drying, limiting the problems connected to the utilization of pilot equipment for what regards the aerodynamic, and to estimate the feasibility of a further scale-up till the industrial level.

## 4.2 Modelling of Cassava drying

The model developed by C. Lambert et al [24] incudes diffusive (internal) and convective (surface) heat and mass transfers, since an evaluation of the thermal and matter Biot numbers (section 2.2.2) does not allow to neglect one of the two types of mechanisms. The main hypothesis and equations of the model, as well as their way of solving, are detailed in Section 2.2.3. For our purposes, product is modelled as a thin layer, since no variation in the air characteristics are detected after crossing the products. Moreover, the model is conceived to consider different geometries as slab, spheres, and cylinders. In our work, powder dried in cross flow is modelled as independent speres, as air surrounds particles while going through the product layer. In this case, the geometrical characterization of the population of particles is achieved thanks to granulometry conducted on dry powder and is used in modelling in the way described in sub-section-2.2.3.4. The behaviour of cassava powder in parallel drying is instead better approximated by a slab of porous material as described in sub-section 3.1.1.6. To account for surface heat and mass transfer, the evaluation of the convective coefficient was required: adimensional correlations (Nusselt) were used to get it in the cases of powder in cross flow and cylinders, direct measurement was instead performed in the case of powder in parallel flow (section 2.1.5)

For modelling purposes, many properties of cassava are being investigated by literature consultation, direct measurement, and parameter identification procedure. The geometrical characterization was obtained by measurement of diameter (cylinders), thickness of the layer (slab) and granulometry (spheres), while the thermo-hydro properties of cassava like heat capacity, thermal conductivity and sorption were investigated by literature review. Since a wide range of value was found in papers for what regards the diffusion coefficient, its identification was needed basing on the experimental drying curves previously obtained, cause no reliable value was found in literature but just a range of higher likelihood (section 2.2.4.4). Based on this, the model was implemented on Python and parameter identification was employed to identify the parameters of the temperature dependent equation for diffusion coefficient. To do this, minimization of the factor $j$ expressing the “distance” between the experimental and simulated curve was done using Nelder-mead method. Initially, the identification was done basing on drying curves of raw cassava cylinders, since for this product a geometrical characterization was easier and more precise. Subsequently the values identified for $D_{eff}$ were applied on the drying curves of cassava powder in cross and parallel flow, and the simulated curve that come out revealed to be a good approximation of the experimental ones. Moreover, the range of values was in agreement both with literature and with the Fourier Abacus (section 2.2.4). A further validation of the found values was obtained by identification of the diffusion coefficient parameters also basing on powder drying curves. Similar values with respect to the previous identification were found. Last, identification was conducted, on a computer with high computational power, on all the available kinetics at the same time, including different geometries and levels of processing for the products. As expected, the new values are very close to the ones identified previously, so we can definitely rely on the truthfulness of our result.

The identification of the diffusion coefficient concludes the part relative to the characterization of the product and opens the way to the following phase of dimensioning of an optimized drying equipment for a given capacity, in a perspective of cost and applicability evaluation of the equipment in real conditions (Africa and South America countries).

## FIGURE INDEX

## TABLE INDEX

# BIBLIOGRAPHY

[1] W. F. Breuninger, K. Piyachomkwan, and K. Sriroth, *Tapioca/Cassava Starch: Production and Use*, Third Edit. Elsevier Inc., 2009.

[2] M. E. Dulloo, J. Hanson, M. A. Jorge, and I. Thormann, "Introduction Regeneration guidelines: general guiding principles," 2008, [Online]. Available: https://cropgenebank.sgrp.cgiar.org/images/file/other_crops/Introduction_ENG.pdf.

[3] A. A. C. Alves, "Cassava botany and physiology.," *Cassava Biol. Prod. Util.*, pp. 67–89, 2001, doi: 10.1079/9780851995243.0067.

[4] A. Fathoni, "The Role of Interconversion of Scopoletin and Scopolin in Cassava Postharvest Physiological Deterioration ( PPD ) The Role of Interconversion of Scopoletin and Scopolin in Cassava Postharvest Physiological," *Thesis degree Dr. Philos.*, p. University of Bath, 2017.

[5] M. K. Mtunguja, H. S. Laswai, E. Kanju, J. Ndunguru, and Y. C. Muzanila, "Effect of genotype and genotype by environment interaction on total cyanide content, fresh root, and starch yield in farmer-preferred cassava landraces in Tanzania," *Food Sci. Nutr.*, vol. 4, no. 6, pp. 791–801, 2016, doi: 10.1002/fsn3.345.

[6] FAO, "Food And Agriculture Organization." https://www.fao.org/faostat.

[7] M. Bokanga, "Cassava: Post-harvest Operations," *INPhO-Post-harvest Compend.*, p. 56, 1999.

[8] R. J. Hillocks, "Cassava in Africa Origins of Cassava in Africa," *Cassava Biol. Prod. Util.*, pp. 41–54, 2002, [Online]. Available: http://ciat-library.ciat.cgiar.org/articulos_ciat/cabi_06ch3.pdf.

[9] A. Westby, "Cassava utilization, storage and small-scale processing.," *Cassava Biol. Prod. Util.*, vol. 1, pp. 281–300, 2001, doi: 10.1079/9780851995243.0281.

[10] B. Ugwu and P. Ay, "Seasonality of cassava processing in Africa and tests of hypotheses: COSCA working paper, No. 6," 1992.

[11] B. James *et al.*, *Producing Gari from Cassava An illustrated guide for smallholder cassava processors U P O CA Unleashing the power of cassava in Africa*. 2012.

[12] A. O. Adebayo-Oyetoro, O. B. Oyewole, A. O. Obadina, and M. A. Omemu, "Cyanide and Heavy Metal Concentration of Fermented Cassava Flour ( Lafun ) Available in the Markets of Ogun and Oyo States of Nigeria," *Int. J. ofFood Sci.*, vol. 7, no. 7, pp. 356–359, 2013.

[13] Abass A.B., "How to make high quality cassava flour," *Int. Inst. Trop. Agric.*, p. 14 pp, 2006.

[14] M. Precoppe, T. Tran, A. Chapuis, J. Muller, and A. Abbas, "Improved energy performance of small-scale pneumatic dryers used for processing cassava in Africa.," *Biosyst. Eng.*, pp. 510–519, 2016, doi: 10.1016/j.biosystemseng.2016.10.001.

[15] T. Tran *et al.*, "A comparison of energy use, water use and carbon footprint of cassava starch production in Thailand, Vietnam and Colombia," *Resour. Conserv. Recycl.*, vol. 100, pp. 31–40, 2015, doi: 10.1016/j.resconrec.2015.04.007.

[16] A. Chiadò Rana, "Cassava mash dewatering in filtration - compression : experimental study and modelling," Politecnico di Torino, 2021.

[17] E. O. Udoro, O. S. Gbadamosi, and K. a Taiwo, “Studies on the Production and Utilization of Dried Cassava Chips as Human Food,” *Int. Union Food Sci. Technol.*, vol. 1, no. 2008, pp. 1–8, 2013.

[18] P. W. Wareing, A. Westby, J. A. Gibbs, L. T. Allotey, and M. Halm, “Consumer preferences and fungal and mycotoxin contamination of dried cassava products from Ghana,” *Int. J. Food Sci. Technol.*, vol. 36, no. 1, pp. 1–10, 2001, doi: 10.1046/j.1365-2621.2001.00419.x.

[19] A. Westby and S. Gallat, “Cassava chips processing in Ghana:participatory postharvest research and technology transfer in response to new market opportunities,” *Enhancing Postharvest Technol. Gener. Dissem. Africa*, pp. 61–65, 1999.

[20] A. Chapuis, M. Precoppe, J. M. Méot, K. Sriroth, and T. Tran, “Pneumatic drying of cassava starch: Numerical analysis and guidelines for the design of efficient small-scale dryers,” *Dry. Technol.*, vol. 35, no. 4, pp. 393–408, 2017, doi: 10.1080/07373937.2016.1177537.

[21] K. Sriroth *et al.*, “Cassava Starch Technology: the Thai experience,” *Starch/Starke*, vol. 52, pp. 439–449, 2000.

[22] L. A. Sanni, O. O. Oke, F. M. Oladimeji, and K. F. Ogbozomivaze, “Thermal Properties and Energy Utilization of Cassava Meal in Conductive Rotary Drying,” *Am. J. Food Sci. Technol.*, vol. 4, no. 6, pp. 160–167, 2016, doi: 10.12691/ajfst-4-6-1.

[23] F. . Ademiluyi, “Developments of predictive models for drying fermented ground cassava in a rottory dryier,” Rivers Rivers State University of Science and Technology, Port Harcourt, Nigeria.

[24] C. Lambert, D. Goujot, H. Romdhana, and F. Courtois, “Toward a generic approach to build up air drying models,” *LDRT*, vol. 34, no. 3, pp. 346–359, 2016, doi: 10.1080/07373937.2015.1054510.

[25] Escobar Salamanca, “Démarche intégrée pour l’indentification de mécanisme et d’opérations unitaires déterminants da la qualité du gari,” école doctorale GAIA, 2018.

[26] I. Defloor, I. Dehing, and J. A. Delcour, “Physico-chemical properties of cassava starch,” *Starch/Staerke*, vol. 50, no. 2–3, pp. 58–64, 1998, doi: 10.1002/(SICI)1521-379X(199803)50:2/3<58::AID-STAR58>3.0.CO;2-N.

[27] P. Action, “Drying of foods,” *Food Technol.*, vol. 60, no. 12, 2006, doi: 10.1201/9780429058769-14.

[28] A. Gevaudan, “Etude du sechage par contact de milieux granulaires agites,” 1989.

[29] S. Romuli, A. Abass, and J. Müller, “Physical Properties of Cassava Grits before and after Pneumatic Drying,” *J. Food Process Eng.*, vol. 40, no. 2, 2017, doi: 10.1111/jfpe.12397.

[30] S. N. Marousis and G. D. Saravacos, “in Drying Starch Materials,” vol. 55, no. 5, pp. 3–8, 1990.

[31] J. H. Hotchkiss, J. M. Jay, S. J. Mulvaney, M. D. Pierson, J. A. Torres, and E. A. Zottola, *PRINCIPLES OF FOOD PROCESSING*. Aspen Publication, 1998.

[32] Z. F. Min Zhang, Bhesh Bhandari, *Handbook of drying of vegetables and vegetable products*,

no. December. 2006.

[33] M. N. Golubovic, H. D. Madhawa Hettiarachchi, W. Belding, and W. M. Worek, “A new method for the experimental determination of Lewis’ relation,” *Int. Commun. Heat Mass Transf.*, vol. 33, no. 8, pp. 929–935, 2006, doi: 10.1016/j.icheatmasstransfer.2006.05.009.

[34] R. B. Bird, W. E. Stewart, and E. N. Lightfoot, *Transport phenomena*. New York, 2002.

[35] F. Courtois, “Dynamic modelling of drying to improve processing quality of corn,” ENSIA, 1991.

[36] H. Romdhana, C. Lambert, D. Goujot, and F. Courtois, “Model reduction technique for faster simulation of drying of spherical solid foods,” *J. Food Eng.*, vol. 170, pp. 125–135, 2015, doi: 10.1016/j.jfoodeng.2015.09.021.

[37] A. Chilton, T Colburn, “Mass Transfer (Absorption) Coefficients - Prediction from data on heat transfer and fluid friction,” *Ind. Eng. Chem.*, pp. 1183–1187, 1934, doi: 10.1021/ie50299a012.

[38] V. Puri and R. Anantheswaran, “The finite element method in food processing - A review,” *J. Food Eng.*, vol. 19, pp. 247–274, 1993.

[39] T. Gulati and A. K. Datta, “Enabling computer-aided food process engineering: property estimation equations for transport phenomena-based models,” *J. Food Eng.*, vol. 116, pp. 483–504, 2013.

[40] D. N. Njie, “Thermal properties of cassava, yam and platain,” *J. Food Eng.*, pp. 63–76, 1998, doi: Njie, D. N., Rumsey, T. R., & Singh, R. P. (1998). Thermal properties of cassava, yam and platain. Journal of Food Engineering, 37(1), 63–76. doi:10.1016/s0260-8774(98)00068-5.

[41] F. T. Ademiluyi and Y. T. Puyate, “Modeling Drying Kinetics of Fermented Ground Cassava in a Rotary Dryer,” *Transnatl. J. Sci. Technol. May*, vol. 3, no. 5, pp. 1–24, 2013.

[42] M. Okos and Y. Choi, “Thermal properties of liquid foods,” *Am. Soc. Agric. Eng.*, 1986.

[43] D. R. Heldmann and R. P. Sight, *Food Procedd engineering*. Springer, 1981.

[44] T. Ademiluyi, T. O. K. Audu, D. O. Njobuenwu, and F. E. Akpan, “Effect of variety on the heat transfer coefficient during drying of fermented ground cassava,” *Int. J. Food Sci. Technol.*, 2008.

[45] R. Niesteruk, “Thermal Properties of Food Products,” *Dry. Technol.*, vol. 10, no. 2, pp. 541–544, 1992, doi: 10.1080/07373939208916455.

[46] D. A.E and S. G.D, “Thermal conductivity of granular starch materials,” *J. Food Sci.*, vol. 53, pp. 1759–1799, 1988.

[47] C. . Chavez-Mendez *et al.*, “Fitting cassava drying kinetic with a high order equation,” *Dry. Technol.*, vol. 16, pp. 323–331, 1998.

[48] A. Chapuis, M. Precoppe, J. M. Méot, K. Sriroth, and T. Tran, “Pneomatic drying on cassava starch: numerical analysis and guidelines for for the design of efficient small-scale dryiers,” *Dry. Technol.*, vol. 35, pp. 393–408, 2017.

[49] L. Van Der Werf, A. Chapuis, and F. Coutois, “A global sorption equation for raw and

processed cassava based on a review and compilation of sorption properties," *Dry. Technol.*, 2022, doi: 10.1080/07373937.2022.2076238.

[50] A. Duquenoy, J. J. Bimbenet, and G. Trystram, *Génie des procédés alimentaires: des basas aux applications*. 2002.

[51] N. M. Panagiotou, M. K. Krokida, Z. B. Maroulis, and G. D. Saravacos, "Moisture Diffusivity : Literature Data Compilation for Foodstuff.," *Int. J. Food Prop.*, pp. 273–299, 2004.

[52] S. Marousis and G. Saravacos, "Density and porosity in drying starch materials," *J. Food Sci.*, vol. 55, pp. 367–1372, 1990.

[53] S. Ajala, "Drying Characteristics and Mathematical Modelling of Cassava Chips," vol. 4, no. June 2012, pp. 1–9, 2012.

[54] T.Tunde-Akintunde and A. A. Afon, "Modeling of hot-air drying of pretreated cassava chips," *Agric. Eng. Int. CIGR J.*, vol. 12, no. 2, pp. 34–41, 2010.

[55] A. Lopez-ortiz, N. Gomez-Gomez, M. Morales-Celaya, and S. S. Torres, "Thickness effect on effective diffusivity and internal temperature profile of cassava (Manihotes-culentumCrantz) during drying," 2013.

[56] O. A. Azaka, S. Ogbonna Enibe, and C. H. Achebe, "Determination of Moisture Diffusivity during Drying of Rectangular Cassava Pellets: Experimental and Modeling Study," *J. Eng. Appl. Sci.*, vol. 15, no. 1, pp. 56–63, 2019.

[57] C. Chávez-Méndez, M. A. Salgado-Cervantes, K. N. Waliszewski-Kubiak, and M. A. Garcia-Alvarado, "Fitting cassava drying kinetic with a high order equation," *Dry. Technol.*, vol. 16, no. 1–2, pp. 323–331, 1998, doi: 10.1080/07373939808917407.

[58] N. . Zogzas and Z. B. Maroulis, "Moisture diffusitivy data compilation in foodstuff," *Dry. Technol.*, no. May 2013, pp. 37–41, 2007.

[59] J. A. Nelder and R. Mead, "A Simplex Method for Function Minimization," *Comput. J.*, vol. 7, no. 4, pp. 308–313, 1965, doi: 10.1093/comjnl/7.4.308.

[60] W. T. V. and B. P. F. William H. Press, Saul A. Teukolsky, *Numerical Recipes*. Cambridge University Press, 1992.

[61] "Math Works, MATLAB, The Math Works, MA, 1994." .

[62] C. Lagarias, Jeffrey, A. Reeds, James, H. Wright, Margaret, and E. Wright, Paul, "Convergence properties of the nelder–mead simplex method in low dimensions," *SIAM J. Optim.*, vol. 9, no. 1, pp. 112–147, 1998.

[63] J. E. Dennis, Jr. and V. Torczon, "Direct Search Methods on Parallel Machines," *SIAM J. Optim.*, vol. 1, no. 4, pp. 448–474, 1991, doi: 10.1137/0801027.

[64] M. H. Wright, "Direct Search Methods: Once Scorned, Now Respectable," *Pittman Research Notes in Mathematics Series: Numerical Analysis 1995*. pp. 191–208, 1996.

[65] D. Parkinson, J.M. and Hutchinson, "An investigation into efficiency of variants on the simplex method"," *Numer. methods nonlinear Optim.*, pp. 115–135, 1972.

[66] McCabe, L. Warren, P. Harriot, and J. C. Smith, *Unit operations of chemical engineering*, 5th ed. McGraw-Hill, 1993.

# Annex 1

## Characterization of the air flow in the pilot equipment

### *CIRAD dryer: characterization of the air*

The air velocity is calculated using the information about the frequency of the fan, that can be read on the screen, and thanks to the following empirical equation:

$$v_{air} = 0.102414 * f - 0.217$$

The minimum value for the frequency is 20 Hz, that corresponds to a velocity of 1.831 m/s. This represents an estimation of the real value, by the time that, in the formula, there is no dependency on the temperature and on the variation of the passage sections between the chambers and the pipe connecting them. For this reason, it was necessary to validate this measurement by means of external sensors placed at certain access points.

The external equipment employed is composed by a hygrometer able to also detect the temperature, and an anemometer, both from Testo company (Figure 1). In the parallel drying chamber, the average value for the air velocity comes out to be around 1.64 m/s when the temperature is set on 60°C, that represents a relative difference of 10.4% with respect to the value estimated with the formula. The temperatures detected respectively with the inline and external sensors were instead 59.4 and 56.8, with a relative error of around 4.37%. In the cross drying chamber, instead, the relative difference detected with the two sensors respectively for air velocity and temperature resulted to be 4.75 % and 18.07%. The mean temperature from the external and inline sensors were indeed respectively 37.9°C and 39.7°C. For the air velocity, an average value of 1.5 m/s is being detected by the testo sensors along the trial

For the experimentation, the trials are made at three different air temperatures: 40°C, 60°C and 80°C. The set-point on the relative humidity is 8% but, by the moment that the dryer has no condenser, it cannot be reached in every temperature conditions. In particular, at the temperature of 40°C the value can be slightly different (between 15% and 21%) depending on the atmospheric air condition of the day.

*Figure 1 Testo sensors for the characterization of the air flow*

### *A.T.A. dryer: characterization of the air*

The Table 1 summarizes the conditions of some of the trials made on the A.T.A. dryer, as well as the characterization of the air flow performed by the inline and Testo sensors. It's worth noting that Testo sensors make measurements in continuum, storing it with a certain frequency: the values in the table are the result of an average made on the data recorded along the entire duration of the trial.

*Table 1 Characterization of air flow in A.T.A. loop dryer: discrepancies noted on the internal air velocity detections*

| **Date** | **Flow Type** | **Air velocity (inline) [m/s]** | **Air velocity (Testo) [m/s]** | **Temperature (Inline) [°C]** | **Temperature (Testo) [°C]** | **HR% (Inline)** | **HR% (Testo)** |
|---|---|---|---|---|---|---|---|
| 21/04/2022 | Parallel | Unavailable | 0.7 | 63.5 | 61.2 | 8.5 | 8.8 |
| 22/04/2022 | Parallel | 1.7 | 1 | 60 | 61.7 | 7 | 6.8 |
| 22/04/2022 | Traversing | 1 | 0,7 | 60,6 | 60,4 | 9,6 | 11,3 |

Relative percentage differences between external and inline measurements:

- Air speed: 26%
- Temperature: 2,27%
- HR: 7.536%

As visible, the measurements on the temperature and on the relative humidity seem to have negligible discrepancies. The value relative to the speed of the air is not enough reliable due to the missing of several measurement repetitions and must be taken by the reader as an indicative value. Nevertheless, the difference between the two measurements appears to be not totally negligible.